

PH.D. DISSERTATION

UNIVERSITY OF NAPLES “FEDERICO II”

DEPARTMENT OF ELECTRICAL ENGINEERING  
AND INFORMATION TECHNOLOGIES

DOCTORATE OF PHILOSOPHY IN  
ELECTRONIC AND TELECOMMUNICATIONS ENGINEERING

---

COOPERATION AND MIGRATION FOR  
FUTURE COMMUNICATION  
NETWORKS

---

**FULVIO MELITO**

Ph.D. Coordinator

Ch.mo Prof. Niccoló RINALDI

Supervisors

Ch.mo Prof. Francesco VERDE

Ch.ma Prof.ssa Donatella DARSENA

XXVII cycle



# Dedication

*To the loving memory of my father, Mario.*

*To my mom, Carmen.*

*To my niece Claudia and to my sister Roberta.*



# Acknowledgements

I would like to thank my supervisors, Professors Francesco Verde and Donatella Darsena, as well as Professor Giacinto Gelli for their guidance and support during the entire Ph.D. course.

I wish also to thank Telecom Italia S.p.A., for having funded my Ph.D. scholarship, and Eng. Antonio Manzalini (Telecom Italia Strategy-Future Centre) for his advice and continuous support.



# Contents

<b>Acknowledgements</b>	<b>V</b>
<b>Introduction</b>	<b>XI</b>
<b>Basic notation</b>	<b>XIX</b>
<b>Glossary of acronyms</b>	<b>XXI</b>
<b>Assumptions</b>	<b>XXV</b>
<b>1 Preliminaries: wireless channel, MIMO, OFDM</b>	<b>1</b>
1.1 The wireless channel . . . . .	2
1.1.1 Attenuation phenomena . . . . .	2
1.1.2 Multipath propagation effects and fading types . . . . .	5
1.1.3 Narrowband and wideband systems . . . . .	6
1.2 Diversity . . . . .	8
1.3 MIMO systems . . . . .	10
1.3.1 Array gain . . . . .	11
1.3.2 Diversity gain . . . . .	12
1.3.3 Multiplexing gain . . . . .	14
1.3.4 Interference reduction . . . . .	14
1.4 OFDM . . . . .	15
1.4.1 OFDM analog implementation . . . . .	17
1.4.2 OFDM digital implementation . . . . .	19
1.5 Cooperative approaches . . . . .	23
1.5.1 Relaying models and protocols . . . . .	23

<b>2</b>	<b>Performance analysis and optimization of MIMO cooperative multiple-relay communications in Gaussian noise</b>	<b>27</b>
2.1	Introduction . . . . .	28
2.2	General network model . . . . .	30
2.3	Case 1: Naive cooperation with ZF equalization . . . . .	33
2.3.1	System model and basic assumptions . . . . .	33
2.3.2	Theoretical performance analysis . . . . .	34
2.3.3	Numerical performance analysis . . . . .	41
2.4	Case 2: Naive cooperation with MMSE equalization . . . . .	47
2.4.1	Signal model . . . . .	47
2.4.2	SEP analysis . . . . .	48
2.4.3	Numerical results . . . . .	54
2.5	Case 3: Optimized cooperation . . . . .	56
2.5.1	Network model and basic assumptions . . . . .	57
2.5.2	Full instantaneous CSI . . . . .	59
2.5.3	Statistical-only CSI . . . . .	62
2.5.4	Numerical results . . . . .	66
2.6	Conclusions . . . . .	69
<b>3</b>	<b>Design of cooperative multiple-relay communications over frequency selective channels corrupted by non-Gaussian noise</b>	<b>71</b>
3.1	Introduction . . . . .	72
3.2	Asynchronous Middleton Class A model . . . . .	73
3.3	Non-cooperative communications over non-Gaussian channels . . . . .	74
3.3.1	OFDM system model . . . . .	74
3.3.2	ICI analysis of sample-by-sample blanking . . . . .	75
3.3.3	Frequency-domain FIR ICI-free equalization . . . . .	76
3.3.4	Numerical performance analysis . . . . .	78
3.4	Cooperative communications over non-Gaussian channels . . . . .	82
3.4.1	Network model . . . . .	82
3.4.2	Numerical results . . . . .	88
3.5	Conclusions . . . . .	92
<b>4</b>	<b>Virtual machine migration in Software-Defined future networks</b>	<b>95</b>
4.1	Introduction . . . . .	96

4.2	Network scenarios . . . . .	98
4.3	Live migration of virtual machines across WANs . . . . .	99
4.4	Numerical performance analysis . . . . .	105
4.5	Conclusions . . . . .	108
<b>Conclusions</b>		<b>109</b>
<b>Appendices</b>		<b>113</b>
<b>A</b>	<b>Proof of Lemma 1</b>	<b>113</b>
<b>B</b>	<b>Proof of Theorem 1</b>	<b>116</b>
<b>C</b>	<b>Proof of Theorem 2</b>	<b>119</b>
<b>D</b>	<b>Proof of Lemma 2</b>	<b>122</b>
<b>E</b>	<b>Proof of Theorem 3</b>	<b>123</b>
<b>Bibliography</b>		<b>139</b>



# Introduction

In the recent past of telecommunication systems, two historical events are worth noting: the first occurred in 1979, when a first generation (1G) mobile network was deployed for the first time by NTT (Nippon Telegraph and Telephone) in Japan; the second occurred in 1995, the year in which the Internet was fully commercialized in the United States of America. Since those years, telecommunication technologies have been characterized by an unprecedented pace of evolution driven by the societal development. This phenomenon, resulting in a corresponding evolution of both our habits and our lifestyle has, consequently, affected all the aspects of the human beings' daily life. As a matter of fact, from those years, both fixed and mobile communications allowed us to get, if properly utilized, improvements such as (between others) a better efficiency in the work environments, a greater level of personal security, and wider social networks. Anyway if, from a technological point of view, we could say that the Internet we have nowadays is essentially unchanged with respect to what it was at the start of its life, the same cannot be stated for the mobile networks. In fact, from the roll out of the 1G mobile networks, two other technologies have been standardized before the introduction of the fourth generation (4G) system we have currently. Unlike the evolutionary processes related to the previous generations of mobile standards, in which the aim has been to implement digital communication systems allowing the transmission of multimedia data, the most important leap ahead to deal with now is mainly related to the improvement of connectivity and capacity. As happened for all the previous major phases of the mobile telecommunication standards, even in this phase, companies and governments have planned to employ a considerable amount of financial and human resources in research activities related to the next generation mobile network. With regard to the government of the old continent only, the European Commission

has already funded research activities on future networks with hundreds of million euro, while other governments and companies in the world have announced investments from hundreds of millions to more than a billion dollars. Globally, there is a huge number of researchers that, currently, are working hard all around the world both to define use cases and requirements of the fifth generation (5G) mobile network and to standardize it. A deep understanding of the future scenario is particularly important for such a kind of activities. As stated in [1], there have been 110 million new mobile subscriptions globally in Q3 (*third quarter*) 2014 and a 60% growth in data traffic globally between Q3 2013 and Q3 2014<sup>1</sup>. Moreover, in the next few years, the number of connected devices (e.g. communicating machines for smart cities, e-health, entertainment, transportation, etc...) will grow up to tens of billions, allowing the so-called Internet of Things (IoT) to complement the actual human-centric communication scenario [2, 3] and contributing to the traffic growing. In this new integrated scenario, the services requested by the connected devices will be extremely heterogeneous both in terms of purpose and in terms of requirements. Therefore, 5G networks will have to ensure connectivity anywhere and anytime to a tremendous number of devices, each of which characterized by a certain service level agreement (SLA) that the networks will have to dynamically manage. In order to deal with the expected traffic growth, the ever increasing number of connected devices and the related requirements and use cases, the future mobile network will have to [4]: (i) **be more efficient** in terms of energy, cost, and resource utilization; (ii) **be more versatile** in terms of availability, mobility, and QoS (*Quality of Service*); (iii) **provide better scalability** in terms of traffic and connected devices. More specifically, it is widely recognized that 5G networks will have to address six challenges that the LTE-A (*Long Term Evolution - Advanced*) is not able to properly deal with. These challenges are the following and are briefly discussed in [5]: (i) higher capacity; (ii) higher data rate; (iii) lower E2E (*End to End*) latency; (iv) massive device connectivity; (v) reduced CapEx (*Capital Expenditure*) and OpEx (*Operational Expenditure*); (vi) consistent QoE (*Quality of Experience*) provisioning. With the aim to address these challenges, the research community is working to identify the set of key candidate technologies that will enable the future mobile network.

---

<sup>1</sup>It is estimated that approximately 55% of mobile traffic will come from video in 2020.

Three of these candidate technologies are related to the **relaying and multi-hop communications** (typical of the cooperative approaches for wireless networks) and to the recently introduced paradigms of **SDN** (*Software Defined Networking*) [6] and **NFV** (*Network Function Virtualization*) [7].

In this thesis work, some original results concerning the above mentioned technologies (relaying/multi-hop communications/cooperative communications, SDN, and NFV) will be presented, by reserving greater emphasis to the first one. The following subsections will represent a short introduction to the basics of such technologies and the relevance of their possible use within future mobile network architectures, by referring also to some literature papers related to the covered topics.

### Cooperative communications

Cooperation concepts in the context of telecommunication systems have been introduced for the first time when Edward C. Van Der Meulen, by considering communication channels between three different terminals, addressed the problem of *how to send information in one specified direction over a two-way communication channel* [8] *as effectively as possible, assuming that all terminals were **cooperating** so as to optimize the transmission procedure* [9, 10]. In his work, Van Der Meulen defined the basis concept of *relay channel* and derived upper and lower bounds on the capacity of such a channel. As intuition could suggest, unlike the so called *direct, single-user* or *point-to-point* communication, in which the communication from a single source (S) to a single destination (D) happens without the help of any other communicating terminal, cooperation is possible whenever there are at least three terminal nodes in the network: more generally, a source, a destination and a set (eventually of unitary cardinality) of nodes that help the communication from S to D. Cooperative relaying techniques can be employed with the aim to improve the coverage and/or the data rates and have recently gained increasing attention within both academic and industrial research activities. Indeed, in LTE (Long Term Evolution) release 10, i.e. the LTE-A (Long Term Evolution-Advanced), support for a decode-and-forward (DF) relaying scheme has been introduced. Specifically, in order for release 8/9 terminals to be served by relays (introduced in release 10) and, therefore, to ensure full compatibility between LTE (release 8, 9) and LTE-A (release

10), a fundamental condition on the transparency of the relays with respect to the terminals has been imposed. This means that the terminal is not aware of whether it is connected to a relay or to a conventional base station [11].

Besides its role in LTE-A standard, cooperative relaying turns out to be also a potential enabling technology for 5G networks. In [4], the authors envision the employment of relay nodes as a mean to implement multi-hop communications and wireless network coding in order to extend coverage and improve reliability, transfer the processing/energy burden from the massive machine communication (MMC) devices to the network, and to have an alternative backhauling solution. In [5], instead, it is argued that a possible way to support the hyperconnectivity, required by the huge number of connected nodes of a future 5G network, will be represented by a combination of advances in air interface design, signaling optimization, intelligent clustering and relaying techniques. Again in [5], joint use of relaying and nesting techniques is expected to ensure 5G features such as support of multiple devices, group mobility and nomadic hotspots. The paper [12], written by N. Bhushan *et al.*, is strongly related to network densification, which represents a combination of spatial densification and spectral aggregation and is considered a key mechanism to improve the wireless communications and meet the requirements, in terms of capacity and connectivity, of the next generation of mobile communications. Moreover, the authors highlight the Martin Cooper's<sup>2</sup> statement for which, so far, three main factors (in decreasing order of impact) have always had a predominant influence in the growth of wireless system capacity: increase in the number of wireless infrastructure nodes, increased use of radio spectrum, and improvement in link efficiency. Within the paper other solutions are also pointed out, such as the use of relay nodes at location without wired backhaul access (as a mean to ensure access to mobile terminals and to backhaul traffic to a base station with wired backhaul) and the use case of D2D (*Device to Device*) relay for traffic offloading.

---

<sup>2</sup>Martin Cooper is a pioneer of wireless communications and is considered the father of the cell phone. Worthy of note is its *law of spectral efficiency*, also known as Cooper's law, which states that *the maximum number of voice conversations or equivalent data transactions that can be conducted in all of the useful radio spectrum over a given area doubles every 30 months.*

## SDN & NFV

SDN [6] is an emerging architecture formally introduced by the Open Networking Foundation (ONF), a not-for-profit organization co-founded by Nick McKeown and Scott Shenker and dedicated to the promotion and adoption of SDN. According to what the ONF has stated, the basic idea of SDN is represented by *the physical separation of the network control plane from the forwarding plane enabling, in this way, the network control to become directly programmable and the underlying infrastructure to be abstracted for applications and network services* [6, 13]. One of the main effects of SDN is that it allows one to modify the network functionalities by simply installing new software in the network but without performing any change at the hardware level. This feature speeds up the network innovation by making it only dependent on the software design speed and no more on the overall process of hardware design, production and installation. A core tool to implement an SDN architecture is *OpenFlow* [14], the first standard communications interface defined between the control and forwarding layers of an SDN architecture and widely supported by various device manufacturers, service providers, and operators.

NFV [7] represents an evolved way to apply virtualization's concepts to the telecommunication networks. It was introduced at the end of 2012 by some of the world's leading telecoms network operators, which selected ETSI (European Telecommunications Standards Institute) to be the home of the Industry Specification Group for NFV (ISG NFV), with the aim to provide a mean to speed up the launch of new network services while, at the same time, saving financial resources. It is a matter of fact that, currently, the amount of time necessary to launch a new network service depends on many factors such as, between others: (i) the presence, within the networks, of proprietary hardware appliances; (ii) the difficulties in designing new and ever more complex hardware-based appliances; (iii) the ever shorter hardware lifecycles. The solution proposed by ISG NFV to address these problems consists in virtualizing all the network functions that could be virtualized and installing them on general purpose hardware. In this way NFV, as well as SDN, allows one to perform faster changes of the network features by reducing CapEx and OpEx.

SDN and NFV, therefore, promise a more flexible network deployment and operation as well as a more efficient resource utilization (that is, maybe, the basic benefit of virtualization).

The key role that SDN and NFV will have in the 5G network architecture is widely recognized. In [5] an architectural vision which addresses the challenges placed on 5G mobile networks with its key architectural elements is proposed. The authors indicate SDN and NFV as technologies capable to allow faster deployment, orchestration and on demand scaling of the functions in the network cloud. Also in the RAS (Radio Access and Spectrum)<sup>3</sup> white paper on 5G radio network architecture [15] the relevance of SDN and NFV as enabling technologies is described. The paper confirm the ability to implement (i.e., virtualize and deploy) critical mobile network functions (MME, HGW,PGW, etc.) on standard IT (Information Technology) platforms by, anyway, highlighting the role of both the highspeed IP (Internet Protocol) networks availability and the possibility to manage them more flexibly through SDN, as necessary conditions. Finally, papers [16,17] again emphasized the significant impact that SDN and NFV will have in applying intelligence in future 5G networks.

### Organization of the thesis

By considering the activities carried out during the Ph.D. programme and the related topics, this work of thesis is organized as follows:

- In **Chapter 1**, the application environment considered in the overall Ph.D. program as well as both the relevant phenomena governing it and the main technologies employed to mitigate their negative effect on performance metrics are described. The chapter, hence, will start with a short introduction of the wireless channel. Specifically, a description of the multipath propagation will be given as well as an overview both of its time and frequency consequences and of the involved attenuation phenomena. Then, the concept of diversity and its role in counteracting the multipath fading will be discussed. In this regard, time, frequency, and

---

<sup>3</sup>RAS is a cluster activity comprising a portfolio of more than 20 research projects participating in the European Commission 7<sup>th</sup> Framework Program and investigating radio access and spectrum aspects of future wireless networks.

space diversity will be described. In addition, the basic principles of multiple-input multiple-output (MIMO) systems will be treated as well as the performance improvements they provide. At that point, orthogonal frequency division multiplexing (OFDM) multi-carrier modulation will be discussed. Besides introducing the basic idea of OFDM, both the analog and the digital OFDM implementations will be described with a particular emphasis, for the case of digital implementation, on the relevance of the cyclic prefix (CP) (similar consideration can be made, in the case of analog implementation, for the time guard) in mitigating the multipath fading when considering wideband systems. Finally, the last section will be devoted to introducing the basics of cooperative approaches.

- In **Chapter 2**, some results related to MIMO cooperative multiple-relay systems will be presented. At first, the general network model will be introduced and, then, the chapter will follow by describing three different original results. The first presented contribution will be mainly related to the performance analysis, in terms of average bit error rate (ABER), of a MIMO cooperative system characterized by non-optimized processing (both at the source and at the relay nodes) and zero-forcing (ZF) reception. Moreover, the study of the optimal relays' positions will be performed in the special case of relay cluster. The second contribution will be related to the performance analysis for a similar system, but in the case of minimum mean square error (MMSE) receiver. The last contribution will be aimed at assessing the improvement provided by the optimization of both the source and the relay processing in an OFDM system, by considering two limit cases of the available channel state information (CSI).
- In **Chapter 3**, the design of cooperative multiple-relay communications over frequency selective channels corrupted by non Gaussian noise is carried out. The motivations which drive the study of wireless networks in impulsive noise stems from the fact that such a noise category, along with the multipath fading, may represent the dominant cause of performance degradation in heavily-congested scenarios. The contributions presented in this chapter are related both to the direct communication and to the cooperative communication. At first, a SISO OFDM system, employing non-linear

blanking preprocessing to mitigate the impulsive noise effects, will be considered and the design of a new equalizer will be presented. Specifically, it will be shown that, by exploiting the presence of *virtual carriers* (a solution present in several multicarrier standards), it is possible to design frequency-domain linear finite impulse response (FIR) equalizers for channels affected by impulsive noise (IN), which are able to compensate for the inter-carrier interference (ICI) introduced by a blanking nonlinearity.<sup>4</sup> In particular, a sufficient condition ensuring the existence of such a FIR ICI-free solution is derived. Moreover, it is shown that, with respect to conventional zero-forcing (ZF) receivers (with or without blanking), a performance gain can be obtained for signal-to-noise ratio (SNR) values of practical interest, with an affordable increase in computational complexity. Then, a cooperative OFDM system, employing a distributed space-time block coding (STBC) technique will be considered to show its beneficial effects, with respect to the direct communication, both in the centralized and decentralized cases.

- In **Chapter 4**, the potential impact of emerging technologies, like software defined networking (SDN) and network virtualization (NV), on future network evolution is addressed. It is argued that the above mentioned technologies could bring a significant disruption at the edge networks, where it will be possible to develop distributed clouds of virtual resources running on standard hardware. The contribution of the chapter is related to a key technical challenge behind this vision: the capability of dynamically moving virtual machines (VMs), which run network services, functions, and users applications, among edge networks across wide area interconnections. Specifically, we focus on the problem of live migrating the memory state of a single VM between two physical machines, which are located at the edge and are inter-connected by a wide area network (WAN). With reference to a pre-copy mechanism, aimed at iteratively transferring the memory content to the destination machine, we will develop a simplified mathematical model that unveils the dependence of the total migration time and downtime of the VM memory transfer on the main WAN parameters, such as capacity, buffering, and propagation delay.

---

<sup>4</sup>The proposed approach can be extended to other memoryless nonlinearities [18], e.g., clipping or combination of blanking and clipping.

# Basic notation

Symbol	Meaning
$\mathbb{N}$	Field of natural numbers
$\mathbb{Z}$	Field of integer numbers
$\mathbb{R}$	Field of real numbers
$\mathbb{C}$	Field of complex numbers
$\mathbb{R}_{++}$	$\{x \in \mathbb{R} : x > 0\}$
$\mathbb{R}^{m \times n}$	Field of $m \times n$ real matrices
$\mathbb{R}^m$	Shorthand for $\mathbb{R}^{m \times 1}$
$\mathbb{C}^{m \times n}$	Field of $m \times n$ complex matrices
$\mathbb{C}^m$	Shorthand for $\mathbb{C}^{m \times 1}$
$\mathcal{B}$	When $\mathcal{B} \subset \mathcal{J}$ , is the complement of the set $\mathcal{B}$ with respect to $\mathcal{J}$
$ \mathcal{B} $	Cardinality of the set $\mathcal{B}$
$\mathbf{a}$	Column vector
$\mathbf{A}$	Matrix
$\mathbf{0}_m$	Null column vector of size $m$
$\mathbf{O}_{m \times n}$	Null matrix of size $m \times n$
$\mathbf{1}_m$	Column vector of size $m$ whose elements are all equal to 1
$\mathbf{I}_m$	Identity matrix of size $m$
$a_n$	$n$ -th element of the column vector $\mathbf{a}$
$\mathbf{a}_n$	$n$ -th column vector of a matrix $\mathbf{A}$
$\mathbf{a}_{n(-n)}$	$n$ -th column vector of a matrix $\mathbf{A}$ deprived of its $n$ th entry
$\{\mathbf{A}\}_{mn}$	$(m, n)$ -th entry of a matrix $\mathbf{A}$
$\mathbf{A}_{(-n)}$	Matrix $\mathbf{A}$ deprived of its $n$ -th column
$\mathbf{A}_{(-n, -n)}$	Matrix $\mathbf{A}$ deprived of its $n$ -th row and $n$ -th column

$\ \mathbf{a}\ $	Euclidean norm of the vector $\mathbf{a}$
$\ \mathbf{A}\ $	Frobenius norm of a matrix $\mathbf{A}$
$(\cdot)^T$	Transpose of a matrix
$(\cdot)^H$	Conjugate transpose of a matrix
$(\cdot)^{-1}$	Inverse of a matrix
$(\cdot)^-$	Generalized (1)-inverse of a matrix
$(\cdot)^\dagger$	Generalized (Moore-Penrose) inverse of a matrix
$\text{tr}(\cdot)$	Trace of a square matrix
$\det(\cdot)$	Determinant of a square matrix
$\text{rank}(\cdot)$	Rank of a matrix
$\mathcal{N}(\cdot)$	Null space of a matrix
$\mathcal{R}(\cdot)$	Range of a matrix
$\text{diag}(\cdot)$	Diagonal matrix formed by the components of the vector argument
$\text{blkdiag}(\cdot)$	Block-diagonal matrix formed by the matrices of its argument
$\lambda_{\max}(\cdot)$	Maximum eigenvalue of a square matrix
$\max(\cdot)$	Maximum of its arguments
$\min(\cdot)$	Minimum of its arguments
$\otimes$	Kronecker product
$*$	Linear convolution
$\circledast$	Circular convolution
$\text{Pr}(\cdot)$	Probability of an event
$\mathbf{x} \sim \mathcal{CN}(\boldsymbol{\mu}, \mathbf{K})$	Circular symmetric complex Gaussian random vector $\mathbf{x} \in \mathbb{C}^n$ with mean $\boldsymbol{\mu} \in \mathbb{C}^n$ and covariance matrix $\mathbf{K} \in \mathbb{C}^{n \times n}$
$\mathbb{E}[\cdot]$	Mean of random variable $\mathbf{A}$ (subscript dropped when obvious)
$\text{VAR}[\cdot]$	Variance of a random variable
$\Gamma(\cdot)$	Gamma function
$U(\cdot)$	Tricomi's (confluent hypergeometric) function
$\mathcal{O}(\cdot)$	$f(x) = \mathcal{O}(g(x)); g(x) > 0$ , states that $f(x)/g(x) < \infty$ as $x \rightarrow \infty$
$R_{\text{code}}$	Code rate

# Glossary of acronyms

Acronym	Meaning
ABER	Average Bit Error Rate
ACK	Acknowledgement
ADSL	Asymmetric Digital Subscriber Line
A/D	Analog-to-Digital
AF	Amplify and Forward
ASEP	Average Symbol Error Probability
ASER	Average Symbol Error Rate
AWGN	Additive White Gaussian Noise
BER	Bit Error Rate
CapEx	Capital Expenditure
CP	Cyclic Prefix
CPU	Central Processing Unit
CSI	Channel State Information
D	Destination
D2D	Device-to-Device
D/A	Digital-to-Analog
DAB	Digital Audio Broadcasting
DF	Decode and Forward
DFT	Discrete Fourier Transform
DPM	Destination Physical Machine
DRBD	Distributed Replicated Block Device
DSTBC	Distributed Space-Time Block Coding
DVB	Digital Video Broadcasting
E2E	End to End
ETSI	European Telecommunications Standards Institute
F-CSI	Full-Channel State Information

FDM	Frequency Division Multiplexing
FEQ	Frequency Domain Equalization
FFT	Fast Fourier Transform
FIFO	First-In First-Out
FIR	Finite Impulse Response
HGW	Home Gateway
ICI	Intercarrier Interference
ICT	Information and Communication Technology
IDFT	Inverse Discrete Fourier Transform
IFFT	Inverse Fast Fourier Transform
i.i.d.	independent and identically distributed
IN	Impulsive Noise
I/O	Input/Output
IoT	Internet of Things
IP	Internet Protocol
I/Q	In-phase/Quadrature-phase
ISG NFV	Industry Specification Group for NFV
ISI	Inter Symbol Interference
IT	Information Technology
LAN	Local Area Network
LE	Large Enterprise
LISP	Locator/Identifier Separation Protocol
LOS	Line Of Sight
LTE	Long Term Evolution
LTE-A	Long Term Evolution-Advanced
MAC	Multiple Access or Medium Access
MCA	Middleton Class A
MGF	Moment Generating Function
MIMO	Multiple-Input Multiple-Output
MISO	Multiple-Input Single-Output
MMC	Massive Machine Communication
MME	Mobility Management Entity
MMSE	Minimum Mean-Square Error
MSE	Mean-Square Error
NBI	NarrowBand Interference
NFV	Network Function Virtualization

$nG$	$n$ -th Generation of mobile communication
NTT	Nippon Telegraph and Telephone
NV	Network Virtualization
OFDM	Orthogonal Frequency-Division Multiplexing
ONF	Open Networking Foundation
OpEx	Operational Expenditure
OS	Operating System
PGW	Packet data network Gateway
PM	Physical Machine
P/S	Parallel-to-Serial
PSK	Phase-Shift Keying
QAM	Quadrature Amplitude Modulation
$Qn$	$n$ -th Quarter of a year
QoE	Quality of Experience
QoS	Quality of Service
QPSK	Quadrature Phase-Shift Keying
RAM	Random Access Memory
RAS	Radio Access and Spectrum
RV	Random Variable
S	Source
S-CSI	Statistical-Channel State Information
SDN	Software Defined Networking
SEP	Symbol Error Probability
SER	Symbol Error Rate
SIMO	Single-Input Multiple-Output
SINR	Signal-to-Interference-plus-Noise Ratio
SIR	Signal-to-Interference Ratio
SISO	Single-Input Single-Output
SLA	Service Level Agreement
SME	Small-to-Medium Enterprise
SNR	Signal-to-Noise Ratio
S/P	Serial to Parallel
SPM	Source Physical Machine
STBC	Space-Time Block Code (or Coding)
STTC	Space-Time Trellis Code (or Coding)
SVD	Singular Value Decomposition

TCP	Transmission Control Protocol
V-BLAST	Vertical Bell Laboratories Layered Space-Time
VC	Virtual Carrier
VM	Virtual Machine
WAN	Wide Area Network
WiMAX	Worldwide Interoperability for Microwave Access
WLAN	Wireless Local Area Network
ZF	Zero-Forcing
ZMCSCG	Zero-Mean Circularly-Symmetric Complex Gaussian

# Assumptions

Label	Argument	Assumption
(a1)	vector $\mathbf{s}$	$\mathbf{s} \in \mathbb{C}^m$ is a zero mean circularly symmetric complex random vector, with correlation matrix $\mathbb{E}[\ \mathbf{s}\mathbf{s}^H\ ^2] = \mathbf{I}_m$ , and whose entries assume i.i.d. (independent and identically distributed) equiprobable values belonging to a QAM constellation, with cardinality $Q$ .
(a2)	vector $\mathbf{w}_i$	$\mathbf{w}_i$ is a ZMCSCG random vector, statistically independent of $\mathbf{s}$ and $\mathbf{H}_i$ , and with autocorrelation matrix $\mathbb{E}[\ \mathbf{w}_i\mathbf{w}_i^H\ ^2] = \sigma_{\mathbf{w},i}^2 \mathbf{I}_{N_R}$ .
(a3)	matrix $\mathbf{H}_i$	The entries of $\mathbf{H}_i$ , which is statistically independent of $\mathbf{s}$ and $\mathbf{H}_l$ , for $l \neq i$ , are i.i.d. ZMCSCG random variables having variance $\sigma_{\mathbf{h},i}^2$ , which depends on the average path loss associated to the link between S and the $i$ -th relay node.
(a4)	matrix $\mathbf{G}_i$	The entries of $\mathbf{G}_i$ , which is statistically independent of $\mathbf{z}_i$ and $\mathbf{G}_l$ , for $l \neq i$ , are i.i.d. ZMCSCG random variables with variance $\sigma_{\mathbf{g},i}^2$ , which depends on the average path loss associated to the link between the $i$ -th relay node and D.

(a5)	vector $\mathbf{d}$	$\mathbf{d}$ is a ZMCSCG random vector, with autocorrelation matrix $\mathbb{E}[\ \mathbf{d}\mathbf{d}^H\ ^2] = \sigma_d^2 \mathbf{I}_{N_D}$ , which is statistically independent of $\mathbf{z}_i$ and $\mathbf{G}_i$ .
(a6)	matrix $\mathbf{C}$	The dual-hop channel matrix $\mathbf{C} \in \mathbb{C}^{m \times n}$ is full column rank, i.e., $m \leq n$ and $\text{rank}(\mathbf{C}) = n$ with probability one.
(a7)	matrix $\mathbf{F}_0$	$\mathbf{F}_0$ is a scaled semi-unitary matrix of size $N_S \times N_B$ , i.e., $\mathbf{F}_0^H \mathbf{F}_0 = \mathbf{I}_{N_B}/N_B$ .
(a8)	scalars $(N_S, N_B)$	$N_S = N_B$ , i.e., the number $N_S$ of source antennas is equal to the number $N_B$ of source symbols (belonging to $\mathbf{s}$ ) to be transmitted within a generic symbol interval.
(a9)	matrices $\{\mathbf{F}_i\}_{i=1}^{N_C}$	$\mathbf{F}_i, \forall i \in \{1, 2, \dots, N_C\}$ , represents a matrix of size $N_R \times N_R$ such that $\text{tr}(\mathbf{F}_i^H \mathbf{F}_i) = N_R$ .

# List of Figures

1.1	MIMO system. . . . .	10
1.2	Transmit precoding and receiver shaping. . . . .	11
1.3	Array gain. . . . .	11
1.4	Receive diversity. . . . .	12
1.5	Transmit diversity. . . . .	13
1.6	Spatial multiplexing. . . . .	14
1.7	Interference reduction. . . . .	15
1.8	OFDM subcarriers overlapping for rectangular pulses. . . . .	16
1.9	OFDM analog implementation - transmitter side. . . . .	18
1.10	OFDM analog implementation - receiver side. . . . .	18
1.11	Digital OFDM implementation - transmitter side. . . . .	19
1.12	Digital OFDM implementation - receiver side. . . . .	19
1.13	Cyclic prefix of length $\mu$ . . . . .	21
1.14	ISI between data block in channel output. . . . .	22
1.15	Three-terminal relay channel. . . . .	24
2.1	General topology. . . . .	30
2.2	ABER vs $d_{SC}$ between S and C for $\theta = 0$ (Ex. 1). . . . .	42
2.3	ABER vs the C's radius $r$ for $N_C \in \{2, 6\}$ (Ex. 1). . . . .	43
2.4	ABER vs SNR for $(N_C, N_S, N_R, N_D) = (2, 2, 2, 2)$ (Ex. 2). . . . .	44
2.5	ABER vs SNR for $(N_C, N_S, N_R, N_D) = (6, 2, 2, 2)$ (Ex. 2). . . . .	45
2.6	ABER vs SNR for $(N_C, N_S, N_R, N_D) = (2, 2, 2, 3)$ (Ex. 2). . . . .	45
2.7	ABER vs SNR for $(N_C, N_S, N_R, N_D) = (6, 2, 2, 3)$ (Ex. 2). . . . .	46
2.8	ABER vs SNR for different values of the number $N_C$ of relays. . . . .	54
2.9	ASEP vs SNR for Naive and F-CSI cases. . . . .	67
2.10	ASEP vs SNR for Naive, S-CSI and F-CSI cases ( $N_C = 2$ ). . . . .	68
3.1	ASER vs $\xi$ for SNR=15 dB. . . . .	79

---

3.2	ASER vs $\xi$ for SNR=25 dB. . . . .	80
3.3	ASER vs SNR with $\xi$ optimally chosen $\forall$ SNR value. . . . .	80
3.4	ASER vs $\xi$ for SNR $\in \{4, 14, 24\}$ dB ( $N_C=2$ - HI). . . . .	88
3.5	ASER vs SNR ( $N_C=2$ - HI). . . . .	89
3.6	ASER vs SNR with and without blanking ( $N_C=2$ - HI). . . . .	90
3.7	ASER vs $\xi$ for SNR $\in \{0, 4, 14\}$ dB ( $N_C=2$ - NG). . . . .	91
3.8	ASER vs SNR ( $N_C=2$ - NG/HI). . . . .	91
3.9	ASER vs SNR ( $N_C \in \{2, 3\}$ - HI). . . . .	92
4.1	Edge networks scenario. . . . .	97
4.2	Average downtime versus $\gamma/\lambda$ . . . . .	107
4.3	Average total migration time versus $\gamma/\lambda$ . . . . .	107

# Chapter 1

## Preliminaries: wireless channel, MIMO, OFDM, cooperation

This first chapter is devoted to introducing preliminary concepts regarding the application environment considered in the overall Ph.D. program, as well as the relevant phenomena governing it and the main technologies employed to mitigate their negative effect on performance metrics. The chapter, hence, will start with a short introduction of the wireless channel. Specifically, a description of the multipath propagation will be given, as well as an overview both of its time and frequency consequences and of the involved attenuation phenomena. Then, the concept of diversity and its role in counteracting the multipath fading will be discussed. In this regard, time, frequency, and space diversity will be described. In addition, the basic principles of multiple-input multiple-output (MIMO) systems will be introduced, as well as the performance improvements they provide. At that point, orthogonal frequency division multiplexing (OFDM) multicarrier modulation will be treated. Besides introducing the basic idea of OFDM, the section will describe both analog and digital OFDM implementations, with a particular emphasis, for the case of digital implementation, on the relevance of the cyclic prefix (CP) (similar considerations can be made, in the case of analog implementation, for the time guard) in mitigating the multipath fading when considering wideband systems. Finally, the last section will introduce the basics of cooperative approaches.

## 1.1 The wireless channel

Unlike wired communications, in which signal propagation is constrained within “wires”, in wireless communications the propagation medium is not a wire but, typically, either the troposphere or the water. In this chapter the first one will be considered. When a signal is transmitted through the wireless channel, it experiences both the inherent properties of the transmitting medium and the environmental characteristics. In fact, besides the wireless medium properties, the propagation depends on static and dynamic entities (buildings, monuments, trees, cars, etc.) which constitute the propagation environment. Therefore, in general, propagation occurs by means of multiple path (*multipath propagation*) and the channel has time-variant properties, mainly due to the relative mobility between transmitter and receiver, as well as the motion of the surrounding objects. As a result, transmitted power experiences both time-independent (*path-loss*) and time-dependent (*fading*) attenuations and, hence, the received power fluctuates. Typically, these received power variations happen over large, medium and short distance scales [19, 20].

### 1.1.1 Attenuation phenomena

Large-scale distance (100-1000 m) attenuations are mainly measured by *path loss*. This kind of attenuation is due to the dissipation, depending on the distance  $d$  between source and destination devices, of the power radiated by the transmitter. Path loss estimations can be taken in the case in which the electromagnetic waves propagate through the wireless medium when the transmitter and receiver have an unobstructed line of sight (LOS) path between them and, typically path loss models assume that path loss is the same at a given  $d$ . In the simplest case of LOS-only transmissions, the so-called free-space path loss is described the ***Friis law***

$$P_{\text{RX}}(d) = P_{\text{TX}} G_{\text{TX}} G_{\text{RX}} \left( \frac{\lambda}{4\pi d} \right)^2 \quad (1.1)$$

which gives the received power  $P_{\text{RX}}$  as a function of the distance  $d$  (between transmitter and receiver) in free space, where  $P_{\text{TX}}$  is the transmitted power,  $G_{\text{TX}}$  and  $G_{\text{RX}}$  are the antenna gains, respectively, of the

transmit and receive antennas, and  $\lambda$  is the wavelength<sup>1</sup>. This law states that, given the transmit and receive antennas, the received power decays as the square of the distance  $d$ . To estimate the path loss in a more practical scenario involving, besides the LOS path, also propagation mechanisms like diffraction, reflection, transmission and scattering, many path-loss models can be formulated. However, for general analysis it is recommended to use a simple model like the simplified path-loss model one

$$P_{\text{RX}} = P_{\text{TX}} K \left( \frac{d_0}{d} \right)^\eta, \quad (1.2)$$

which is valid for  $d > d_0$ , where  $K$  is a dimensionless constant that depends on the antenna characteristics and the average channel attenuation at  $d = d_0$ ,  $d_0$  is a reference distance for the antenna far-field, and  $\eta$  is the path-loss exponent (between 2 and 6). In particular, the free-space path-loss model, the two-ray model, the Hata model, and the COST extension to the Hata model are all of the same form as (1.2) [20].

Medium-scale distance (10-100 m outdoor, <10 m indoor) random fluctuations of the attenuation, instead, are mainly due to obstruction by large objects and changes in reflecting surfaces and scattering objects. This phenomenon is called *shadowing* or *shadow fading* (sometimes referred to as *medium-scale fading*). With regards to large objects obstruction, it is worth noting that the transition from the non-shadowed zone to the shadowed one it is not sharp but gradual and, specifically, by supposing a fixed transmitter, the receiver has to move over large distances (from a few meters up to several hundreds of meters) in order to pass from the “light” zone to the “dark” zone. This is why shadowing is associated to the so called medium-scale distance movements. Since the properties of the blocking objects and the changes in reflecting surfaces and scattering objects are generally unknown, statistical models must be used to characterize these fluctuations. The most commonly employed model for shadow fading is the *log-normal* one, which has been empirically confirmed for indoor and outdoor environments. In this model, the transmit-to-receive power ratio  $\psi = P_{\text{TX}}/P_{\text{RX}}$  is assumed to be random with a log-normal distribution given by:

$$p_{\Psi}(\psi) = \frac{\xi}{\sqrt{2\pi}\sigma_{\psi_{\text{dB}}}\psi} \exp \left[ -\frac{(\log_{10}(\psi) - \mu_{\psi_{\text{dB}}})^2}{2\sigma_{\psi_{\text{dB}}}^2} \right], \quad \psi > 0, \quad (1.3)$$

---

<sup>1</sup>The factor  $(\frac{\lambda}{4\pi d})^2$  is called *free space loss factor* or *geometric attenuation*.

where  $\xi = 10/\ln(10)$ ,  $\mu_{\psi_{\text{dB}}}$  is the mean of  $\psi_{\text{dB}} = 10 \log_{10}(\psi)$  in decibels, and  $\sigma_{\psi_{\text{dB}}}$  is the standard deviation of  $\psi_{\text{dB}}$  (also in dB). Some observations are now in order. First, since  $\psi$  is log-normal distributed,  $\psi_{\text{dB}} = 10 \log_{10}(\psi)$  is Gaussian distributed. Secondly, this log-normal model jointly treats path loss and shadow fading effects. In fact, the mean  $\mu_{\psi_{\text{dB}}}$ , can be based on an analytical model or empirical measurements: for empirical measurements  $\mu_{\psi_{\text{dB}}}$  equals the empirical path loss, while for analytical models  $\mu_{\psi_{\text{dB}}}$  must incorporate both the path loss (e.g., from a free-space or ray-tracing model) as well as average attenuation from blockage [20]. However, path loss can also be treated separately from shadowing by considering the following model, based on (1.2):

$$\frac{P_{\text{RX}}}{P_{\text{TX}}} \text{ dB} = 10 \log_{10}(K) - 10\eta \log_{10}\left(\frac{d}{d_0}\right) - \psi_{\text{dB}}, \quad (1.4)$$

where  $\psi_{\text{dB}}$  is a Gaussian random variable with zero mean and variance  $\sigma_{\psi_{\text{dB}}}^2$ .

Finally, small-scale (at a distance approximately equal to the wavelength) random fluctuations of the received power are due to constructive/destructive interference between the multipath components of the received signal. In fact, each path involved in the propagation is characterized by its own attenuation delay. Therefore, when the multipath waves are added up at the receiver end, they can mutually interfere either constructively or destructively (depending on their own phases), thus producing variations in the received signal strength. Since the phases associated to each multipath component depends on the relative position of transmitter, receiver and surrounding objects, the interference and, therefore, the amplitude of the total signal, changes with time when either the transmitter, the receiver or the surrounding objects change their position. This effect is called *small-scale fading*, because even a relatively (with respect to the wavelength) small movement can result in a large change in the signal amplitude. As well as for medium-scale distance fluctuations, due to the random nature of the phenomena involved, even small-scale fading requires statistical models for its characterization. In this case, the most considered fading models for the statistical distribution of the complex attenuations are both the Rayleigh and the Rice models.

**Rayleigh model:** in urban environments it is likely to have no dominant scatterers (there is no LOS between transmitter and receiver)

and, hence, it is reasonable to assume that the receiver observes reflected waves only. When the number of reflected waves is large, according to the central limit theorem, both the components (in-phase and in-quadrature) of the received signal can be expressed as uncorrelated real and jointly Gaussian random processes with zero mean and variance  $\sigma^2$ . In this case, the envelope of the received signal is distributed, at each time instant, according to the Rayleigh statistical model, while its phase obeys a uniform distribution in  $[-\pi, \pi)$ .

**Rice model:** in some propagation environments, such the satellite mobile radio channel or the microcellular one, there are no obstacles along the LOS path between transmitter and receiver. Hence, one can consider to have a dominant scatterer (typically related to the LOS) in addition to many others, whose contributions are approximately equal. This allows one to express the received signal as the sum of a direct wave (LOS component) and a certain number of reflected waves, whose sum represents the so called “scattered component” of the received signal. The direct wave is a stationary, fading-free and constant-amplitude signal, while the reflected waves are independent random signals. When the number of reflected waves is large, again, the components (in-phase and in-quadrature) of the scattered signal can be characterized as real and jointly Gaussian random processes with zero mean and variance  $\sigma^2$ . The scattered component envelope is distributed according to the Rayleigh model while the overall signal<sup>2</sup> has a Rice distributed envelope.

### 1.1.2 Multipath propagation effects and fading types

Multipath propagation is characterized by four main phenomena: **time shift**, **time dispersion**, **frequency shift** and **frequency dispersion**.

Time-domain phenomena are closely related to the different lengths of the paths involved in the propagation and thus to the delays associated to each multipath component. Specifically, besides the time shift due to the propagation delay, when a very short pulse is transmitted over a multipath channel, the receiver observes a train of pulses and, therefore, a signal whose duration is greater than that of the transmitted signal.

---

<sup>2</sup>The overall signal is the sum of the direct component, with constant amplitude, and the scattered component, which is Rayleigh distributed.

With regards to the time dispersion, it is useful to introduce the channel delay spread  $T_m$  (or, equivalently, the channel coherence bandwidth  $B_C \cong 1/T_m$ ) which represents a measure of the time delay between the arrival of the first received multipath component and the last received multipath component associated with a single transmitted pulse.

Frequency-domain phenomena, instead, are mainly due to the time variations in the structure of the medium. Specifically, they are associated to the possible motion either of transmitter, receiver or surrounding objects. This movements produce a frequency shift equals to the Doppler frequency  $f_D$  and a frequency dispersion due to a Doppler spread caused by amplitude modulation. With regards to the frequency dispersion, it is useful to introduce the channel coherence time  $T_C$  (or, equivalently, the Doppler spread  $B_D \cong 1/T_C$ ), which represents a statistical measure of the time in which the fading is correlated.

Given the channel delay spread, the channel coherence time, and the signalling interval  $T_u$  (or, equivalently, the bandwidth  $B_u$ ) of the transmitted signal, two distinctions between fading types can be made. Specifically, with regards to the channel coherence time, the fading is said to be **flat** (or, equivalently, **frequency-nonselctive**) when  $T_m < T_u$ ; otherwise, the fading is **frequency selective**. On the other hand, with regards to the channel delay spread, the fading is said to be **slow** if  $T_C > T_u$ ; otherwise, the fading is **fast**.

### 1.1.3 Narrowband and wideband systems

The signal observed by a receiver in the case of transmission over a multipath channel turns out to be, in general, a distorted version of the transmitted signal. In the case of discrete multipath delays, the general expression of the equivalent low-pass response of the multipath channel at time  $t$  due to an impulse at  $t - \tau$  can be expressed as

$$h(\tau, t) = \sum_{l=0}^{L(t)} \alpha_l(t) e^{-j\phi_l(t)} \delta[\tau - \tau_l(t)]; \quad \phi_l(t) = 2\pi f_c \tau_l(t). \quad (1.5)$$

Therefore, if a bandpass signal

$$s(t) = \text{Re} \left\{ u(t) e^{j2\pi f_c t} \right\}, \quad (1.6)$$

where  $u(t)$  is the equivalent low pass signal for  $s(t)$  (with bandwidth  $B_u$ ) and  $f_c$  is its carrier frequency, is transmitted, the general expression for

the received signal is the following one:

$$r(t) = \text{Re} \left\{ \left[ \sum_{l=0}^{L(t)} \alpha_l(t) e^{-j\phi_l(t)} u[t - \tau_l(t)] \right] e^{j2\pi f_c t} \right\}. \quad (1.7)$$

The impact of multipath on the received signal depends on the product between the multipath delay spread  $T_m$  and the bandwidth of the transmitted signal  $B_u$ . Depending on this product, it is possible to define two different classes of fading models.

The first class is that of the “**narrowband fading models**” and is characterized by the relation  $T_u \gg T_m$ , i.e.,  $B_u T_m \ll 1$ . In this case,  $u[t - \tau_l(t)] \approx u(t)$ , for all  $l$ , the multipath components are not resolvable, and the temporal dispersion is negligible. Thus, the channel impulse response turns out to be

$$h(\tau, t) = \left[ \sum_{l=0}^{L(t)} \alpha_l(t) e^{-j\phi_l(t)} \right] \delta(\tau) \quad (1.8)$$

and the received signal can be expressed as

$$r(t) = \text{Re} \left\{ u(t) e^{j2\pi f_c t} \left[ \sum_{l=0}^{L(t)} \alpha_l(t) e^{-j\phi_l(t)} \right] \right\}. \quad (1.9)$$

which differs from the transmitted one by the complex scale factor in the round brackets. Therefore, the resulting constructive and destructive interference causes narrowband fading of the signal and a negligible time dispersion, which does not introduce *intersymbol interference* (ISI) in digital communications.

The second class, instead, is that of the “**wideband fading models**” and is characterized by the relation  $T_u \ll T_m$ , i.e.,  $B_u T_m \gg 1$ . In this case the approximation  $u[t - \tau_l(t)] \approx u(t)$ , for all  $l$ , is no longer valid, the multipath components are all resolvable and interfere with the subsequently transmitted signals producing ISI. In this case, the general expressions both for the channel impulse response and for the received signal reported, respectively, in (1.5) and (1.7), have to be considered.

## 1.2 Diversity

One of the best solutions to counteract the effects of fading is represented by diversity techniques. When burst of errors occur at the receiver, it means that the channel is in a deep fade and, then, one of the possible solution to improve the performance is to give at the receiver the possibility to have independent replicas of the transmitted signal. A diversity technique, indeed, is any technique by means of which the same signal is allowed to experience statistically independent fading channels. Specifically, if any signal has a probability  $p$  to be faded below a critical threshold, then  $L$  independently fading replicas of the same signal have a probability  $p^L$  to be all faded below that threshold [21]. Therefore, diversity allows one to increase the probability to have at least one replica of the transmitted signal that is above the critical threshold at the receiver end. Some of the ways considered to implement diversity are based on introducing redundancy in time, frequency and space.

**Time diversity:** Time diversity consists in transmitting the same signal, a certain number of times, over successive time slots. To ensure the independence between the channels, time slots have to be spaced at least of a period equal to the channel coherence time  $T_C$ . Indeed, the channel coherence time represents a statistical measure of the time interval in which the fading is correlated. In order to achieve practical time diversity in mobile communication systems, error detecting codes are combined with interleaving techniques. In this case, the time redundancy is introduced by the error detection coding, while the time spacing between the replicas is provided by the interleaving depth. Anyway, since excessive interleaving depth leads to decoding delays, this technique is not effective in the case of very slow fading (when  $T_C \gg T$ ) when interleaving could introduce to significant delays that are not acceptable for real-time applications. Although time diversity does not require increased transmit power, it has the drawback of a spectral efficiency worsening, due to the redundancy introduced in the time domain.

**Frequency diversity:** Frequency diversity is achieved by sending the same message over different carrier frequencies. In order to obtain independent fading channels, an appropriate spacing between the carriers has to be designed. Specifically, the adjacent carrier frequencies have to be separated, at least, by the coherence

bandwidth  $B_C$  of the channel in order to ensure incorrelation between the fading statistics associated to different frequencies. Unlike time diversity, frequency diversity requires additional power at the transmitter. One of the way to achieve frequency diversity is to employ spread-spectrum techniques. Indeed, although this is not equivalent to send the same message over independent fading paths, such techniques provide a kind of frequency diversity by leading to a channel gain that is variable across the bandwidth of the transmitted signal. Spread-spectrum techniques represent modulation methods that are applicable to digitally modulated signals. They have been applied to antijam<sup>3</sup> systems, code-division multiple-access systems and systems designed to counteract the multipath.

**Space diversity:** A notable way to achieve independent fading paths is space diversity. Such a technique is implemented by employing multiple antennas (antenna array) either at the transmitter or at the receiver (or at both sides). The antenna elements constituting the array have to be spatially arranged and physically spaced by a distance necessary to allow the signals to experiment independent fading paths. In general, antenna spacing depends on both the considered frequency range and the propagation environment: typically, a spacing of some wavelengths is sufficient for the scope. Space diversity provides the receiver with signal replicas that represent a space-domain redundancy and, unlike both time and frequency diversity, it does not lead to spectral efficiency losses. Such a characteristic is very attractive for high data-rate wireless systems. Two similar techniques are polarization diversity and angular diversity, which employ, respectively, antenna polarization and angular orientation to generate independent fading paths.

---

<sup>3</sup>Jamming indicates any narrowband interference disturbance

### 1.3 MIMO systems

A wireless system can be labeled as a “MIMO system” if both the transmitter and the receiver nodes are equipped with multiple antennas. MIMO systems represent a standard method to counteract fading by means of spatial diversity without incur in spectral efficiency losses. Therefore, they are, by construction, inherently robust with respect to fading phenomena. Besides the space diversity, MIMO systems can also implement time, frequency or mixed diversity techniques, with the aim to obtain either diversity or capacity gains. A generic MIMO system in which the transmitter and the receiver are equipped, respectively, with  $M_T$  and  $M_R$  antennas is reported in Figure 1.1. Such a system can be

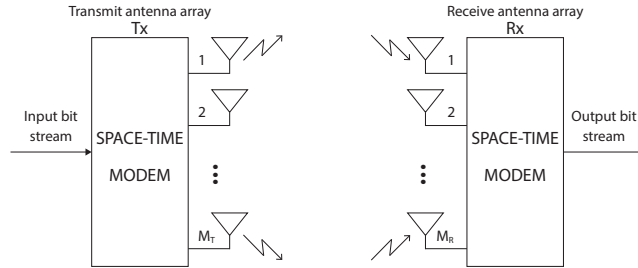


Figure 1.1: MIMO system.

decomposed in a certain number of independent parallel channels (SISO links). To show this, let us consider a MIMO channel characterized by the channel matrix  $\mathbf{H} \in \mathbb{C}^{M_R \times M_T}$ , having rank  $R_H$ . From the matrix theory, every matrix  $\mathbf{H}$  can be decomposed, according to the singular value decomposition (SVD), as

$$\mathbf{H} = \mathbf{U}\mathbf{\Sigma}\mathbf{V}^H \quad (1.10)$$

where  $\mathbf{U} \in \mathbb{C}^{M_R \times M_R}$  and  $\mathbf{V} \in \mathbb{C}^{M_T \times M_T}$  are unitary matrices, while  $\mathbf{\Sigma} \in \mathbb{C}^{M_R \times M_T}$  is a (pseudo) diagonal matrix whose main diagonal entries correspond to the singular values of the channel  $\mathbf{H}$ . Since the rank of a matrix cannot exceed the number of rows and columns, than it straightforward to observe that  $R_H \leq \min(M_T, M_R)$ . In the case of rich scattering environment  $\mathbf{H}$  is of full rank and, hence,  $R_H = \min(M_T, M_R)$ . Parallel decomposition of the channel is obtained by defining a transformation on the channel input and output by means of *transmit precoding*

and *receiver shaping* operations. Specifically, as shown in Fig. 1.2 [20], with transmit precoding the input  $\mathbf{x}$  of the antennas is generated by means of a linear transformation of the input vector  $\tilde{\mathbf{x}}$  as  $\mathbf{x} = \mathbf{V}^H \tilde{\mathbf{x}}$ , while receiver shaping performs a similar operation by elaborating the antenna output as  $\tilde{\mathbf{y}} = \mathbf{U}^H \mathbf{y}$ . In general, multiple antennas can be used

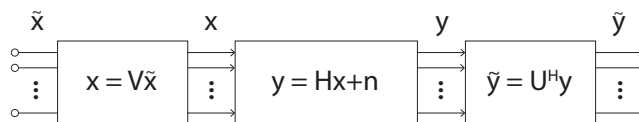


Figure 1.2: Transmit precoding and receiver shaping.

to increase the data rates through **multiplexing** or to improve performance through **diversity** [20]. One of the main MIMO techniques aims at improving power efficiency by maximizing space diversity, and includes delay diversity, space-time block codes (STBCs) and space-time trellis codes (STTCs). Another approach is represented by *layered space-time architectures*, such as the vertical Bell Laboratories layered space-time (V-BLAST) [22, 23] employed to increase capacity. Performance improvements achieved by using MIMO systems are due to four different leverages, which are array gain, diversity gain, spatial multiplexing and interference reduction [24, 25].

### 1.3.1 Array gain

Fig. 1.3 shows a single-input multiple-output (SIMO) system with one transmit antenna and two receive antennas. The receive antennas observe different versions,  $s_1$  and  $s_2$ , of the transmitted signal  $s$ . The signal

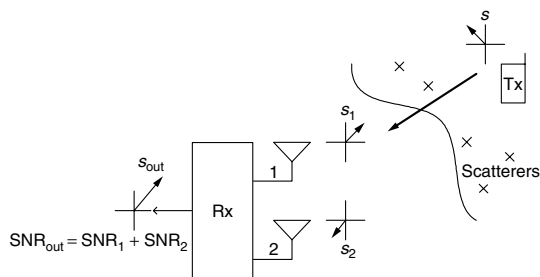


Figure 1.3: Array gain.

version  $s_1$  and  $s_2$  have different amplitudes and phases, both depending on the propagation conditions. If the CSI is known at the receiver, it is possible to apply suitable processing techniques in order to coherently combine  $s_1$  and  $s_2$  to improve the power of the received signal component and, therefore, the signal quality. In this case, the SNR at the output of the combiner equals the sum of the SNRs related to the single links. Obviously, this result can be extended to SIMO systems with more than two receive antennas. In such systems, the average increase of the signal power at the receiver is referred to as *array gain* and is proportional to the number of receive antennas. If the CSI is known at the transmitter, an array gain can also be achieved in systems with multiple transmit antennas (multiple-input single-output - MISO systems) while, if the CSI is known at both the ends of the link, it can also be achieved with multiple antennas at both ends.

### 1.3.2 Diversity gain

In wireless channel the power of the signals changes in the time, frequency and space domains. When the power level goes below a certain threshold, the channel is said to be in fade and, as already seen in the previous section, suitable diversity techniques can be employed to mitigate fading and, therefore, to stabilize the wireless links. In the following, receive and transmit diversity will be briefly described by considering space diversity as a reference diversity system.

Receive diversity is achieved by systems with multiple antennas only at the receiver (SIMO systems). Fig. 1.4 shows a system employing receive diversity. When the signal  $s$  is transmitted, the receive antennas

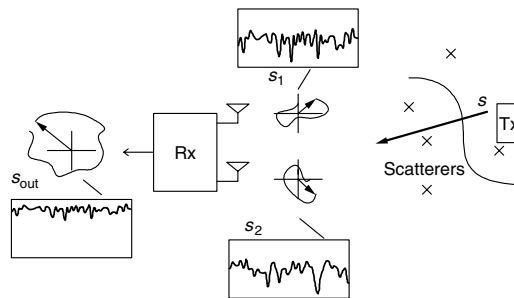


Figure 1.4: Receive diversity.

observe, independently, the fading-corrupted signal transmit versions,  $s_1$  and  $s_2$ . The receiver, then, combine  $s_1$  and  $s_2$ , by means of suitable processing techniques, in order to mitigate the fading effects<sup>4</sup>. The system in Fig. 1.4 has a diversity order of 2: in general, the diversity order equals the number of receive antennas,  $M_R$ , of the SIMO system.

Transmit diversity can be applied to systems with multiple transmit antennas. To achieve diversity with such a system, CSI at the transmitter is not necessarily required, but a suitable shaping of the transmit signal is needed, which can be designed by means, e.g., of space-time coding techniques. A classical example of transmit diversity scheme is represented by the Alamouti's scheme. Fig. 1.5 shows a generic transmit diversity scheme with two transmit antennas and one receive antenna. At the transmitter,  $s$  is subject to a coding scheme whose output is repre-

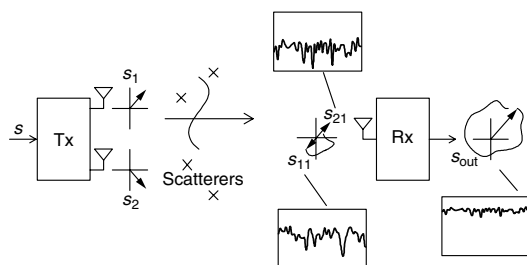


Figure 1.5: Transmit diversity.

sented by the signals  $s_1$  and  $s_2$  to be transmitted over different antennas. At the receiver end, then, suitable processing techniques are employed in order to recover the source signal while mitigating the fading effects. The system in Fig. 1.5 has a diversity order of 2: in general, the diversity order depends on the number of the transmit antennas,  $M_T$ , of the MISO system.

Finally, diversity gain in MIMO systems can be obtained by suitably combining transmit and receive diversity schemes: in general, the diversity order depends on the product  $M_R M_T$  between the number of transmit and receive antennas of the MIMO system.

---

<sup>4</sup>A better degree of fading mitigation can be obtained by considering a larger number of receive antennas.

### 1.3.3 Multiplexing gain

Unlike SIMO and MISO, MIMO systems provide an additional performance gain, called *multiplexing gain*. Such a capacity (in terms of data rates) enhancing leverage results from the fact that a MIMO channel can be decomposed into  $R_H$  parallel independent channels [20] and can be achieved by means of a technique that is called *spatial multiplexing*. Fig. 1.6 shows the basic principle of spatial multiplexing in the case of two transmit antennas and two receive antennas. In this case, the source

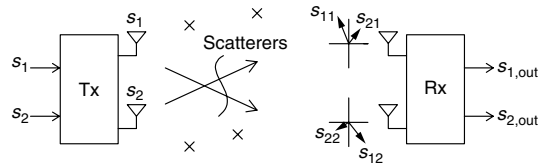


Figure 1.6: Spatial multiplexing.

symbol stream  $s$  is splitted into two substreams (serial-to-parallel conversion) each having half data rate with respect to the source stream. The obtained substreams are, then, modulated to obtain the signals  $s_1$  and  $s_2$  to be transmitted simultaneously by means of two different antennas. In the case of good channel conditions, the spatial representations of these signals,  $[s_{11} \ s_{12}]^T$  e  $[s_{21} \ s_{22}]^T$ , are well separated (ideally orthogonal) at the receive antennas. The receiver can, then, extract the substreams,  $s_1$  and  $s_2$ , to combine them in order to recover the source symbol stream  $s$ .

### 1.3.4 Interference reduction

Co-channel interference is due to the frequency reuse in wireless networks and adds to the noise leading to a serious performance degradation. Fig. 1.7 shows the general concept of interference reduction for a receiver with two antennas. Typically, the desired signal  $s$  and the interference signal  $i$  are characterized by well-separated spatial representations,  $[s_1 \ s_2]^T$  and  $[i_1 \ i_2]^T$ , at the receiver that, in its turn, can exploit the difference between the representations with the aim to reduce the interference and, therefore, improve the signal to interference ratio (SIR). Interference reduction requires the knowledge of the channel related to the desired signal, while the knowledge of the channel related to the in-

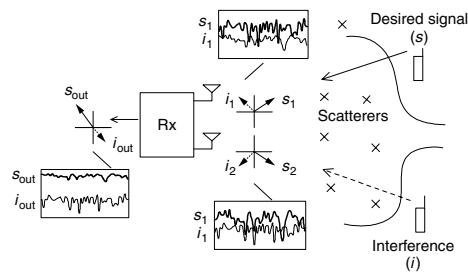


Figure 1.7: Interference reduction.

terfering component is not required. Moreover, interference reduction can also be implemented at the transmitter side and, in general, enables the use of high reuse factors by improving, in this way, network capacity.

## 1.4 OFDM

The idea of multicarrier modulation has been introduced in the late 1950s [26], with the Kineplex system, and used for military scopes. At that time it was not feasible to have orthogonal frequency division multiplexing (OFDM) commercial products because of both the costs and the dimensions of the system<sup>5</sup>. When digital operations, like discrete Fourier transform (DFT), for frequency multiplexing mapping were considered [27, 28], practical implementations became feasible and were, then, introduced in the early 1990s [29]. Multicarrier modulation is employed in many wired and wireless applications, some of which are: digital audio broadcasting (DAB), digital video broadcasting (DVB), asymmetric digital subscriber line (ADSL), wireless local area network (WLAN), Worldwide Interoperability for Microwave Access (WiMAX), and LTE-A. OFDM turns out to be also a good candidate for the 5G radio interface. With regards to the wireless communications, the widespread use of OFDM is mainly due to its capacity in mitigating the fading effects when considering wideband systems. Indeed, because of the ever increasing request of wideband services, the ratio between the signal bandwidths and the channel coherence bandwidth has led to an increasing concern about ISI problems. The basic idea of OFDM is to provide a kind of frequency diversity by splitting the information stream, whose bandwidth is likely

<sup>5</sup>Kineplex multiplexers were totally implemented with analogic technologies.

to exceed the channel coherence bandwidth  $B_C$ , into a certain number of substreams, each of which having a bandwidth smaller than  $B_C$  and modulating carriers at different frequencies. The idea is, therefore, to break a wideband channel into multiple parallel narrowband channels by means of an orthogonal channel partition [20]. The spectrum of the OFDM signal is similar to that obtained with frequency division multiplexing (FDM) but, as shown in Fig. 1.8, the OFDM substreams are allowed to be partially overlapped in frequency (of about 50%). OFDM

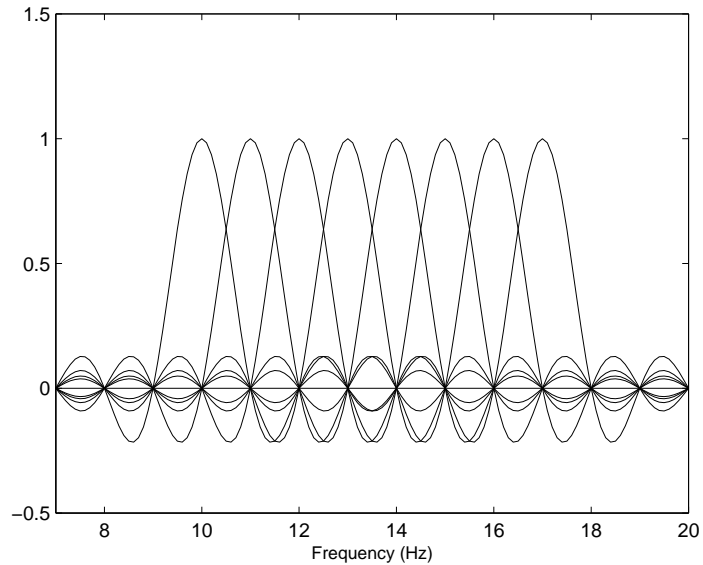


Figure 1.8: OFDM subcarriers overlapping for rectangular pulses.

spectrum is given by the envelope of the cardinal sine (*sinc*) functions shown in figure, each of which representing a subcarrier at a specified frequency. This partial overlapping ensure a better spectral efficiency at the price of time and frequency orthogonality constraints. The number of subcarriers is related to the need to allow each subchannel to have a bandwidth contained in  $B_C$ , in such a way to have near-flat fading and mitigated ISI. Moreover, it can be shown that subcarrier spacing  $\Delta f$  has to be chosen as  $\Delta f = k/T$ , with  $k \in \mathbb{N}$ , where  $T$  represents the symbol period.

### 1.4.1 OFDM analog implementation

A generic analog OFDM implementation scheme is shown in Fig. 1.9 and Fig. 1.10 [30], which report, respectively, the multicarrier transmitter and the multicarrier receiver block diagrams. With regard to the transmitter side, the first operation to perform is a serial-to-parallel (S/P) conversion of the input binary symbols  $d(n)$  with bit rate  $R_b$ . By denoting with  $T$  ( $T \gg T_b$ ) the symbol period, the S/P conversion can be performed by means of a buffer which stores  $B = R_b T$  bit during the  $n$ -th symbol interval  $[nT, (n+1)T]$ ,  $n \in \mathbb{Z}$ . At the buffer output, therefore, there is a vector  $\mathbf{d}(n) \triangleq [d_0(n), d_1(n), \dots, d_{B-1}(n)]^T$ , whose generic entry is  $d_i(n) \triangleq d(nB + i)$ ,  $i = 0, 1, \dots, B-1$ . It is worth noting that the buffer output rate turns out to be  $R = R_b/B$ . By indicating with  $M$  the number of subcarriers, the  $B$ -dimensional vector  $\mathbf{d}(n)$  is, then processed by an encoder whose output is an  $M$ -dimensional ( $M \leq B$ ) vector  $\mathbf{a}(n) = [a_0(n), a_1(n), \dots, a_{M-1}(n)]^T$ . Finally, the entries of  $\mathbf{a}(n)$  are transmitted over different subcarriers. In the case of linear modulation, the multichannel frame related to the considered symbol interval,  $[nT, (n+1)T]$ , can be written as:

$$f_n(t) = \sum_{i=0}^{M-1} a_i(n) p_i(t - nT) \quad (1.11)$$

where  $\{p_i(t)\}_{i=0}^{M-1}$ , represents a class of functions satisfying the following time and frequency biorthogonality (in time and frequency domains) condition:

$$\langle p_k(t - mT), p_i(t - nT) \rangle = \delta_{k-i} \delta_{m-n}, \quad (1.12)$$

where  $i, k \in \{0, 1, \dots, M-1\}$  and  $n, m \in \mathbb{Z}$  are, respectively, subcarrier and temporal indexes. A possible choice for a class of functions satisfying biorthogonality and, consequently, unitary norm conditions, is the following:

$$p_i(t) = T^{-\frac{1}{2}} \text{rect} \left[ \frac{t - (n + 0.5)T}{T} \right] e^{\frac{j2\pi it}{T}}; \quad i \in \{0, 1, \dots, M-1\}, n \in \mathbb{Z}. \quad (1.13)$$

The transmitted signal, denoted by  $x(t)$ , can be expressed as

$$x(t) = \sum_{n=-\infty}^{\infty} f_n(t) = \sum_{n=-\infty}^{\infty} \sum_{i=0}^{M-1} a_i(n) p_i(t - nT). \quad (1.14)$$

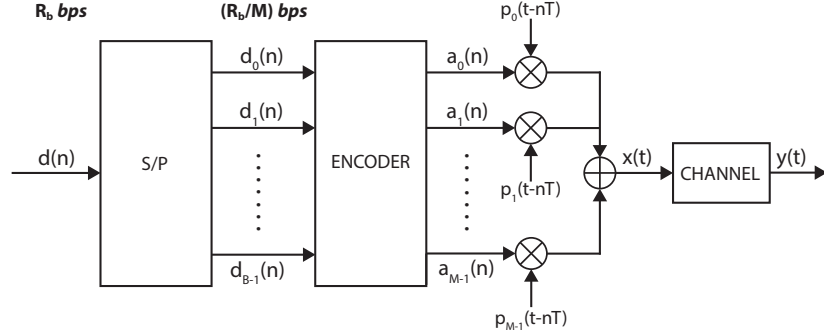


Figure 1.9: OFDM analog implementation - transmitter side.

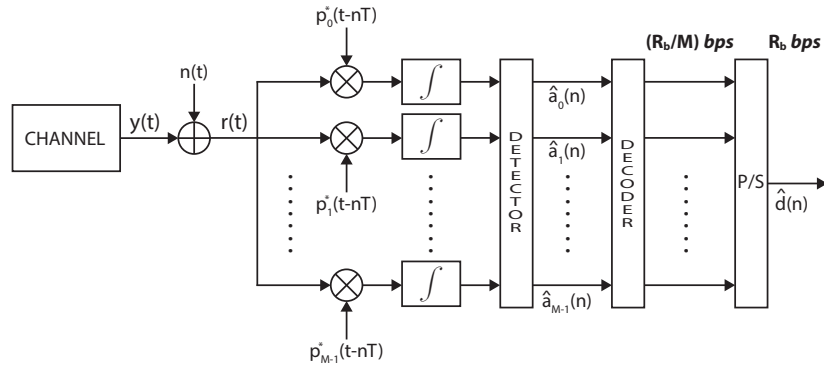


Figure 1.10: OFDM analog implementation - receiver side.

By assuming propagation over a linear time-invariant channel  $h(t)$  corrupted by additive white Gaussian noise (AWGN), the received signal is

$$r(t) = y(t) + n(t), \quad (1.15)$$

where  $y(t)$  is the channel output [convolution between  $x(t)$  and the channel impulse response  $h(t)$ ] and  $n(t)$  is an AWGN random process.

At the receiver end,  $r(t)$  is projected over the  $M$  basis functions and, thus, demodulation is carried out by means of correlators. At this point, the demodulator outputs are subject to detection. Finally, the transmit symbol estimates  $\hat{a}_i(n), \forall i \in \{0, 1, \dots, M-1\}$ , are processed by the decoder and the parallel-to-serial (P/S) converter in order to obtain an estimate  $\hat{d}(n)$  of the source bit stream  $d(n)$ .

### 1.4.2 OFDM digital implementation

The generic OFDM digital implementation with DFT is shown in Fig. 1.11 and Fig. 1.12 [20], from which it is worth observing the duality between

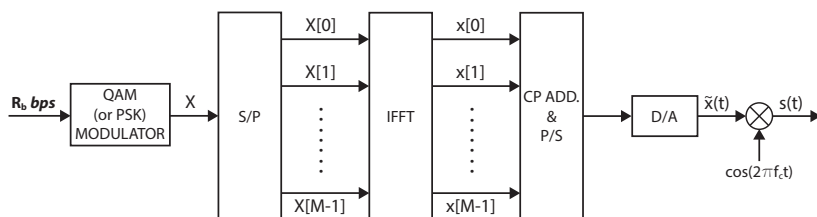


Figure 1.11: Digital OFDM implementation - transmitter side.

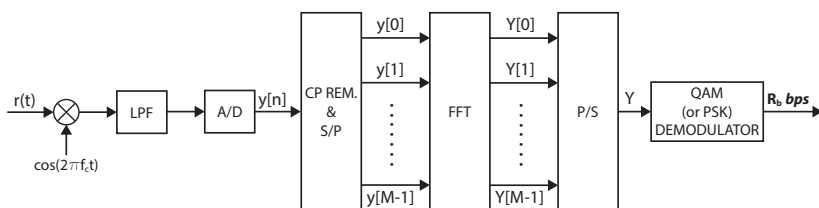


Figure 1.12: Digital OFDM implementation - receiver side.

transmitter and receiver processings [20].

#### Transmitter processing

Hereinafter, the discussion will be related to a single, i.e., the  $n$ -th, OFDM symbol. The source data stream is digitally modulated, according to either a quadrature amplitude modulation (QAM) or a phase shift keying (PSK) format, to obtain the modulated symbol stream  $X[m]$ ,  $0 \leq m \leq M - 1$ , which feeds an S/P converter. The S/P converter output symbols represent the discrete frequency components of the OFDM modulator output,  $s(t)$ . Therefore, the first operation needed to generate  $s(t)$  is to convert the frequency components in time components by means of an  $M$ -point inverse discrete Fourier transform (IDFT) performed with inverse fast Fourier transform (IFFT) algorithms. At the output of the IFFT, the time-domain OFDM symbol is represented by

$x[m]$ ,  $0 \leq m \leq M - 1$ , where

$$x[m] = \frac{1}{\sqrt{M}} \sum_{i=0}^{M-1} s(i) e^{j \frac{2\pi i m}{M}}; \quad m = 0, 1, \dots, M - 1 \quad (1.16)$$

At this point the cyclic prefix is added to the OFDM symbol in order to obtain the new length- $(M + \mu)$  sequence  $\tilde{x}[m]$ ,  $0 \leq m \leq M + \mu - 1$ . After CP insertion, the samples of the sequence  $\tilde{x}[m]$ ,  $0 \leq m \leq M + \mu - 1$  are, then, serialized by means of a P/S converter and processed by a digital-to-analog (D/A) converter, whose output represents the base-band OFDM signal  $\tilde{x}(t)$ . Finally, this OFDM signal will modulate a carrier at a frequency  $f_c$  in order to generate the signal  $s(t)$  to be transmitted.

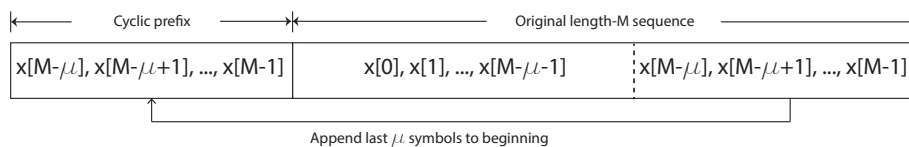
### Cyclic prefix

To understand what the cyclic prefix is and why it is employed in OFDM modulation, some considerations on the input-output relationship of the channel are useful. It is well known that, in the case of discrete-time systems, the output of a channel is obtained as the discrete-time linear convolution between the channel input and the channel impulse response. If, however, one considers the circular convolution, then the channel input could be recovered at the receiver by performing the IDFT of the ratio between the DFT of the channel output and the DFT of the channel impulse response. Anyway since, as already said, the input-output relationship of the channel is given by the linear convolution, it is useful to find a way to make sure that the receiver “see” the convolution as circular. The way to do this is to introduce the *cyclic prefix*.

Let us consider an  $M$ -sequence  $x[m]$ ,  $0 \leq m \leq M - 1$ , and a discrete-time channel with finite impulse response (FIR)  $h[m]$ ,  $0 \leq m \leq \mu - 1$ , where  $\mu + 1 = \lceil T_m/T_s \rceil = L_h$ <sup>6</sup>. The cyclic prefix (CP) for the  $M$ -sequence  $x[m]$ ,  $0 \leq m \leq M - 1$ , is defined as  $\{x[M - \mu], x[M - (\mu - 1)], \dots, x[M - 1]\}$  and, therefore, as the last  $\mu$  entries of the sequence  $x[m]$ ,  $0 \leq m \leq M - 1$ . For each input  $M$ -sequence, the related cyclic prefix is appended at the beginning of the sequence in order to obtain a new one which is denoted by  $\tilde{x}[m]$ ,  $-\mu \leq m \leq M - 1$ , and is called

---

<sup>6</sup> $L_h$  represents the channel memory and is defined as the ceiling of the ratio between the channel delay spread (FIR channel duration) and the sampling period of the discrete time sequence.

Figure 1.13: Cyclic prefix of length  $\mu$ .

*extended sequence.* This new sequence has size  $M + \mu$  and is defined as  $\{\tilde{x}[-\mu], \dots, \tilde{x}[M - 1]\} = \{x[M - \mu], \dots, x[M - 1], x[0], \dots, x[M - 1]\}$ . This CP definition allows to state that, for  $0 \leq k \leq \mu$ ,  $\tilde{x}[m - k] = x[m - k]_{\text{M}}$ ,<sup>7</sup> for  $0 \leq m \leq M - 1$ . Then, if  $\tilde{x}[m]$ ,  $-\mu \leq m \leq M - 1$ , is the input of a discrete time channel with impulse response  $h[m]$ ,  $0 \leq m \leq \mu - 1$ , the output  $y[m]$ ,  $-\mu \leq m \leq M - 1$ , is given by

$$\begin{aligned}
 y[m] &= \tilde{x}[m] * h[m] \\
 &= \sum_{k=0}^{\mu-1} h[k] \tilde{x}[m - k] = \sum_{k=0}^{\mu-1} h[k] x[m - k]_{\text{M}} \\
 &= x[m] \circledast h[m], \tag{1.17}
 \end{aligned}$$

where  $\circledast$  is the circular convolution operator and the third equality follows from  $\tilde{x}[m - k] = x[m - k]_{\text{M}}$ .

Therefore, by appending the CP at the beginning of the input sequence, linear convolution becomes circular. Moreover, if the channel output DFT is performed, in the free-noise case, the following relation is obtained:

$$\begin{aligned}
 \text{DFT}\{y[m] = x[m] \circledast h[m]\} &= Y[i] = X[i] H[i] = \\
 &= \text{DFT}\{x[m]\} \text{DFT}\{h[m]\}; \tag{1.18}
 \end{aligned}$$

where  $0 \leq m, i \leq M - 1$  and the input sequence  $x[m]$ ,  $0 \leq m \leq M - 1$ , can be obtained as

$$\begin{aligned}
 x[m] &= \text{IDFT}\{Y[i]/H[i]\} = \\
 &= \text{IDFT}\{\text{DFT}\{y[m]\}/\text{DFT}\{h[m]\}\}, \tag{1.19}
 \end{aligned}$$

<sup>7</sup> $[m - k]_{\text{M}}$  means  $[m - k]$  modulo  $M$ . Therefore, given a sequence  $x[m - k]$ ,  $x[m - k]_{\text{M}}$  turns out to be a periodic version of  $x[m - k]$  with period  $M$ .

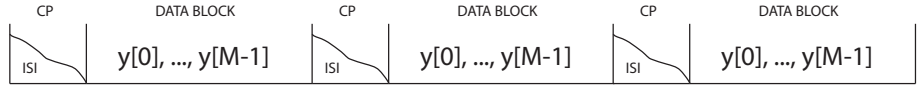


Figure 1.14: ISI between data block in channel output.

if  $h[m]$ ,  $0 \leq m \leq \mu$ , is known at the receiver side.

It is worth noting that  $y[m]$ ,  $-\mu \leq m \leq M-1$ , has size  $M + \mu$  and that in (1.19) the first  $\mu$  samples,  $\{y[-\mu], \dots, y[-1]\}$ , are not necessary to recover  $x[m]$ ,  $0 \leq m \leq M-1$ , since they represent redundancy associated to the CP. By supposing that the channel input  $x[m]$ ,  $0 \leq m \leq M-1$ , is broken into data blocks of size  $M$ , each having the CP at the beginning in order to obtain the sequence  $\tilde{x}[m]$ ,  $-\mu \leq m \leq M-1$ , then the first  $\mu$  samples of  $y[m] = h[m] * \tilde{x}[m]$ , in every block, are corrupted by ISI as shown in Fig. 1.14 [20]. CP insertion is crucial to create a suitable edge between adjacent data blocks and, hence, provide a way to mitigate ISI by simply removing it from each data block. In continuous time, this is equivalent to insert a guard band of duration  $T_g$  (greater or equal to the channel delay spread  $T_m$ ) after each block of  $M$  symbols, of duration  $MT_s$ . The benefits achieved thanks to the CP insertion comes at a cost that can be summarized as follows:

1. since the CP has size  $\mu$ , it implies an overhead of  $\mu/M$  which results in a data rate reduction of  $M/(\mu + M)$ ;
2. power inefficiency due to the transmission of the necessary overhead.

In order not to suffer for the second drawback, it is possible to design the CP as an all-zero prefix (zero-padded OFDM) [20].

### Receiver processing

The signal  $s(t)$  will be filtered by the channel impulse response  $h(t)$  and corrupted by additive noise. The signal at the input of the receiver is

$$y(t) = s(t) * h(t) + n(t),$$

where  $*$  is the linear convolution operator.

The received signal is downconverted to baseband and low-pass filtered in order to remove the high frequency components (double frequency). Then, the analog-to-digital (A/D) converter samples its input to obtain

$$y[m] = \tilde{x}[m] * h[m] + \nu[m]; \quad -\mu \leq m \leq M - 1.$$

At this point the first  $\mu$  samples of  $y[m]$ , which represents the CP, are removed. Thanks to the CP removal, before the S/P conversion there are  $M$  time samples whose DFT, in the noise-free case, can be written as  $Y[i] = H[i] X[i]$ . These time samples, then, feed the S/P converter and, after, the fast Fourier transform (FFT) device. The output of the FFT turns out to be a scaled version of the original symbols  $H[i] X[i]$ <sup>8</sup> and feeds the P/S converter and the QAM (or PSK) demodulator in order to recover the information.

OFDM systems decompose the wideband channel in a set of narrowband subchannels, each of which transmitting one of the QAM (or PSK) symbols. Unlike other techniques (e.g., *vector coding*), such a decomposition does not require the knowledge, at the transmitter, of the channel gains  $H[i]$ , for  $i = 0, \dots, M - 1$ .

## 1.5 Cooperative approaches

Cooperative approaches represent a relatively new class of protocols in which, unlike the *direct* (*single-user* or *point-to-point*) communication, the transmission from a source device  $S$  to a destination device  $D$  is supported at least by another terminal (called a *relay*) willing to help the communication. Cooperative communication schemes can be considered both to improve the data rates and to improve the performance, in terms of bit error rate (BER), for a given transmission rate. When cooperative communication is used primarily to leverage the spatial diversity with the aim to improve the communication reliability, the resulting cooperative approach is referred to as *cooperative diversity*.

### 1.5.1 Relaying models and protocols

The basics of cooperative communications date back to the late 1960s and early 1970s [9, 10], when E.C. Van Der Meulen introduced the so-called *relay channel* and derived upper and lower bounds on its capacity. The relay channel is a three single-antenna terminal communication channel like the one shown in Fig. 1.15. Based on this simple scheme, in

---

<sup>8</sup> $H[i] = H(f_i)$  represents the channel (affected by flat-fading) gain associated to the  $i$ -th subcarrier.

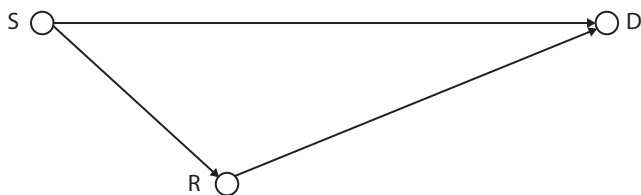


Figure 1.15: Three-terminal relay channel.

general, the information is relayed in two *phases* (or *modes*)<sup>9</sup>: the first one, when  $S$  transmit and  $(R, D)$  receive, is called **broadcast phase**; the second one, when  $(S, R)$  transmit and  $D$  receives is called **multiple access** (MAC) , or **relaying, phase**. By starting from this simple and general scheme, four different relaying models can be introduced [31]: these models are reported in compact way in Table 1.1.

Table 1.1: Relaying models

#	phase 1	phase 2	short description
1	$S \rightarrow (R, D)$	$(S, R) \rightarrow D$	most general form of relaying
2	$S \rightarrow R$	$(S, R) \rightarrow D$	$D$ ignores signal from $S$ in first mode
3	$S \rightarrow (R, D)$	$R \rightarrow D$	$S$ does not transmit in second mode
4	$S \rightarrow R$	$R \rightarrow D$	multi-hop communication

Among these models, the first one is the most general, while the last one is the oldest as well as simplest way to implement relaying. Moreover, unlike the other three, multi-hop communication model does not yield diversity benefits, and it is mainly employed to counteract power decay (path-loss) in long-range transmissions and, therefore, to allow communication between network nodes that are not in the coverage range of each other. Besides the distinction made according to the two relaying phases, another classification can be carried out based on orthogonality properties of the relaying. Specifically, if transmitted and received signals turns out to be orthogonal (in some sense), relaying is said to be **orthogonal**; otherwise, relaying is said to be **non-orthogonal**<sup>10</sup>. Or-

<sup>9</sup>The terms *phase* and *mode* do not indicate a temporal sequence of events but only represent a conceptual way to describe how, in general, the information sent by  $S$  can reach  $D$  with the help of  $R$ . Different time scheduling of these phases can be, then, considered.

<sup>10</sup>Similarly, the concept of orthogonality can be associated directly to the relay

thogonality properties between transmitted and received signals can be referred either to the time domain, to the frequency domain, or in the joint time-frequency domain (biorthogonality). A further classification about cooperative communication can be made according to the way in which the source and relay nodes can share their resources to achieve the highest performance improvement. In this sense, cooperation strategies based on resource sharing result in different *relay protocols*. There exist different strategies that relays can adopt, two of which are mainly employed in practice. The first strategy is known as ***decode and forward*** (DF) and the second is called ***amplify and forward*** (AF). As suggested by its name, in DF protocols, the relay decodes the signal transmitted from the source before forwarding it towards the destination. On the other hand, in AF protocols, the relays scale up or down (according to some power constraint) the received signal before retransmission.

---

nodes rather than to the relaying mechanism. In this case, the distinction turns out to be made between orthogonal and non-orthogonal relays.



## Chapter 2

# Performance analysis and optimization of MIMO cooperative multiple-relay communications in Gaussian noise

This chapter deals with analysis and optimization of Multiple-Input Multiple-Output (MIMO) cooperative networks, employing multiple amplify-and-forward (AF) relays. In such networks, the availability of channel state information (CSI) at the cooperating nodes is crucial to fully exploit the spatial diversity arising from the presence of the relays. On the other hand, the use of linear equalization structures at the destination is important to avoid unaffordable computational complexity. When the source and the relays have no CSI, channel-independent precoding strategy can be employed at the source and at the destination. In this case, a performance analysis of the cooperative network has been performed in order to enlighten potential gains with respect to a direct transmission (i.e., without recruiting relays), by considering at the destination zero-forcing (ZF) and minimum mean square error (MMSE) equalization criteria. It has been shown that, when the source and the relays have no CSI at all, the diversity order is independent of the number of cooperating nodes and, compared to a direct communication, a signifi-

cant coding gain can be achieved only if the positions of the relays are carefully planned. To achieve an additional gain in terms of diversity order, CSI at the source and at the relays is needed. In this case, the main problem is the design of optimal precoding strategies, which can be (approximatively) implemented in closed form with a manageable computational complexity. In this respect, a closed-form optimization design has been developed in the case of multiple MIMO orthogonal-frequency division multiplexing (OFDM) relays, operating over frequency selective channels, which ensures a performance gains in terms of both diversity order and coding gain.

## 2.1 Introduction

In fading channels, the use of MIMO systems is a well-known approach to achieve diversity and/or multiplexing gains [32]. In recent years, a significant attention has also been devoted to cooperative diversity techniques [33, 34], due to their ability to improve coverage and quality of service through relaying, both in infrastructure-based [35, 36] and *ad-hoc* [37–39] wireless networks. Cooperative schemes can be conveniently adopted in MIMO systems, in order to further improve their diversity and/or multiplexing gains [40]. The most considered relaying protocols in the literature are decode-and-forward and amplify-and-forward (AF): in the former one, the relays decode, re-encode, and retransmit the source messages; in the latter one, the relays simply scale the received signal according to a power constraint and forward it to the destination. However, among the cooperative techniques [41], the AF relaying protocol allows one to gain most of the benefits of cooperation without a significant increase in system complexity [42–44] and, therefore, this relaying strategy has gained recently a lot of attention. According to a multi-hop communication model (see model 4 of Table 1.1), the relays receive data from the source during the first time slot (*first hop*), and forward an amplified version of the received signal during the second time slot (*second hop*), while the source remains silent. Moreover, albeit suboptimal, linear designs of cooperative MIMO transceivers have received a great deal of attention [45–49], since they offer a good trade-off between performance and complexity.

Although the aforementioned designs allow one to keep computational requirements low, they require that full CSI about the first and

second hops of the MIMO cooperative transmission are known to all the cooperating nodes: in practice, acquisition of such a large amount of CSI might lead to an unsustainable waste of communication resources, especially in cooperative networks with multiple MIMO relays. According to these drawbacks, all the works [45–49] and the related theoretical performance analyses [50–53] deal only with the single-relay case.

With reference to cooperative MIMO systems employing a single AF relay, performance analysis and optimization of source precoding and relaying matrices have been tackled in several papers (see e.g. [48] and references therein), under the assumption that both source and relay have complete CSI, and considering different design criteria, such as, e.g., maximization of the source-destination mutual information, minimization of the mean-square error (MSE) or maximization of the signal-to-interference-plus-noise ratio (SINR) at the destination.

Both performance analysis and optimization are much more challenging when the cooperative network encompasses multiple relays. Performance analysis of a MIMO-OFDM network with multiple relays, in terms of error probability, has been considered in [54], with reference to a system employing non-optimized relay matrices (so called *non coherent* or “naive” AF relaying) and zero-forcing (ZF) equalization at the destination. However, it is known [55] that, in order to fully exploit the benefits of distributed MIMO diversity, full CSI at the relays is required and the relaying matrices must be optimized in order to allow for *coherent* combining of the relayed signals at the destination.

Acquisition of complete and reliable CSI in a multiple-relay network can represent a challenging task, especially in rapidly changing channels. Several algorithms for channel estimation in AF relay systems are available in literature. In [56] and [57], the estimation of both the source-relay and relay-destination channels is performed resorting to pilot-based schemes. As regards to CSI acquisition at the transmitter, one viable solution consists in exploiting the possible channel reciprocity between the forward and reverse link; an alternative approach relies on forwarding the (possibly quantized [58]) CSI acquired at the destination to the source over a reliable feedback link.

Recently, the multiple-relay optimization problem has been tackled in [59], under the MMSE criterion and assuming either weighted sum power constraint or per-relay power constraint. A similar optimization scenario is considered in [60], where the power constraint is enforced at

the destination rather than at the relays.

## 2.2 General network model

Throughout this chapter, a MIMO cooperative multiple-relay network composed by a source, a destination and  $N_C$  relay nodes is considered, where it is assumed to be no direct link between source and destination, and thus communication takes place through a set of intermediate AF relay nodes. In addition, there is no relay-to-relay communication. Therefore, we consider a dual-hop communication relaying protocol (see Tab. 1.1 in Subsec. 1.5.1 of Ch. 1) in which the relay nodes, after performing a linear processing (typical of the AF protocols) on the received source signal, forward it to the destination in the relaying phase. Moreover, non-orthogonal and half-duplex relay nodes are employed so that, respectively, they operate within the same frequency band and cannot transmit and receive simultaneously. The general network topology is represented in Fig. 2.1, in which the positions of the  $N_C$  relay nodes are

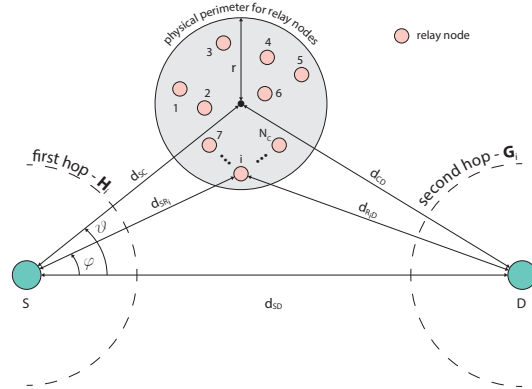


Figure 2.1: General topology.

randomly chosen within the circle of radius  $r$  whose center is identified by the couple of polar coordinates  $(d_{SC}, \theta)$ , taken with respect to the source node  $S$  which, in this regard, plays the role of the origin of the polar coordinate system. All the nodes are equipped with multiple antennas, with the number of antennas at source, relays, and destination denoted by  $N_S$ ,  $N_R$ , and  $N_D$ , respectively, and spatial multiplexing transmission is employed. Communications supported by the network insist across

a frequency-flat quasi-static Rayleigh fading channel and the received signals are affected by a Gaussian distributed thermal noise.

Since the processing of the considered system is on a symbol-by-symbol basis, for the sake of notation simplicity, we avoid indicating the functional dependence on the  $k$ -th symbol interval ( $k \in \mathbb{Z}$ ) in all the following derivations.

### Source processing

The signal transmitted by S during the first time slot is denoted by  $\mathbf{s} \in \mathbb{C}^{N_B}$ , where  $N_B \leq N_S$ , which satisfies assumption **(a1)** (see the assumptions section). The symbol block  $\mathbf{s}$  is processed by a *full-column rank* precoding matrix  $\mathbf{F}_0 \in \mathbb{C}^{N_S \times N_B}$ , thus obtaining  $\tilde{\mathbf{s}} = \mathbf{F}_0 \mathbf{s} \in \mathbb{C}^{N_S}$ .

### $i$ -th relay processing

The received signal at the  $i$ -th relay, during the second time slot, is given by  $\mathbf{z}_i = \mathbf{H}_i \tilde{\mathbf{s}} + \mathbf{w}_i$ , where  $\mathbf{H}_i \in \mathbb{C}^{N_R \times N_S}$  represents the  $i$ -th *first-hop* (i.e., between the source and the  $i$ -th relay) MIMO channel,<sup>1</sup> and  $\mathbf{w}_i \in \mathbb{C}^{N_R}$  accounts for noise. At the relay nodes, assumptions **(a2)** and **(a3)** hold (see the assumptions section). Specifically, the variance of the entries of the matrix  $\mathbf{H}_i, \forall i$ , is defined as  $\sigma_{h,i}^2 \triangleq (d_{SD}/d_{SR_i})^\eta$ , where  $d_{SD}$  is the distance between the source and the destination,  $d_{SR_i}$  is the distance between the source and the  $i$ -th relay node, and  $\eta \geq 2$  represents the path loss exponent. The vector  $\mathbf{z}_i \in \mathbb{C}^{N_R}$  is scaled by  $\sqrt{\alpha_i}$  and processed by a forwarding matrix  $\mathbf{F}_i \in \mathbb{C}^{N_R \times N_R}$ , hence yielding

$$\begin{aligned} \tilde{\mathbf{z}}_i &\triangleq \sqrt{\alpha_i} \mathbf{F}_i \mathbf{z}_i = \sqrt{\alpha_i} \mathbf{F}_i (\mathbf{H}_i \tilde{\mathbf{s}} + \mathbf{w}_i) \\ &= \sqrt{\alpha_i} \mathbf{F}_i \mathbf{H}_i \mathbf{F}_0 \mathbf{s} + \sqrt{\alpha_i} \mathbf{F}_i \mathbf{w}_i \in \mathbb{C}^{N_R}, \end{aligned} \quad (2.1)$$

### Destination processing

At the destination, the received signal can be expressed as  $\mathbf{r} = \mathbf{C} \mathbf{s} + \mathbf{v}$ , with

$$\mathbf{C} \triangleq \left[ \sum_{i=1}^{N_C} \sqrt{\alpha_i} \mathbf{G}_i \mathbf{F}_i \mathbf{H}_i \right] \mathbf{F}_0 \in \mathbb{C}^{N_D \times N_B} \quad (2.2)$$

---

<sup>1</sup>This channel is also referred to as *backward* or *broadcast* channel.

$$\mathbf{v} \triangleq \sum_{i=1}^{N_C} \sqrt{\alpha_i} \mathbf{G}_i \mathbf{F}_i \mathbf{w}_i + \mathbf{d} \in \mathbb{C}^{N_D} \quad (2.3)$$

denoting the overall non-Gaussian dual-hop channel matrix and the effective noise at the destination, respectively, where  $\mathbf{G}_i \in \mathbb{C}^{N_D \times N_R}$  represents the  $i$ -th *second-hop* (i.e., between the  $i$ -th relay and the destination) MIMO channel matrix,<sup>2</sup> whereas  $\mathbf{d} \in \mathbb{C}^{N_D}$  is the thermal noise vector at the destination. Assumptions **(a4)**, **(a5)** and **(a6)** (see the assumptions section) hold at the receiver end where, similarly to the backward channels, the variance of the entries of the matrix  $\mathbf{G}_i, \forall i$ , is defined as  $\sigma_{g,i}^2 \triangleq (d_{SD}/d_{R_iD})^\eta$ , where  $d_{R_iD}$  is the distance between the  $i$ -th relay and the destination.

In the following two sections, a performance analysis of a cooperative system is carried out under the assumption that no CSI is available at the cooperative transmitters. On the other hand, in the last section, CSI is exploited at the source and relays to design optimal precoding strategies.

---

<sup>2</sup>This channel is also referred to as *forward* or *MAC* channel.

## 2.3 Case 1: Naive cooperation with ZF equalization

In this first case, we consider the performance analysis, in terms of symbol error probability (SEP), of a cooperative system, where multiple MIMO AF relays simultaneously transmit in the second hop, and the destination adopts linear ZF equalization. To avoid incurring in significant signaling overhead, a *non-coherent* [40, 61, 62] or *blind* [63] relaying system is considered, where CSI is not available at the source and relays. Although noncoherent relaying simplifies the analysis, since precoding at the source and relays does not depend on the channel coefficients, there are two additional problems with respect to single-relay theoretical studies [50–53]: (i) the correlation between noise samples at the destination, due to the simultaneous relay transmissions; (ii) the different locations of the relays, which imply different variances of the fading channel coefficients. Relying on the strong law of large numbers [64] and on properties of the linear combination of Wishart matrices with unequal covariances [65], we develop an approximation of the noise correlation matrix that allows us to derive an accurate yet simple approximation of the SEP in the high-SNR regime, for an arbitrary number and locations of relays. According to [61], we show that noncoherent schemes cannot achieve distributed spatial diversity, but only coding and multiplexing gain. Additionally, by specializing our results in the case of a *relaying cluster*, for which the distances between the different relays are negligible with respect to the distance between the source and the destination, we discuss the placement of the cluster that maximizes the coding gain and, moreover, we present a comparison between cooperative and direct transmissions.

### 2.3.1 System model and basic assumptions

We consider the network of Fig. 2.1 in which source and destination cannot communicate directly due to large shadowing effects. All nodes are perfectly synchronized and  $\mathbf{H}_i \in \mathbb{C}^{N_R \times N_S}$  and  $\mathbf{G}_i \in \mathbb{C}^{N_D \times N_R}$  denote the first- and second-hop MIMO channels, respectively, for  $i \in \{1, 2, \dots, N_C\}$ . Instantaneous CSI is known only at the destination via training, but is unknown at both the source and relays [40, 61–63].

The source symbol block  $\mathbf{s}$ , satisfying assumption (a1) (see the assumptions section), is processed by a full-column rank precoding matrix

$\mathbf{F}_0 \in \mathbb{C}^{N_s \times N_B}$ , thus obtaining  $\tilde{\mathbf{s}} = \mathbf{F}_0 \mathbf{s} \in \mathbb{C}^{N_s}$ , with  $\text{tr}(\mathbf{F}_0^H \mathbf{F}_0) = 1$ , which ensures that  $\mathbb{E}[\|\tilde{\mathbf{s}}\|^2] = 1$ . At the  $i$ th relay, the vector  $\mathbf{z}_i$  is scaled by  $\sqrt{\alpha_i}$  and processed by a nonsingular forwarding matrix  $\mathbf{F}_i \in \mathbb{C}^{N_R \times N_R}$ , hence yielding  $\tilde{\mathbf{z}}_i \triangleq \sqrt{\alpha_i} \mathbf{F}_i \mathbf{z}_i \in \mathbb{C}^{N_R}$ , with  $\text{tr}(\mathbf{F}_i^H \mathbf{F}_i) = N_R$ . Although the signal at the destination is given by the general model of Sec. 2.2, for the sake of convenience, in the following the main equations are reported again:

$$\mathbf{r} = \mathbf{C} \mathbf{s} + \mathbf{v} \quad (2.4)$$

$$\mathbf{C} \triangleq \left[ \sum_{i=1}^{N_C} \sqrt{\alpha_i} \mathbf{G}_i \mathbf{F}_i \mathbf{H}_i \right] \mathbf{F}_0 \in \mathbb{C}^{N_D \times N_B} \quad (2.5)$$

$$\mathbf{v} \triangleq \sum_{i=1}^{N_C} \sqrt{\alpha_i} \mathbf{G}_i \mathbf{F}_i \mathbf{w}_i + \mathbf{d} \in \mathbb{C}^{N_D} \quad (2.6)$$

where, again,  $\mathbf{r}$  represents the signal received by the destination node,  $\mathbf{C}$  denotes the dual-hop channel matrix, and  $\mathbf{v}$  the overall noise at the destination, where  $\mathbf{w}_i$  and  $\mathbf{d}$  fulfill, respectively, assumptions **(a2)** and **(a5)** (see the assumptions section), with  $\sigma_{w,i} = \sigma_d \triangleq \sigma^2$ .

When the source and relays have no CSI, a sensible choice [66, 67] is to assume that  $\mathbf{F}_0$  and  $\{\mathbf{F}_i\}_{i=1}^{N_C}$  are scaled semi-unitary matrices, i.e.,  $\mathbf{F}_0^H \mathbf{F}_0 = \mathbf{I}_{N_B}/N_B$  and  $\mathbf{F}_i^H \mathbf{F}_i = \mathbf{F}_i \mathbf{F}_i^H = \mathbf{I}_{N_R}$ : in this case,  $\mathbf{F}_0$  is employed to adjust the multiplexing rate and the set of relaying matrices  $\{\mathbf{F}_i\}_{i=1}^{N_C}$  is used to avoid possible rank deficiency of  $\mathbf{C}$  (see **(a6)** in the assumptions section). Therefore, here we consider the set  $\{\mathbf{F}_i\}_{i=0}^{N_C}$  of matrices satisfying both the assumptions **(a7)** and **(a9)** (see the assumptions section). Each scaling factor  $\alpha_i$  is chosen so as to satisfy the average power scaling constraint  $\mathbb{E}[\|\tilde{\mathbf{z}}_i\|^2] = N_R P_i$ , where  $P_i$  is the power available at the  $i$ th relay for each antenna, thus obtaining

$$\alpha_i = \frac{\gamma P_i}{1 + \gamma \sigma_{h,i}^2}, \quad (2.7)$$

with  $\gamma \triangleq \sigma^{-2}$  denoting the average signal-to-noise ratio (SNR) per transmitted symbol block.

### 2.3.2 Theoretical performance analysis

Let us introduce

$$\mathbf{G} \triangleq [\mathbf{G}_1, \mathbf{G}_2, \dots, \mathbf{G}_{N_C}] \in \mathbb{C}^{N_D \times (N_C N_R)}$$

and

$$\mathbf{H} \triangleq [\mathbf{H}_1^T, \mathbf{H}_2^T, \dots, \mathbf{H}_{N_C}^T]^T \in \mathbb{C}^{(N_C N_R) \times N_S}.$$

By applying the conditional expectation rule, the error probability in detecting the  $n$ th entry of  $\mathbf{s}$ ,  $P_{\text{coop},n}(e)$ , can be calculated as

$$P_{\text{coop},n}(e) = \mathbb{E}_{\mathbf{H}}\{\mathbb{E}_{\mathbf{G}|\mathbf{H}}[P_{\text{coop},n}(e|\mathbf{G}, \mathbf{H})]\}, \quad (2.8)$$

where  $P_{\text{coop},n}(e|\mathbf{G}, \mathbf{H})$  represents the SEP conditioned on  $\mathbf{H}$  and  $\mathbf{G}$ . The conditional SEP  $P_{\text{coop},n}(e|\mathbf{H})$  is given [68] by

$$\begin{aligned} P_{\text{coop},n}(e|\mathbf{H}) &\triangleq \mathbb{E}_{\mathbf{G}|\mathbf{H}}[P_{\text{coop},n}^{(m)}(e|\mathbf{G}, \mathbf{H})] \\ &= \frac{2b}{\pi} \int_0^{\pi/2} \Phi_{\text{SINR}_n} \left( -\frac{u}{\sin^2 x}; \mathbf{H} \right) dx \end{aligned} \quad (2.9)$$

where  $b \triangleq 2(1 - 1/\sqrt{Q})$  and  $u \triangleq 3/[2(Q - 1)]$  are modulation-dependent parameters, whereas

$$\Phi_{\text{SINR}_n}(y; \mathbf{H}) \triangleq \mathbb{E}_{\mathbf{G}|\mathbf{H}}[\exp(y \text{SINR}_n)] \quad (2.10)$$

is the moment generating function (MGF), conditioned on  $\mathbf{H}$ , of the signal-to-interference-plus-noise ratio

$$\text{SINR}_n \triangleq \frac{1}{\{\mathbf{C}^\dagger \mathbf{K}_{\mathbf{v}\mathbf{v}} \mathbf{C}^{\dagger H}\}_{nn}}, \quad (2.11)$$

with  $\mathbf{K}_{\mathbf{v}\mathbf{v}} \triangleq \mathbb{E}[\mathbf{v}\mathbf{v}^H | \mathbf{G}]$  denoting the correlation matrix of the noise at the output of the ZF equalizer.

### SINR approximation

It can be shown that  $\mathbf{K}_{\mathbf{v}\mathbf{v}}$  can be decomposed as  $\mathbf{K}_{\mathbf{v}\mathbf{v}} = \sigma^2 (\mathbf{S}_{N_C} + \mathbf{I}_{N_D})$ , with  $\mathbf{S}_{N_C} \triangleq \sum_{i=1}^{N_C} \alpha_i \mathbf{G}_i \mathbf{G}_i^H$  being a sum of complex central Wishart matrices [69]  $\alpha_i \mathbf{G}_i \mathbf{G}_i^H$ , each one having  $N_R$  degrees of freedom and covariance matrix  $\alpha_i^2 \sigma_{g,i}^2 \mathbf{I}_{N_D}$ , respectively. Matrix  $\mathbf{S}_{N_C}$  has mean  $\mathbf{M}_{N_C} \triangleq$

$\mathbb{E}[\mathbf{S}_{N_C}] = \varrho N_R \mathbf{I}_{N_D}$ , with  $\varrho \triangleq \sum_{i=1}^{N_C} \alpha_i \sigma_{g,i}^2 > 0$ , and variance given by

$$\begin{aligned}
\text{VAR}(\mathbf{S}_{N_C}) &\triangleq \mathbb{E} \left[ \|\mathbf{S}_{N_C} - \mathbf{M}_{N_C}\|^2 \right] \\
&= -2 \varrho N_R \sum_{i=1}^{N_C} \alpha_i \mathbb{E} \left[ \text{tr} (\mathbf{G}_i \mathbf{G}_i^H) \right] + \varrho^2 N_R^2 N_D \\
&\quad + \sum_{i=1}^{N_C} \sum_{\substack{k=1 \\ k \neq i}}^{N_C} \alpha_i \alpha_k \mathbb{E} \left[ \text{tr} (\mathbf{G}_i \mathbf{G}_i^H \mathbf{G}_k \mathbf{G}_k^H) \right] \\
&\quad + \sum_{i=1}^{N_C} \alpha_i^2 \mathbb{E} \left\{ \text{tr} \left[ (\mathbf{G}_i \mathbf{G}_i^H)^2 \right] \right\} \\
&= N_R N_D^2 \sum_{i=1}^{N_C} \alpha_i^2 \sigma_{g,i}^4 \tag{2.12}
\end{aligned}$$

where we observed [69] that  $\mathbb{E}\{\text{tr}[(\mathbf{G}_i \mathbf{G}_i^H)^2]\} = \sigma_{g,i}^4 N_R N_D (N_R + N_D)$ . When the number of relays  $N_C$  is sufficiently large, matrix  $\mathbf{S}_{N_C}$  converges *almost surely* to the constant matrix  $\mathbf{M}_{N_C}$ , as stated by the following Lemma whose proof relies on a generalization of the Kolmogorov's inequality [64] to the case of random matrices.

**Lemma 1.** *Under the assumption that*

$$\sum_{i=1}^{+\infty} \frac{\alpha_i^2 \sigma_{g,i}^4}{i^2} < +\infty \tag{2.13}$$

*the matrix sequence  $\{\alpha_i \mathbf{G}_i \mathbf{G}_i^H\}_{i=1}^{N_C}$  obeys the strong law of large numbers, i.e.,  $\forall \epsilon > 0$  and  $\forall \Delta > 0$ , there is  $N > 0$  such that,  $\forall K > 0$ , the probability of the simultaneous fulfilment of the  $K$  inequalities  $\|\mathbf{S}_{N_C} - \mathbf{M}_{N_C}\|/N_C < \epsilon$  is greater than or equal to  $1 - \Delta$ , for  $N_C \in \{N, N + 1, \dots, N + K\}$ .*

**Proof.** See App. A.

Fulfilment of (2.13) depends on the sequence  $\{\alpha_i^2 \sigma_{g,i}^4\}_{i=1}^{+\infty}$  whose general term can be upper bounded as

$$\alpha_i^2 \sigma_{g,i}^4 = \gamma^2 P_i^2 \left[ \frac{\sigma_{g,i}^2}{1 + \gamma \sigma_{h,i}^2} \right]^2 \leq \gamma^2 P_{\max}^2 \left[ \frac{\sigma_{g,i}^2}{1 + \gamma \sigma_{h,i}^2} \right]^2, \tag{2.14}$$

where  $P_{\max} > 0$  is the maximum (finite) power available at each relay. Thus, one can argue that (2.13) is trivially satisfied when the average path losses do not depend on  $i$ , i.e.,  $\sigma_{h,i}^2 = (d_{SD}/d_{SR_i})^\eta = \sigma_h^2$  and  $\sigma_{g,i}^2 = (d_{SD}/d_{R_iD})^\eta = \sigma_g^2$ : in this case, the sum of the series in (2.13) is upper bounded by  $(\pi^2 \alpha_{\max}^2 \sigma_g^4)/6$ , with  $\alpha_{\max} \triangleq (\gamma P_{\max})/(1 + \gamma \sigma_h^2)$ . From a physical viewpoint, this happens when the relays form a relaying cluster, wherein the distances between the different relays are negligible with respect to the distance  $d_{SD}$  between the source and destination. When the cooperative relays do not belong to a cluster, the general term of  $\{\alpha_i^2 \sigma_{g,i}^4\}_{i=1}^{+\infty}$  can be further upper bounded as

$$\alpha_i^2 \sigma_{g,i}^4 \leq \gamma^2 P_{\max}^2 \left[ \frac{\sigma_{g,\max}^2}{1 + \gamma \sigma_{h,\min}^2} \right]^2 < P_{\max}^2 \left( \frac{d_{SR_{\max}}}{d_{R_{\min}D}} \right)^{2\eta}, \quad (2.15)$$

with  $\sigma_{h,\min}^2 \triangleq (d_{SD}/d_{SR_{\max}})^\eta$  and  $\sigma_{g,\max}^2 \triangleq (d_{SD}/d_{R_{\min}D})^\eta$ , where  $d_{SR_{\max}}$  is the distance of the farthest relay from the source, while  $d_{R_{\min}D}$  is the distance of the nearest relay to the destination, i.e.,

$$d_{SR_{\max}} \triangleq \max_{i \in \{1,2,\dots,N_C\}} d_{SR_i} \quad (2.16)$$

$$d_{R_{\min}D} \triangleq \min_{i \in \{1,2,\dots,N_C\}} d_{R_iD}. \quad (2.17)$$

Hence, for any value of  $\gamma$ , a *sufficient condition* for fulfilment of (2.13) is that  $d_{SR_{\max}}/d_{R_{\min}D} \leq \chi$ , for some finite constant  $0 < \chi < +\infty$ , which, besides requiring that  $d_{SR_{\max}}$  is finite, imposes that  $d_{R_{\min}D}$  must be sufficiently large, i.e., the relays cannot be too close the destination; in this case, the sum of the series in (2.13) is upper bounded by  $(\pi^2 P_{\max}^2 \chi^{2\eta})/6$ .

### SEP approximation

Roughly speaking, Lemma 1 states that, with high probability,  $\|\mathbf{S}_{N_C} - \mathbf{M}_{N_C}\|/N_C$  remains small for all  $N_C \geq N$ , provided that (2.13) holds. Therefore, if  $N_C$  is sufficiently large, by replacing  $\mathbf{S}_{N_C}$  with  $\mathbf{M}_{N_C}$ , thus obtaining  $\mathbf{K}_{\mathbf{v}\mathbf{v}} \approx \sigma^2 (\varrho N_R + 1) \mathbf{I}_{N_D}$ , the SINR is approximated as

$$\text{SINR}_n \approx \frac{\gamma}{\beta} \cdot \frac{1}{\{(\mathbf{C}^H \mathbf{C})^{-1}\}_{nn}}, \quad (2.18)$$

where  $\beta \triangleq \varrho N_R + 1$ . At this point, we state the main result of the paper.

**Theorem 1.** Let  $N_R \geq N_B$ ,  $D \triangleq N_D - N_B + 1$  and  $N_C N_R > N_D$ . In the high-SNR region, i.e., for  $\gamma \gg 1$ , one has

$$P_{coop,n}(e) \approx \bar{P}_{coop}(e) \triangleq \Upsilon_{coop} \left[ \frac{3\gamma \sum_{i=1}^{N_C} (\alpha_i \sigma_{h,i}^2 \sigma_{g,i}^2)^2}{2N_B(Q-1)\beta \sum_{i=1}^{N_C} \alpha_i \sigma_{h,i}^2 \sigma_{g,i}^2} \right]^{-D} \quad (2.19)$$

where

$$\Upsilon_{coop} \triangleq 2\Theta(D) \left(1 - \frac{1}{\sqrt{Q}}\right) \frac{(N_C N_R - N_D - 1)!}{(N_C N_R - N_B)!}. \quad (2.20)$$

with  $\Theta(v) \triangleq (2/\pi) \int_0^{\pi/2} [\sin^2(x)]^v dx$ ,  $v \in \mathbb{R}$ .

**Proof.** See App. B.

As a first remark, we highlight that  $\bar{P}_{coop}(e)$  turns out to be independent of the symbol index  $n$ . Furthermore, it is worth noting that, in the high-SNR regime, the scaling factor  $\alpha_i \approx P_i/\sigma_{h,i}^2$  becomes independent of  $\gamma$ . Consequently,  $\{\alpha_i \sigma_{h,i}^2 \sigma_{g,i}^2\}_{i=1}^{N_C}$  and  $\beta$  in (2.19) turn out to be independent of  $\gamma$  and, thus, the SEP can be simply approximated as  $\bar{P}_{coop}(e) \approx (C_{coop} \gamma)^{-D}$ , where  $D \triangleq N_D - N_B + 1$  is the *diversity order*, whereas the *coding gain*  $C_{coop}$  is given by

$$C_{coop} \triangleq \frac{3\Upsilon_{coop}^{-1/D} \sum_{i=1}^{N_C} P_i^2 \sigma_{g,i}^4}{2N_B(Q-1) \left( N_R \sum_{i=1}^{N_C} P_i \sigma_{h,i}^{-2} \sigma_{g,i}^2 + 1 \right) \sum_{i=1}^{N_C} P_i \sigma_{g,i}^2}. \quad (2.21)$$

It is noteworthy that, as stated in [61], the diversity order of the system does not depend on the number of relays  $N_C$ : such a result stems from the fact that the forwarding matrices are channel-independent. Moreover, we highlight that the SEP is independent of the precoding and forwarding matrices  $\{\mathbf{F}_i\}_{i=0}^{N_C}$ , i.e., all AF MIMO cooperative systems with linear equalization at the destination and (semi-)unitary precoding and forwarding matrices exhibit the same SEP given by (2.19).

### Optimal placement of the relaying cluster

To streamline the subsequent discussions, we assume hereinafter that the relays use the same maximum transmitting power,<sup>3</sup> i.e.,  $P_i = P_{\max}$ ,  $\forall i \in \{1, 2, \dots, N_C\}$ . Furthermore, we focus on the case when the relays form a relaying cluster (see Fig. 2.1 when the distances  $\{d_{i,j}\}_{i,j=1}^{N_C}$ , for  $i \neq j$ , between every pair of relays are all negligible with respect to  $d_{SD}$ , i.e.,  $d_{i,j} \ll d_{SD} \forall i, j \in \{1, 2, \dots, N_C\}, i \neq j$ ) and, thus, the average path losses are approximately independent of  $i$ , i.e.,  $\sigma_{h,i}^2 \approx \sigma_h^2 \triangleq (d_{SD}/d_{SC})^\eta$  and  $\sigma_{g,i}^2 \approx \sigma_g^2 \triangleq (d_{SD}/d_{CD})^\eta$ , where  $d_{SC}$  is the source-cluster distance and  $d_{CD}$  is the cluster-destination distance.<sup>4</sup> Particularizing (2.21) to the case when  $P_i = P_{\max}$ ,  $\sigma_{h,i}^2 \approx \sigma_h^2$ , and  $\sigma_{g,i}^2 \approx \sigma_g^2$ ,  $\forall i \in \{1, 2, \dots, N_C\}$ , one has

$$C_{\text{coop}} \approx \frac{3 P_{\max} \Upsilon_{\text{coop}}^{-1/D} \sigma_g^2 \sigma_h^2}{2 N_B (Q-1) (N_C N_R P_{\max} \sigma_g^2 + \sigma_h^2)}. \quad (2.22)$$

We say that the relaying cluster is optimally placed if the coding gain  $C_{\text{coop}}$  in (2.22) is maximized. Our aim is to calculate the optimal values of  $d_{SC}$  and  $d_{CD}$  that maximize the coding gain (2.22). Assuming  $d_{SD}$  fixed and applying the Carnot's cosine law to the triangle in Fig. 2.1, one obtains that

$$d_{CD} = \sqrt{d_{SC}^2 + d_{SD}^2 - 2 d_{SC} d_{SD} \cos(\theta)},$$

where  $\theta \in [0, 2\pi)$  is the angle between the source-cluster and source-destination directions. At this point, the problem boils down to computing  $d_{SC}$  and  $\theta$ . It is easily shown that  $C_{\text{coop}}$  in (2.22) reaches its maximum value when  $d_{SC}^{\eta-1} + N_C N_R P_{\max} d_{CD}^{\eta-2} [d_{SC} - d_{SD} \cos(\theta)] = 0$  and  $\sin(\theta) = 0$ : the latter equation imposes that  $\theta = \theta_{\text{opt}} = 0$ , i.e., the relaying cluster lies on the line joining the source and destination, and, thus,  $d_{CD} = |d_{SD} - d_{SC}|$ ; in this case, one can infer, from the former equation, that  $d_{SD}$  is necessarily greater than  $d_{SC}$ , i.e.,  $d_{SD} > d_{SC}$ , and thus

$$d_{SC} = (d_{SC})_{\text{opt}} = \frac{d_{SD}}{1 + \eta^{-1} \sqrt{N_C N_R P_{\max}}} \quad (2.23)$$

<sup>3</sup>Joint optimization of the relays' transmitting powers  $P_1, P_2, \dots, P_{N_C}$ , which is a complicated task in the considered decentralized framework, is outside the scope of this paper.

<sup>4</sup>We will show by numerical simulations in Subsection 3.3.4 that results in this case turn out to be valuable design guidelines even when the average path losses are different, provided that the distances between the different relays are sufficiently small with respect to the distance between the source and destination.

and

$$d_{\text{CD}} = (d_{\text{CD}})_{\text{opt}} = d_{\text{SD}} - (d_{\text{SC}})_{\text{opt}}. \quad (2.24)$$

It is apparent from (2.23)-(2.24) that  $0 < (d_{\text{SC}})_{\text{opt}} < d_{\text{SD}}$ . More specifically, in the case where  $P_{\max} N_{\text{C}} N_{\text{R}} = 1$ , which implies that  $(d_{\text{SC}})_{\text{opt}} = d_{\text{SD}}/2$ , the coding gain is maximized when the cluster is equidistant from the source and destination. Moreover, when  $P_{\max} N_{\text{C}} N_{\text{R}} > 1$ , it results that  $(d_{\text{SC}})_{\text{opt}} < d_{\text{SD}}/2$ , i.e., the maximum value of  $C_{\text{coop}}$  in (2.22) is achieved if the relaying cluster is closer to the source than the destination. Finally, if  $P_{\max} N_{\text{C}} N_{\text{R}} < 1$ , then  $(d_{\text{SC}})_{\text{opt}} > d_{\text{SD}}/2$ , i.e., the coding gain reaches its maximum when the cluster is closer to the destination than the source. In these last two cases, the best location of the cluster is also dictated by the path-loss exponent  $\eta$ .

### Comparison between cooperative and direct transmissions

It is interesting to compare (2.19) with the SEP of the direct transmission between the source and destination, i.e., when there are no relays. In this case, it can be verified [68] that, for  $\gamma \gg 1$ , the SEP in detecting the  $n$ th symbol  $s_n$ , in the case of direct transmission with ZF equalization at the destination, can be approximated as  $P_{\text{dir},n}(e) \approx \bar{P}_{\text{dir}}(e) \triangleq (C_{\text{dir}} \gamma)^{-D}$ , where  $C_{\text{dir}} \triangleq 3 \Upsilon_{\text{dir}}^{-1/D} / [2 N_{\text{B}} (Q - 1)]$  represents the coding gain of the direct transmission, with  $\Upsilon_{\text{dir}} \triangleq 2 \Theta(D) (1 - 1/\sqrt{Q})$ . Comparison with (2.19) reveals that the cooperative scheme and direct transmission achieve the same diversity order, but exhibit different coding gains. The ratio between such coding gains can be expressed as

$$\xi \triangleq \frac{C_{\text{coop}}}{C_{\text{dir}}} = \frac{\Omega \sum_{i=1}^{N_{\text{C}}} P_i^2 \sigma_{\text{g},i}^4}{\left( N_{\text{R}} \sum_{i=1}^{N_{\text{C}}} P_i \sigma_{\text{h},i}^{-2} \sigma_{\text{g},i}^2 + 1 \right) \sum_{i=1}^{N_{\text{C}}} P_i \sigma_{\text{g},i}^2} \quad (2.25)$$

where  $\Omega \triangleq \sqrt[D]{(N_{\text{C}} N_{\text{R}} - N_{\text{B}})! / (N_{\text{C}} N_{\text{R}} - N_{\text{D}} - 1)!} \geq 1$ . Henceforth, the cooperative transmission is advantageous with respect to the direct one if  $\xi > 1$ . By substituting in (2.25) the simplified expression of  $C_{\text{coop}}$  given by (2.22), the ratio  $\xi$  becomes

$$\xi \approx \frac{\Omega P_{\max} \sigma_{\text{g}}^2 \sigma_{\text{h}}^2}{N_{\text{C}} N_{\text{R}} P_{\max} \sigma_{\text{g}}^2 + \sigma_{\text{h}}^2}. \quad (2.26)$$

If  $N_C N_R P_{\max} \sigma_g^2 \ll \sigma_h^2$ , which happens when the cluster is much closer to the source than the destination, then  $\xi \approx \Omega P_{\max} \sigma_g^2$ , which unveils that the performance comparison between cooperative and direct transmissions does not depend on the first-hop path loss; in this case, the cooperative scheme outperforms the direct one if  $\Omega P_{\max} \sigma_g^2 > 1$  and, thus, recalling that  $\Omega \geq 1$ , it suffices that  $P_{\max} \gg 1$ , i.e., the maximum transmitting power at the relays has to be sufficiently large. On the other hand, if  $N_C N_R P_{\max} \sigma_g^2 \gg \sigma_h^2$ , which happens when the relaying cluster is much closer to the destination than the source, we obtain from (2.26) that  $\xi \approx (\Omega \sigma_h^2)/(N_C N_R)$ , which does not depend on the second-hop path loss. We observe that, in the latter case, the condition  $\Omega \sigma_h^2 > N_C N_R$ , which ensures that the cooperative scheme is advantageous with respect to the direct one, is independent of  $P_{\max}$ .

### 2.3.3 Numerical performance analysis

To corroborate and complete our theoretical results, we compare the high-SNR approximations  $\bar{P}_{\text{coop}}(e)$  and  $\bar{P}_{\text{dir}}(e)$  with the value of the probabilities  $P_{\text{coop},n}(e)$  and  $P_{\text{dir},n}(e)$ , respectively, calculated by a semi-analytical approach, where the averages (with respect to all the relevant fading channels) are evaluated through  $10^6$  independent Monte Carlo runs, with each run employing a different configuration of relays' positions, a different set of fading channels, and a different set of random scaled unitary matrices  $\{\mathbf{F}_i\}_{i=0}^{N_C}$ . Additionally, we report the ABER performances of both cooperative and direct transmissions when the MMSE equalizer is used at the destination, calculated by a semi-analytical approach similar to that used for the ZF case. Cooperative and direct schemes are referred to as ‘‘Coop’’ and ‘‘Dir’’ in the plots, respectively.

We consider the planar network topology depicted in Fig. 2.1, with the source located at the origin of the reference system, and the destination positioned at  $(d_{SD}, 0)$ , with  $d_{SD} = 1$ ; moreover, the  $N_C$  relays are randomly (uniformly) and independently distributed in the circle of radius  $r$ , whose center is identified by the polar coordinates  $(d_{SC}, \theta)$ . A Gray-labeled QAM modulation with  $Q = 4$  is considered, with  $N_B = N_S$ . All the channels are generated according to assumptions **(a3)**-**(a4)** (see the assumptions section), with  $\eta = 3$ , and all the relays transmit in the second hop with the same power level  $P_i = P_{\max} = 1$ ,  $\forall i \in \{1, 2, \dots, N_C\}$ .

**Example 1: ABER performance for different values of relaying cluster's geometrical parameters**

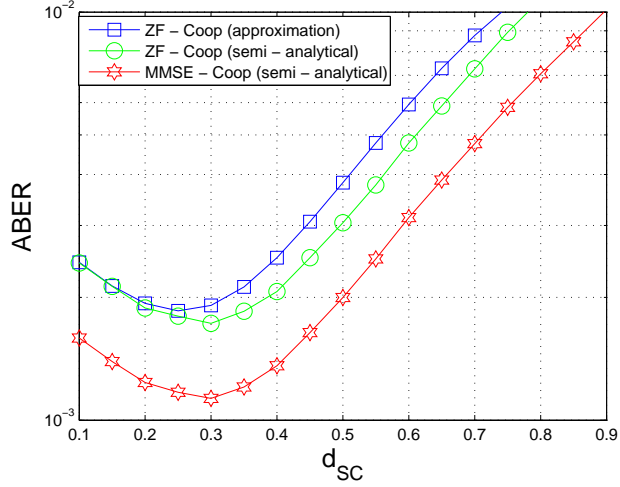


Figure 2.2: ABER versus the distance  $d_{SC}$  between the source and the cluster for  $\theta = 0$  (Example 1).

In this example, we consider the  $(N_S, N_R, N_D) = (2, 2, 2)$  antenna configuration (diversity order  $D = 1$ ), by setting  $\theta = \theta_{opt} = 0$  and  $SNR = 20$  dB. Specifically, we depict in Fig. 2.2 the ABER performances of the considered cooperative transmission schemes as a function of the distance  $d_{SC}$ , with  $r = 0.1$  and  $N_C = 4$ , whereas Fig. 2.3 reports the ABER performances of the same schemes as a function of cluster's radius  $r$  for two values of  $N_C \in \{2, 6\}$ , with  $d_{SC} = (d_{SC})_{opt}$  being the optimal source-cluster distance given by (2.23).

Results of Figs. 2.2 and 2.3 evidence that, as expected, the MMSE equalizer slightly outperforms the ZF one, with a performance gain that does not significantly depend on the position and radius of the relaying cluster, provided that  $r \ll d_{SD}$ . All the curves in Figs. 2.2 and 2.3 show a good agreement between the semi-analytical performance of the ZF equalizer and its approximation (2.19). With reference to the ZF case, the ABER approximation curve in Fig. 2.2 has a minimum point at  $d_{SC} = 0.25$ , which corresponds to a global maximum of the coding gain. By setting  $d_{SD} = 1$ ,  $P_{max} = 1$ ,  $N_C = 4$ ,  $N_R = 2$ , and  $\eta = 3$  in (2.23), one obtains  $(d_{SC})_{opt} = 0.2612$ , thus further confirming that the

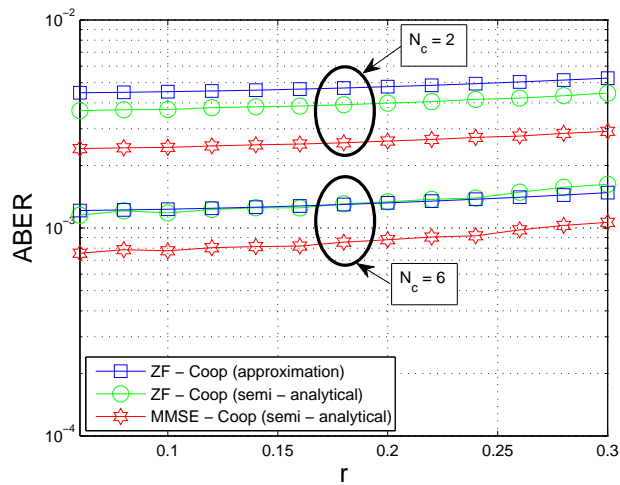


Figure 2.3: ABER versus the cluster's radius  $r$  for two different values of the number  $N_C \in \{2, 6\}$  of relays (Example 1).

results of Subsection 2.3.2 are valid also for a cluster whose radius  $r$  is not infinitesimal, provided that  $r \ll d_{SD}$ .

**Example 2: ABER performance versus SNR for different number of antennas and relays**

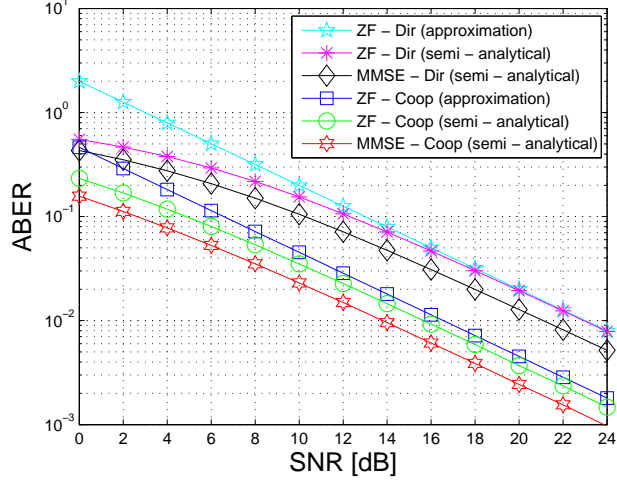


Figure 2.4: ABER vs SNR for  $(N_C, N_S, N_R, N_D) = (2, 2, 2, 2)$  - (Ex. 2).

In this example, we report the ABER performances of both the considered direct and cooperative transmission schemes as a function of the SNR for two different values of  $N_C \in \{2, 6\}$ , with  $d_{SC} = (d_{SC})_{\text{opt}}$ ,  $\theta = \theta_{\text{opt}} = 0$ , and  $r = 0.1$ .

Figs. 2.4 and 2.5 refer to the  $(N_S, N_R, N_D) = (2, 2, 2)$  antenna configuration, whereas Figs. 2.6 and 2.7 refer to at the  $(N_S, N_R, N_D) = (2, 2, 3)$  antenna configuration. In accordance with the results of Subsection 2.3.2, the ABER curves for the cooperative and direct schemes exhibit the same diversity order ( $D = 1$  in Figs. 2.4 and 2.5,  $D = 2$  in Figs. 2.6 and 2.7), but different coding gains. Specifically, with reference to ZF equalization and the  $(N_S, N_R, N_D) = (2, 2, 2)$  antenna configuration, let  $\Delta\text{SNR}(N_C) > 0$  be the SNR gain (in dB) of the cooperative scheme over its corresponding direct counterpart, evaluated for convenience at the ABER value of  $8 \cdot 10^{-3}$ , it results from Figs. 2.4 and Figs. 2.5 that  $\Delta\text{SNR}(2) = 6$  dB and  $\Delta\text{SNR}(6) = 12$  dB, respectively. Such gains can also be reported in terms of the ratio between the coding gain  $C_{\text{coop}}$  of the cooperative scheme and the coding gain  $C_{\text{dir}}$  of the direct transmission as  $\xi_{\text{semi-an}} \triangleq C_{\text{coop}}/C_{\text{dir}} = 10^{\frac{\Delta\text{SNR}(N_C)}{10}}$ . Interestingly, such a

performance gain can be reliably predicted by resorting to (2.26), which refers to a relaying cluster with infinitesimal radius, i.e.,  $r \rightarrow 0$ : for instance, in the case of  $N_C = 6$ , one has that  $\xi_{\text{semi-an}} = 15.8489$  (12 dB); by setting  $P_{\text{max}} = 1$ ,  $N_C = 6$ ,  $N_R = N_S = N_D = 2$ ,  $\eta = 3 \Rightarrow D = 1$ ,  $(d_{SC})_{\text{opt}} = 0.2240$ ,  $\sigma_h^2 = (1/0.2240)^3 = 88.9725$ , and  $\sigma_g^2 = [1/(1 - 0.2240)]^3 = 2.1400$  in (2.25), one gets  $\xi \approx 16.6068$  (12.2 dB).

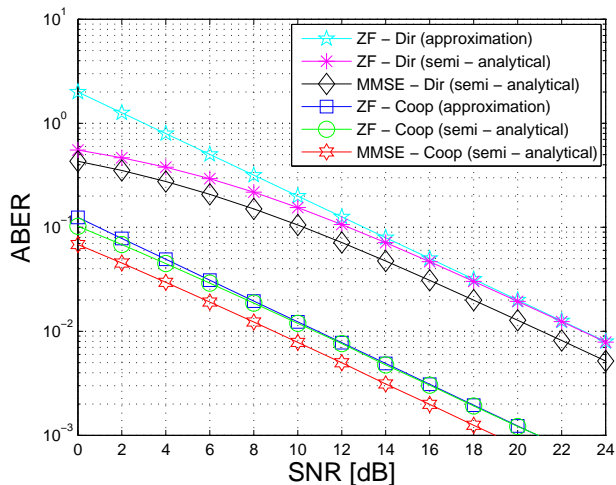


Figure 2.5: ABER vs SNR for  $(N_C, N_S, N_R, N_D) = (6, 2, 2, 2)$  - (Ex. 2).

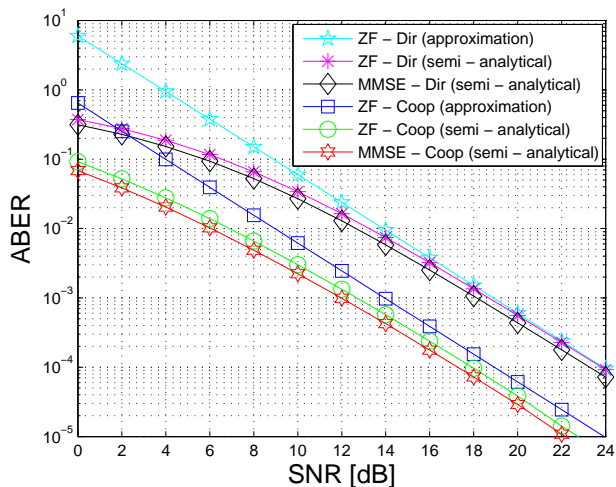


Figure 2.6: ABER vs SNR for  $(N_C, N_S, N_R, N_D) = (2, 2, 2, 3)$  - (Ex. 2).

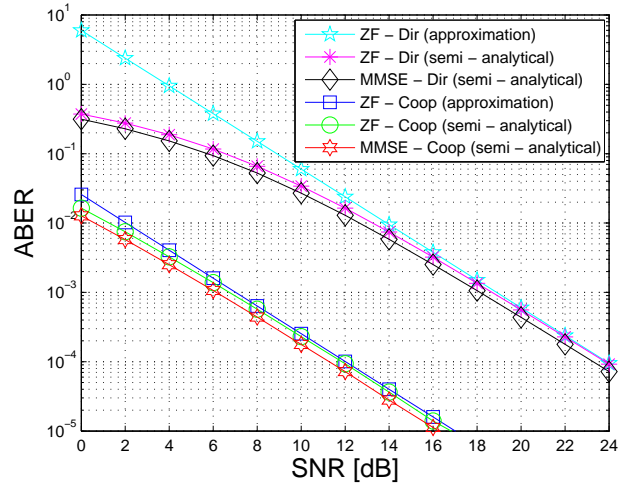


Figure 2.7: ABER vs SNR for  $(N_C, N_S, N_R, N_D) = (6, 2, 2, 3)$  - (Ex. 2).

## 2.4 Case 2: Naive cooperation with MMSE equalization

In this section, we study the SEP performance of the cooperative network considered in case 1, with the only difference that the MMSE criterion is used to design equalizer at the destination. Dual-hop relaying schemes are relevant whenever the signal received via the direct link is below the noise level, due to deep fading or large obstructions. Moreover, it is widely recognized that complete and reliable CSI can be acquired at the relays with a reasonable overhead only in slowly-changing channels and by recruiting only a few closely located relays.

Performance analysis of dual-hop noncoherent AF relaying MIMO schemes over fading channels has been widely carried out in the literature. To name a few, in [40] closed-form expressions and upper/lower bounds on the ergodic capacity are derived in high SNR conditions, whereas in [63] the outage performance of a dual-hop single-antenna/single-relay system is assessed in closed form.

To the best of our knowledge, a complete study of the SEP at the output of a linear MMSE receiver, in the case of an arbitrary (possibly large) number of multiple relays placed in different positions, has not been considered yet. An approximate SEP expression for linear ZF equalization at the destination has been obtained in [54], but the extension to the MMSE case is not straightforward. The contribution consists in the derivation of a closed-form approximation of the SEP at the output of the MMSE equalizer, which proves to be fairly accurate as long as the number of relays exceeds two.

### 2.4.1 Signal model

We consider the network of Fig. 2.1 and assume, again, that there is no direct link, and thus communication between source S and destination D takes place exclusively through  $N_C$  intermediate relay nodes. Moreover, the wireless channel is modeled as an independent and identically distributed (i.i.d.) slow Rayleigh fading channel [70]. Relay nodes employ the AF protocol by simply scaling their received signals, according to a power constraint, and forwarding them to the destination. With regard to the precoding and relaying matrices, in this second result assumptions **(a6)**, **(a7)**, **(a8)** and **(a9)** (see the assumptions section) hold. In addition, we assume that source and relays are not aware of channel

conditions, and thus CSI is available at the destination only (e.g., by training).

According to the model of Sec. 2.2, the received signal at D can be written (see also [40]) (we drop the discrete time-index for simplicity) as

$$\mathbf{r} = \sum_{i=1}^{N_C} \mathbf{G}_i \tilde{\mathbf{z}}_i + \mathbf{d} \quad (2.27)$$

where the signal forwarded by the  $i$ th relay towards D is

$$\tilde{\mathbf{z}}_i \triangleq \sqrt{\alpha_i} (\mathbf{H}_i \mathbf{s} + \mathbf{w}_i) \in \mathbb{C}^{N_R} \quad (2.28)$$

in which  $\alpha_i > 0$  is the scaling factor at the  $i$ th relay. In this case, the general assumptions from **(a1)** to **(a5)** (see the assumptions section) are considered with  $\sigma_{h,i}^2 \triangleq (d_{SD}/d_{SR_i})^\eta$ ,  $\sigma_{g,i}^2 \triangleq (d_{SD}/d_{R_iD})^\eta$ , and  $\sigma_{w,i}^2 = \sigma_d^2 \triangleq \sigma^2$ . In addition, as in the previous section, the scaling factor  $\alpha_i$ ,  $\forall i \in \{1, 2, \dots, N_C\}$  are chosen so as to satisfy the average power constraint  $\mathbb{E}[\|\tilde{\mathbf{z}}_i\|^2] = N_R P_i$ ,  $\forall i \in \{1, 2, \dots, N_C\}$ , where  $P_i$  is the power available at the  $i$ th relay for each antenna, thus obtaining  $\alpha_i = P_i/(\sigma_{h,i}^2 + \sigma^2)$ ,  $\forall i \in \{1, 2, \dots, N_C\}$ .

### 2.4.2 SEP analysis

Let  $\mathbf{C} \triangleq \sum_{i=1}^{N_C} \sqrt{\alpha_i} \mathbf{G}_i \mathbf{H}_i \in \mathbb{C}^{N_D \times N_S}$  denote the equivalent dual-hop MIMO channel, and define  $\mathbf{G} \triangleq [\mathbf{G}_1, \mathbf{G}_2, \dots, \mathbf{G}_{N_C}] \in \mathbb{C}^{N_D \times (N_C N_R)}$ . According to **(a6)** (see the assumptions section), we assume<sup>5</sup> that  $\text{rank}(\mathbf{C}) = N_S \leq N_D$  with probability 1, i.e.,  $\mathbf{C}$  is full-column rank. The received signal (2.27) at D is subject to MMSE equalization, thus yielding

$$\mathbf{y} = \mathbf{C}^H (\mathbf{C} \mathbf{C}^H + \mathbf{R}_{\mathbf{v}\mathbf{v}})^{-1} \mathbf{r}, \quad (2.29)$$

where  $\mathbf{R}_{\mathbf{v}\mathbf{v}} \triangleq \mathbb{E}[\mathbf{v} \mathbf{v}^H | \mathbf{G}]$ , with  $\mathbf{v} \triangleq \sum_{i=1}^{N_C} \sqrt{\alpha_i} \mathbf{G}_i \mathbf{w}_i + \mathbf{d}$ , is the correlation matrix of the overall noise at the destination, conditioned on  $\mathbf{G}$ , which can be expressed as

$$\mathbf{R}_{\mathbf{v}\mathbf{v}} = \sigma^2 \left( \sum_{i=1}^{N_C} \alpha_i \mathbf{G}_i \mathbf{G}_i^H + \mathbf{I}_{N_D} \right). \quad (2.30)$$

---

<sup>5</sup>This assumption is made to avoid that the MMSE equalizer matrix  $\mathbf{C}^H (\mathbf{C} \mathbf{C}^H + \mathbf{R}_{\mathbf{v}\mathbf{v}})^{-1}$  becomes rank-deficient in the high-SNR regime.

Let  $\mathbf{H} \triangleq [\mathbf{H}_1^T, \mathbf{H}_2^T, \dots, \mathbf{H}_{N_C}^T]^T \in \mathbb{C}^{(N_C N_R) \times N_S}$ . By applying the conditional expectation rule, the error probability  $P_n(e)$  in detecting the  $n$ th entry of  $\mathbf{s}$  can be calculated as  $P_n(e) = \mathbb{E}_{\mathbf{H}}\{\mathbb{E}_{\mathbf{G}|\mathbf{H}}[P_n(e|\mathbf{G}, \mathbf{H})]\}$ , where  $P_n(e|\mathbf{G}, \mathbf{H})$  represents the SEP conditioned on  $\mathbf{H}$  and  $\mathbf{G}$ . The conditional SEP  $P_n(e|\mathbf{H}) \triangleq \mathbb{E}_{\mathbf{G}|\mathbf{H}}[P_n(e|\mathbf{G}, \mathbf{H})]$  can be upper-bounded as (see, e.g., [36])  $P_n(e|\mathbf{H}) \leq b \Phi_{\text{SINR}_n^{\text{mmse}}}(-u)$ , with  $b \triangleq 2(1 - Q^{-1/2})$  and  $u \triangleq (3/2)(Q - 1)^{-1}$ , where  $\Phi_{\text{SINR}_n^{\text{mmse}}}(s) \triangleq \mathbb{E}_{\mathbf{G}|\mathbf{H}}[\exp(s \text{SINR}_n^{\text{mmse}})]$  is the moment generating function (MGF), conditioned on  $\mathbf{H}$ , of the random variable (RV)  $\text{SINR}_n^{\text{mmse}}$ , representing the SINR at the output of the MMSE equalizer on the  $n$ th spatial stream. For fixed values of  $\mathbf{H}$  and  $\mathbf{G}$ , the SINR on the  $n$ th spatial stream is given by

$$\text{SINR}_n^{\text{mmse}} = \frac{1}{\text{MMSE}_n} - 1 = \frac{1}{\{(\mathbf{I}_{N_S} + \mathbf{C}^H \mathbf{R}_{\mathbf{v}\mathbf{v}}^{-1} \mathbf{C})^{-1}\}_{nn}} - 1 \quad (2.31)$$

where  $\{\mathbf{A}\}_{nn}$  stands for the  $(n, n)$  entry of matrix  $\mathbf{A}$ . Derivation of the exact distribution of  $\text{SINR}_n^{\text{mmse}}$ , conditioned on  $\mathbf{H}$ , is complicated by the presence in (2.31) of the noise correlation matrix  $\mathbf{R}_{\mathbf{v}\mathbf{v}}$ . To render the problem mathematically tractable, let us first focus on the term  $\mathbf{S}_{N_C} \triangleq \sum_{i=1}^{N_C} \alpha_i \mathbf{G}_i \mathbf{G}_i^H$  in (2.30), which is the sum of  $N_C$  complex central Wishart matrices [71], each one having  $N_R$  degrees of freedom and covariance matrix  $\alpha_i^2 \sigma_{g,i}^2 \mathbf{I}_{N_D}$ . As shown in [54], as the number  $N_C$  of cooperative relays increases, matrix  $\mathbf{S}_{N_C}$  converges almost surely to its mean  $\mathbf{M}_{N_C} \triangleq \varrho N_R \mathbf{I}_{N_D}$ , with  $\varrho \triangleq \sum_{i=1}^{N_C} \alpha_i \sigma_{g,i}^2$ ; in this case, the noise correlation matrix (2.30) can be well approximated as  $\mathbf{R} \approx \sigma^2 (\varrho N_R + 1) \mathbf{I}_{N_D}$ , which, accounting for (2.31), leads to the following SINR approximation

$$\text{SINR}_n^{\text{mmse}} \approx \frac{1}{\{(\mathbf{I}_{N_S} + \gamma \mathbf{C}^H \mathbf{C})^{-1}\}_{nn}} - 1 \quad (2.32)$$

where  $\gamma \triangleq 1/(\sigma^2 \delta)$ , with  $\delta \triangleq \varrho N_R + 1$ .

Let  $\mathbf{C}_{(-n)} \in \mathbb{C}^{N_D \times (N_S - 1)}$  denote the matrix  $\mathbf{C}$  with its  $n$ th column  $\mathbf{c}_n$  removed. We consider the economy-size singular value decomposition  $\mathbf{C}_{(-n)} = \mathbf{U}_n \mathbf{D}_n \mathbf{V}_n^H$ , where the semi-unitary matrix  $\mathbf{U}_n \in \mathbb{C}^{N_D \times (N_S - 1)}$  and the unitary matrix  $\mathbf{V}_n \in \mathbb{C}^{(N_S - 1) \times (N_S - 1)}$  contain the left and right singular vectors, respectively, associated with the nonzero singular values of  $\mathbf{C}_{(-n)}$ , gathered in matrix  $\mathbf{D}_n \triangleq \text{diag}(d_{n,0}, d_{n,1}, \dots, d_{n,N_S-2}) \in \mathbb{R}^{(N_S - 1) \times (N_S - 1)}$ . It can be shown [72] that the SINR at the output of the MMSE receiver can be decomposed into the sum of two statistically independent RVs as  $\text{SINR}_n^{\text{mmse}} = \zeta_n + \text{SINR}_n^{\text{zf}}$ , where  $\text{SINR}_n^{\text{zf}} \approx$

$\gamma/\{(\mathbf{C}^H \mathbf{C})^{-1}\}_{nn}$  is the approximate SINR at the output of the ZF equalizer on the  $n$ th spatial stream, whereas  $\zeta_n \triangleq \gamma \tilde{\mathbf{c}}_n^H [\mathbf{I}_{N_S-1} + \gamma \mathbf{D}_n^2]^{-1} \tilde{\mathbf{c}}_n$ , with  $\tilde{\mathbf{c}}_n \triangleq \mathbf{U}_n^H \mathbf{c}_n$ .

Given  $\mathbf{H}$ , the approximate  $\text{SINR}_n^{\text{zf}}$  is a Gamma RV [73] with shape parameter  $k = N_D - N_S + 1$  and scale parameter  $\theta = \gamma \Sigma_n$ , with  $\Sigma_n \triangleq 1/(\mathbf{R}^{-1})_{nn}$ , where  $\mathbf{R} \triangleq \tilde{\mathbf{H}}^H (\boldsymbol{\Omega} \otimes \mathbf{I}_{N_D}) \tilde{\mathbf{H}} \in \mathbb{C}^{N_S \times N_S}$  represents the covariance matrix of each row of  $\mathbf{C}$ ,

$$\tilde{\mathbf{H}} \triangleq [\text{diag}(\sigma_{h,1}^2, \sigma_{h,2}^2, \dots, \sigma_{h,N_C}^2)^{-1} \otimes \mathbf{I}_{N_D}] \mathbf{H} \quad (2.33)$$

is the normalized channel matrix, with i.i.d. unit-variance ZMCSCG entries,

$$\boldsymbol{\Omega} \triangleq \text{diag}(\alpha_1 \sigma_{h,1}^2 \sigma_{g,1}^2, \alpha_2 \sigma_{h,2}^2 \sigma_{g,2}^2, \dots, \alpha_{N_C} \sigma_{h,N_C}^2 \sigma_{g,N_C}^2), \quad (2.34)$$

and  $\otimes$  denotes Kronecker product [74]. From the statistical independence between  $\text{SINR}_n^{\text{zf}}$  and  $\zeta_n$ , it follows that

$$\begin{aligned} \Phi_{\text{SINR}_n^{\text{mmse}}}(-u) &= \Phi_{\zeta_n}(-u) \Phi_{\text{SINR}_n^{\text{zf}}}(-u) \\ &\approx \Phi_{\zeta_n}(-u) (1 + u \gamma \Sigma_n)^{-(N_D - N_S + 1)} \end{aligned} \quad (2.35)$$

where we approximated  $\Phi_{\text{SINR}_n^{\text{zf}}}(-u)$  with the MGF of a Gamma RV. At this point, we need to evaluate the MGF of  $\zeta_n$ . By writing  $\zeta_n$  as a function of the entries of  $\tilde{\mathbf{c}}_n \triangleq [\tilde{c}_{n,0}, \tilde{c}_{n,1}, \dots, \tilde{c}_{n,N_S-2}]^T$  and the singular values  $d_{n,i}$ , and applying the conditional expectation rule, one obtains the expression of  $\Phi_{\zeta_n}(-u)$  reported in (2.36) at the top of this page.

$$\begin{aligned} \Phi_{\zeta_n}(-u) &= \mathbb{E}_{\mathbf{C}_{(-n)}|\mathbf{H}} \left[ \mathbb{E}_{\mathbf{C}|\mathbf{H}\mathbf{C}_{(-n)}} \left( e^{-u\gamma \sum_{i=0}^{N_S-2} \frac{|t_{n,i}|^2}{1+\gamma d_{n,i}^2}} \right) \right] \\ &= \mathbb{E}_{\mathbf{C}_{(-n)}|\mathbf{H}} \left[ \prod_{i=0}^{N_S-2} \mathbb{E}_{\mathbf{C}|\mathbf{H},\mathbf{C}_{(-n)}} \left( e^{-\frac{u\gamma |t_{n,i}|^2}{1+\gamma d_{n,i}^2}} \right) \right]. \end{aligned} \quad (2.36)$$

In the last-hand of (2.36), we have exploited the statistical independence, conditioned on  $\mathbf{C}_{(-n)}$ , among the circular Gaussian RVs  $\tilde{c}_{n,i}$ , having mean [72]  $\mu_{n,i} \triangleq d_{n,i} \{ \mathbf{V}_n^H [\mathbf{R}_{(-n,-n)}]^{-1} \mathbf{r}_{n(-n)} \}_i$  and variance  $\Sigma_n$ , where  $\mathbf{R}_{(-n,-n)}$  is the covariance matrix  $\mathbf{R}$  with its  $n$ th row and  $n$ th column removed, whereas  $\mathbf{r}_{n(-n)}$  denotes the  $n$ th column of  $\mathbf{R}$  with its  $n$ th removed.

Given  $\mathbf{H}$  and  $\mathbf{C}^{(-n)}$ , it turns out that the RV  $|\tilde{c}_{n,i}|^2$  has a noncentral Chi-squared distribution [73] with MGF

$$\begin{aligned} & \mathbb{E}_{\mathbf{C}|\mathbf{H},\mathbf{C}^{(-n)}} \left[ \exp \left( -u\gamma \cdot \frac{|t_{n,i}|^2}{1+\gamma d_{n,i}^2} \right) \right] \\ &= \left( 1 + \frac{u\gamma \Sigma_n}{1+\gamma d_{n,i}^2} \right)^{-1} \exp \left( -\frac{|\mu_{n,i}|^2}{\Sigma_n + \frac{(1+\gamma d_{n,i}^2)}{u\gamma}} \right) \\ &\leq \frac{1+\gamma d_{n,i}^2}{1+\gamma d_{n,i}^2 + u\gamma \Sigma_n} \end{aligned} \quad (2.7)$$

where the last inequality stems from the fact that  $\exp(-ax) \leq 1$ , for any  $x \geq 0$  and  $a > 0$ .

Substituting (2.7) into (2.36) and recalling that  $\mathbf{C}^{(-n)} = \mathbf{U}_n \mathbf{D}_n \mathbf{V}_n^H$ , after straightforward calculations, one obtains

$$\begin{aligned} \Phi_{\zeta_n}(-u) &\lesssim \mathbb{E}_{\mathbf{C}^{(-n)}|\mathbf{H}} \left[ \prod_{i=0}^{N_S-2} \left( \frac{d_{n,i}^2}{d_{n,i}^2 + u \Sigma_n} \right) \right] \\ &\lesssim \mathbb{E}_{\mathbf{C}^{(-n)}|\mathbf{H}} \left[ \frac{\det(\mathbf{D}_n^2)}{\det(u \Sigma_n \mathbf{I}_{N_S-1} + \mathbf{D}_n^2)} \right] \\ &\lesssim \mathbb{E}_{\mathbf{C}^{(-n)}|\mathbf{H}} \left\{ \frac{\det[\mathbf{\Xi}]}{\det[u \Sigma_n \mathbf{R}_{(-n,-n)}^{-1} + \mathbf{\Xi}]} \right\} \\ &\lesssim \chi^{(N_S-1)} \cdot \mathbb{E}_{\mathbf{C}^{(-n)}|\mathbf{H}} \left\{ \frac{\det[\mathbf{\Xi}]}{\det[\mathbf{I}_{N_S-1} + \chi \mathbf{\Xi}]} \right\} \end{aligned} \quad (2.8)$$

which holds for moderate-to-high values of the SNR, where the last term comes from Weyl's inequality [74], with  $\chi \triangleq (u \Sigma_n \lambda_{\max})^{-1}$  and  $\lambda_{\max}$  denoting the largest eigenvalue of  $\mathbf{R}_{(-n,-n)}$ , conditioned on  $\mathbf{H}$ . At this point, provided that  $N_S > 1$ , approximating the expectation in (2.8) as in [36], one obtains

$$\begin{aligned} \Phi_{\zeta_n}(-u) &\lesssim \binom{N_D}{N_S-1} (N_S-1) \underbrace{\int_0^{+\infty} \frac{t^{N_S-2} e^{-t/\chi}}{(1+t)^{N_D+1}} dt}_{=(N_S-2)! U(N_S-1, N_S-N_D-1, 1/\chi)} \\ &\lesssim \binom{N_D}{N_S-1} (N_S-1)! U(N_S-1, N_S-N_D-1, 1/\chi) \end{aligned} \quad (2.9)$$

where  $U(\cdot, \cdot, \cdot)$  is Tricomi's (confluent hypergeometric) function [73]. Substituting (2.9) into (2.35) and using again the approximation for moderate-to-high SNR values, one has

$$\begin{aligned} \Phi_{\text{SINR}_n^{\text{mmse}}}(-u) &\lesssim \binom{N_D}{N_S - 1} \frac{N_S - 1}{(u\gamma\Sigma_n)^{N_D - N_S + 1}} \\ &\times \int_0^{+\infty} \frac{t^{N_S - 2} e^{-t/\chi}}{(1+t)^{N_D + 1}} dt. \end{aligned} \quad (2.10)$$

Thus, accounting for the expression of  $\chi$ , by substituting (2.10) into the upper bound on  $P_n(e|\mathbf{H})$  and averaging with respect to  $\mathbf{H}$ , the SEP on the  $n$ th spatial stream assumes the form

$$\begin{aligned} P_n(e) &\lesssim b \binom{N_D}{N_S - 1} \frac{N_S - 1}{(u\gamma)^{N_D - N_S + 1}} \\ &\times \mathbb{E}_{\mathbf{H}} \left[ \int_0^{+\infty} \frac{t^{N_S - 2} e^{-ut\lambda_{\max}\Sigma_n}}{(1+t)^{N_D + 1}} \Sigma_n^{-(N_D - N_S + 1)} dt \right]. \end{aligned} \quad (2.11)$$

To calculate (2.11), it can be shown [65] that matrix  $\mathbf{R}$  has approximately a complex central Wishart distribution with

$$\nu_0 \triangleq N_R \frac{\left( \sum_{i=1}^{N_C} \alpha_i \sigma_{h,i}^2 \sigma_{g,i}^2 \right)^2}{\sum_{i=1}^{N_C} \left( \alpha_i \sigma_{h,i}^2 \sigma_{g,i}^2 \right)^2} \quad (2.12)$$

degrees of freedom and covariance matrix

$$\mathbf{K}_{\mathbf{R}} = \frac{\sum_{i=1}^{N_C} \left( \alpha_i \sigma_{h,i}^2 \sigma_{g,i}^2 \right)^2}{\sum_{i=1}^{N_C} \alpha_i \sigma_{h,i}^2 \sigma_{g,i}^2} \mathbf{I}_{N_S} = \vartheta_0 \mathbf{I}_{N_S}. \quad (2.13)$$

Therefore, provided that  $\nu_0 > N_D$ , it turns out that  $\Sigma_n$  is a Gamma RV with shape parameter  $k_0 = \nu_0 - N_S + 1$  and scale parameter  $\vartheta_0$ . In addition, from [71] we know that, for  $(N_S - 1)$  and  $\nu_0$  approaching infinity in such a way that  $(N_S - 1)/\nu_0$  tends to a finite limit  $\ell \geq 0$ , the largest eigenvalue of the complex Wishart matrix  $\mathbf{R}_{(-n, -n)}$  converges almost surely to  $\lambda_\infty \triangleq 2(N_S - 1)(1 + \sqrt{\ell})^2$ ; thus, in order to simplify the calculus of the expectation in (2.11), we replace  $\lambda_{\max}$  with its limiting (nonrandom) value  $\lambda_\infty$ . Relying on Fubini-Tonelli theorem to switch

the order of expectation and integration in the expression of  $P_n(e)$ , we obtain the following final expression of the SEP.

$$\begin{aligned}
P_n(e) &\lesssim b \binom{N_D}{N_S - 1} \frac{N_S - 1}{(u\gamma)^{N_D - N_S + 1}} \\
&\int_0^{+\infty} \frac{t^{N_S - 2}}{(1+t)^{N_D + 1}} \mathbb{E}_{\mathbf{H}} \left[ e^{-ut\lambda_\infty \Sigma_n \Sigma_n^{-(N_D - N_S + 1)}} \right] dt \\
&\lesssim b \binom{N_D}{N_S - 1} \frac{N_S - 1}{(u\gamma\vartheta_0)^{N_D - N_S + 1}} \frac{\Gamma(\nu_0 - N_D)}{\Gamma(\nu_0 - N_S + 1)} \\
&\int_0^{+\infty} \frac{t^{N_S - 2}}{(1+t)^{N_D + 1} (1 + u\lambda_\infty \vartheta_0 t)^{\nu_0 - N_D}} dt \quad (2.14)
\end{aligned}$$

Evaluation of (2.14) entails a computational complexity that is basically dominated by the calculus of the integral, which can be accurately evaluated by using numerical techniques, e.g., Gaussian quadrature methods.<sup>6</sup> Such a computational burden is significantly smaller than the complexity of a Monte Carlo simulation: indeed, since  $P_n(e)$  might assume extremely low values in the high-SNR region, especially for  $N_C > 2$  (see Section 2.4.3), a large number of Monte Carlo runs are required to obtain accurate SEP estimates.

Some remarks about (2.14) are finally in order. First, we highlight that  $P_n(e)$  turns out to be independent of the symbol index  $n$ . Furthermore, it is worth noting that, in the high-SNR regime, the scaling factors  $\alpha_i$ ,  $\forall i \in \{1, 2, \dots, N_C\}$ , can be approximated as  $\alpha_i \approx P_i / (N_S \sigma_{1,i}^2)$ ,  $\forall i \in \{1, 2, \dots, N_C\}$ , i.e., they become independent of  $\gamma$ . Consequently,  $\vartheta_0$  in (2.14) turns out to be independent of  $\gamma$  and, thus, the SEP can be expressed as  $P(e) \approx G_c \gamma^{-D}$ , where  $D \triangleq N_D - N_S + 1$  is the diversity order of the system, which does not depend on the number  $N_C$  of relays, since no CSI is available, and the coding gain is denoted by

$$\begin{aligned}
G_c &\triangleq b \binom{N_D}{N_S - 1} \frac{N_S - 1}{(u\vartheta_0)^{N_D - N_S + 1}} \frac{\Gamma(\nu_0 - N_D)}{\Gamma(\nu_0 - N_S + 1)} \\
&\times \int_0^{+\infty} \frac{t^{N_S - 2}}{(1+t)^{N_D + 1} (1 + u\lambda_\infty \vartheta_0 t)^{\nu_0 - N_D}} dt. \quad (2.12)
\end{aligned}$$

---

<sup>6</sup>As an example, the Matlab routine `quadgk` uses Gaussian quadrature by implementing the Gauss-Kronrod method.

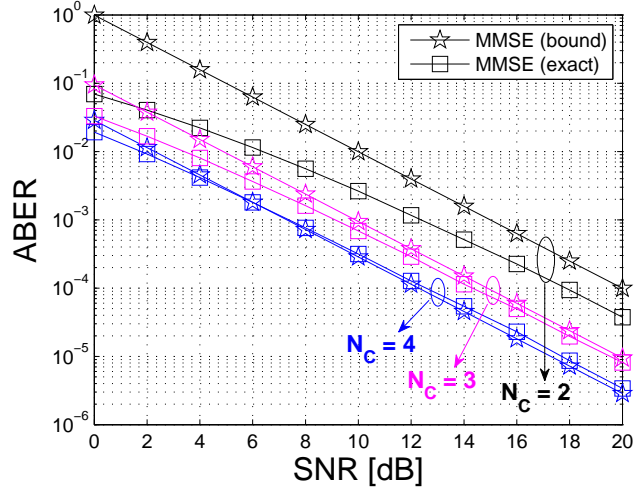


Figure 2.8: ABER vs SNR for different values of the number  $N_C$  of relays.

### 2.4.3 Numerical results

We consider a network geometry consisting of a S-D pair spaced by the distance  $d_{SD} = 1$ , plus  $N_C$  relaying nodes, which are randomly and independently distributed in a circle of radius  $r = 0.1$ , positioned on the line joining S to D at distance  $d_{SC} = 0.2$  from the source. Source, destination and relays are equipped with  $N_S = 2$ ,  $N_D = 3$ , and  $N_R = 2$  antennas, respectively. The employed modulation is Gray-labeled QPSK ( $Q = 4$ ). Both the first-hop and second-hop MIMO channels are generated according to assumptions **(a3)** and **(a4)** (see the assumptions section), with  $\eta = 3$ ; in addition, all the relays transmit with the same power  $P_i = 1$ ,  $\forall i \in \{1, 2, \dots, N_C\}$  (simulations not reported for brevity show that the ABER does not vary significantly if the relays transmit with slightly different powers.) In Fig. 2.8 we plot, for different values of  $N_C \in \{2, 3, 4\}$ , the average bit-error-rate (ABER) of the MMSE receiver. In particular, we compare the ABER values when the SEP  $P_n(e)$  is calculated from the bound (2.14) [labeled as “MMSE (bound)” in the plots], with the exact ones [labeled as “MMSE (exact)”], evaluated by means of a semi-analytical approach, by averaging  $P_n(e|\mathbf{H}, \mathbf{G})$  with respect to  $\mathbf{H}$  and  $\mathbf{G}$  over  $10^6$  Monte Carlo trials. Both curves are reported as a function of  $\text{SNR} \triangleq 1/\sigma^2$ , ranging from 0 to 20 dB.

It is apparent from Fig. 2.8 that the exact performance of the MIMO

AF system with MMSE reception, which exhibits in this scenario a diversity order equal to  $D = N_D - N_S + 1 = 2$ , is well predicted by the proposed bound (2.14), as the SNR increases. The coding gain of the cooperative system rapidly increases as the number of relays  $N_C$  rises. Furthermore, the approximation (2.14) becomes more and more accurate as the number  $N_C$  of cooperating relays grows, which is in part due to the fact that the accuracy of the approximation (2.32) improves.

## 2.5 Case 3: Optimized cooperation

The third case deals with the multiple-relay optimization problem for a MIMO-OFDM cooperative network employing spatial multiplexing, source and relay channel-dependent precoding, and ZF equalization at the destination. Unlike [59] and [60], which adopt the MMSE criterion, here we leverage on the approximate yet accurate results of the performance analysis carried out in [54] and [75], to jointly optimize the precoding and relaying matrices in a minimum SEP sense, for the two limit cases of a full instantaneous CSI and statistical-only CSI. Our criteria lead to compact closed-form solutions, which exhibit significant performance advantages over the simple “naive” AF approach, as corroborated by Monte Carlo computer simulations.

In the considered scenario at hand, designs of the precoding matrix  $\mathbf{F}_0$  and forwarding matrices  $\{\mathbf{F}_i\}_{i=1}^{N_C}$  critically depend on the available CSI at the source and at the relays, respectively. When the source and each relay have full CSI (coherent relay network), optimization of the precoding and forwarding matrices can be carried out in accordance with different design objectives [48] such as, e.g., the maximization of the mutual information between the source and destination, minimization of the MSE at the equalizer output, or maximization of the instantaneous SINR given by (2.18). However, it is widely-recognized that complete and reliable CSI in a coherent relay network can be acquired with a reasonable overhead only in slowly changing channels and, additionally, by recruiting few relays. On the other hand, when the source and relays have no CSI (noncoherent relay network), the precoding matrix  $\mathbf{F}_0$  and the forwarding matrices  $\{\mathbf{F}_i\}_{i=1}^{N_C}$  turn out to be channel-independent necessarily. In the following, by evaluating SEP bounds, we develop different designs for the precoding and forwarding matrices, according to the aforementioned CSI levels provided to the source and relays. As design criterion, we rely on the minimization of the arithmetic mean, over all the  $N_B$  substreams, of the SEP

$$P_{\text{coop},n}(e) \triangleq \Pr(E_{\text{coop},n}) = \mathbb{E}_{\mathbf{G},\mathbf{H}} [\Pr(E_{\text{coop},n} | \mathbf{G}, \mathbf{H})] \quad (2.13)$$

that is,

$$P_{\text{coop},a}(e) \triangleq \frac{1}{N_B} \sum_{n=1}^{N_B} P_{\text{coop},n}(e) \quad (2.14)$$

and express each problem in convex form so that the well-known theory

of convex optimization can be used to obtain efficient optimal solutions using, for example, the interior-point method [76].

### 2.5.1 Network model and basic assumptions

The network under study is, again, compliant with Fig 2.1: in the broadcasting phase, the source sends a data packet to the relays, which simultaneously forward it to the destination during the relaying phase. Moreover, all nodes employ MIMO-OFDM modulation with spatial multiplexing over  $M$  subcarriers [32, 77].

The wireless channel between each pair of antennas is modeled as a quasi-static linear finite-impulse response system, whose order does not exceed the OFDM CP length  $L_{cp}$ . A timing quasi-synchronous MIMO-OFDM network is assumed, wherein the relays belong to a sufficiently small cluster and the CP can jointly compensate for the combined effects of the multipath channel dispersion and the time offset for each relay. In addition, instantaneous CSI is known not only at the destination, but also at the source and relays (*coherent* relaying).

#### Source processing

Let  $\mathbf{s} \in \mathbb{C}^{N_B}$  gather the block of symbols to be transmitted by the source in the  $k$ th ( $k \in \mathbb{Z}$ ) symbol interval and on the  $m$ th OFDM subcarrier, with  $N_B \leq N_S$  and for  $m \in \{0, 1, \dots, M-1\}$ ,<sup>7</sup> Again, at the source node assumption **(a1)** (see the assumptions section) holds. The symbol block  $\mathbf{s}$  is processed by a precoding matrix  $\mathbf{F}_0 \in \mathbb{C}^{N_S \times N_B}$ , obtaining thus  $\tilde{\mathbf{s}} = \mathbf{F}_0 \mathbf{s} \in \mathbb{C}^{N_S}$ , with  $\text{tr}(\mathbf{F}_0^H \mathbf{F}_0) = 1$ , which ensures that  $\mathbb{E}[\|\tilde{\mathbf{s}}\|^2] = 1$ . The design of  $\mathbf{F}_0$  will be discussed in the following subsections. The source adopts a multicarrier spatial multiplexing transmitting technique: before being transmitted, the elements of vectors  $\tilde{\mathbf{s}}$  for different subcarriers corresponding to the same antenna index are subject to conventional OFDM processing, encompassing  $M$ -point IDFT followed by CP insertion.

---

<sup>7</sup>Since the processing of the considered system is on a symbol-by-symbol basis and subcarrier-independent, for the sake of notation simplicity, we avoid indicating the functional dependence on  $k$  and  $m$  in the following derivations.

### Relay processing

After discarding the CP and performing  $M$ -point DFT, the received signal on each subcarrier of the  $i$ th relay, for  $i \in \{1, 2, \dots, N_C\}$ , is given by  $\mathbf{z}_i = \mathbf{H}_i \tilde{\mathbf{s}} + \mathbf{w}_i$ , where  $\mathbf{H}_i \in \mathbb{C}^{N_R \times N_S}$  collects the  $m$ th DFT samples of the  $i$ th first-hop MIMO channel, and  $\mathbf{w}_i \in \mathbb{C}^{N_R}$  accounts for noise at the relay. At the relay nodes assumptions **(a2)**-**(a3)** (see the assumptions section) are considered. The vector  $\mathbf{z}_i \in \mathbb{C}^{N_R}$  is scaled by  $\sqrt{\alpha_i}$  and processed by a forwarding matrix  $\mathbf{F}_i \in \mathbb{C}^{N_R \times N_R}$ , hence yielding  $\tilde{\mathbf{z}}_i \triangleq \sqrt{\alpha_i} \mathbf{F}_i \mathbf{z}_i \in \mathbb{C}^{N_R}$ , where  $\alpha_i > 0$  is determined by the average power scaling [78] constraint  $\mathbb{E}[\|\sqrt{\alpha_i} \mathbf{z}_i\|^2] = N_R P_i$ , thus obtaining  $\alpha_i = \gamma P_i / (1 + \gamma \sigma_{h,i}^2)$ , where  $P_i$  is the power available at the  $i$ th relay and  $\gamma \triangleq \sigma^{-2}$  denotes the average SNR per transmitted symbol block. The design of  $\mathbf{F}_i$  will be discussed in the following subsections. The block  $\tilde{\mathbf{z}}_i$ , after passing through an OFDM modulator, is forwarded by the  $i$ th relay toward the destination.

### Destination processing

After discarding the CP and performing  $M$ -point DFT, the received signal on each subcarrier can be expressed, according to the general model of Section 2.2, as  $\mathbf{r} = \mathbf{C} \mathbf{s} + \mathbf{v}$ . For the sake of convenience, the main relations are again reported below

$$\mathbf{C} \triangleq \left[ \sum_{i=1}^{N_C} \sqrt{\alpha_i} \mathbf{G}_i \mathbf{F}_i \mathbf{H}_i \right] \mathbf{F}_0 \in \mathbb{C}^{N_D \times N_B} \quad (2.15)$$

$$\mathbf{v} \triangleq \sum_{i=1}^{N_C} \sqrt{\alpha_i} \mathbf{G}_i \mathbf{F}_i \mathbf{w}_i + \mathbf{d} \in \mathbb{C}^{N_D} \quad (2.16)$$

where the matrix  $\mathbf{G}_i \in \mathbb{C}^{N_D \times N_R}$  collects the DFT samples of the  $i$ th second-hop MIMO channel,  $\mathbf{d} \in \mathbb{C}^{N_D}$  is the noise vector at the destination, and assumptions **(a4)**-**(a5)**-**(a6)** (see the assumptions section) are considered. In order to recover  $\mathbf{s}$ , the received vector  $\mathbf{r}$  is subject to linear ZF equalization, yielding  $\hat{\mathbf{s}} = \mathbf{C}^\dagger \mathbf{r}$ , with  $(\cdot)^\dagger$  denoting the Moore-Penrose generalized inverse [79], whose entries are finally quantized to the nearest symbols of the QAM constellation. Note that the existence of the ZF equalizer is assured by **(a6)** (see the assumptions section).

### 2.5.2 Full instantaneous CSI

In this subsection, we provide an optimized design procedure for the precoding  $\mathbf{F}_0$  and the relaying  $\{\mathbf{F}_i\}_{i=1}^{N_C}$  matrices when a coherent relay network is considered (i.e., both the source and relays have perfect knowledge of the instantaneous network CSI). To begin with, let  $E_n$  denote the error event in detecting the  $n$ th entry  $s_n$  of  $\mathbf{s}$ , and let

$$\mathbf{G} \triangleq [\mathbf{G}_1, \mathbf{G}_2, \dots, \mathbf{G}_{N_C}] \in \mathbb{C}^{N_D \times N_C N_R}$$

and

$$\mathbf{H} \triangleq [\mathbf{H}_1^T, \mathbf{H}_2^T, \dots, \mathbf{H}_{N_C}^T]^T \in \mathbb{C}^{N_C N_R \times N_S}$$

gather all the forward and backward MIMO channels, respectively. The SEP conditioned on  $\mathbf{G}$  and  $\mathbf{H}$  can be calculated (see, e.g., [36]) as

$$P_{\text{coop},n}(e) \triangleq \Pr(E_n | \mathbf{G}, \mathbf{H}) = \frac{2b}{\pi} \int_0^{\pi/2} \exp\left(-\frac{u}{\sin^2 \vartheta} \text{SINR}_n\right) d\vartheta \quad (2.17)$$

where  $b \triangleq 2(1 - Q^{-1/2})$  and  $u \triangleq 3/[2(Q - 1)]$  are modulation-dependent parameters, whereas  $\text{SINR}_n$  represents the instantaneous (i.e., conditioned on  $\mathbf{G}$  and  $\mathbf{H}$ ) SINR at the output of the ZF equalizer, which admits [36] the following expression:

$$\text{SINR}_n = \frac{1}{\{\mathbf{C}^\dagger \mathbf{K}_{\mathbf{v}\mathbf{v}} \mathbf{C}^{\dagger H}\}_{nn}}. \quad (2.18)$$

In (2.18), taking into account **(a2)** and **(a4)**, the equivalent noise covariance matrix  $\mathbf{K}_{\mathbf{v}\mathbf{v}} \triangleq \mathbb{E}[\mathbf{v} \mathbf{v}^H | \mathbf{H}, \mathbf{G}] = \mathbb{E}[\mathbf{v} \mathbf{v}^H | \mathbf{G}]$  can be expressed as

$$\mathbf{K}_{\mathbf{v}\mathbf{v}} = \sigma^2 \left( \sum_{i=1}^{N_C} \alpha_i \mathbf{G}_i \mathbf{F}_i \mathbf{F}_i^H \mathbf{G}_i^H + \mathbf{I}_{N_D} \right). \quad (2.19)$$

In order to simplify the design of both the precoding and relaying matrices, we observe [54] that the noise correlation matrix (2.19) can be equivalently rewritten as  $\mathbf{K}_{\mathbf{v}\mathbf{v}} = \sigma^2 (\mathbf{S}_{N_C} + \mathbf{I}_{N_D})$ , where

$$\mathbf{S}_{N_C} \triangleq \sum_{i=1}^{N_C} \alpha_i \mathbf{G}_i \mathbf{F}_i \mathbf{F}_i^H \mathbf{G}_i^H = \sum_{i=1}^{N_C} \alpha_i \boldsymbol{\Theta}_i; \quad \boldsymbol{\Theta}_i \triangleq \mathbf{G}_i \mathbf{F}_i \mathbf{F}_i^H \mathbf{G}_i^H$$

is a sum of complex central matrix-variate quadratic forms  $\alpha_i \boldsymbol{\Theta}_i$  [80], for  $i \in \{1, 2, \dots, N_C\}$ . According to **(a5)** (see the assumptions section),

it can be proven that matrix  $\mathbf{S}_{N_C}$  has mean  $\mathbf{M}_{N_C} \triangleq \mathbb{E}[\mathbf{S}_{N_C}] = \varrho \mathbf{I}_{N_D}$ , where  $\varrho \triangleq \sum_{i=1}^{N_C} \alpha_i \sigma_{g,i}^2 > 0$  depends on the path losses over all first and second hops through the scaling factor  $\alpha_i$ .

It is shown in [54] that, under mild conditions, the matrix  $\mathbf{S}_{N_C}$  converges almost surely to the constant matrix  $\mathbf{M}_{N_C}$ , as the number  $N_C$  of relays grows. Therefore, assuming that  $N_C$  is sufficiently large, we replace  $\mathbf{S}_{N_C}$  in  $\mathbf{K}_{\mathbf{v}\mathbf{v}}$  with  $\mathbf{M}_{N_C}$ , obtaining  $\mathbf{K}_{\mathbf{v}\mathbf{v}} \approx \sigma^2 (\varrho + 1) \mathbf{I}_{N_D}$ . Thus, eq. (2.18) can be approximated as

$$\text{SINR}_n \approx \frac{\gamma}{\beta} \text{SINR}_n \quad (2.20)$$

where  $\beta \triangleq \varrho + 1$ , whereas  $\xi_n \triangleq \{(\mathbf{C}^H \mathbf{C})^{-1}\}_{nn}$  depends on the matrices  $\mathbf{F}_0$  and  $\{\mathbf{F}_i\}_{i=1}^{N_C}$  to be optimized through  $\mathbf{C}$ .

We perform the optimization by minimizing the arithmetic mean of the SEPs (2.17), defined as

$$\bar{P}(e) \triangleq \frac{1}{N_B} \sum_{n=0}^{N_B-1} P_{\text{coop},n}(e) = \frac{2b}{\pi} \sum_{n=0}^{N_B-1} \int_0^{\pi/2} \exp\left(-\frac{u}{\sin^2 \vartheta} \text{SINR}_n\right) d\vartheta. \quad (2.21)$$

By substituting (2.20), minimization of (2.21) is equivalent to minimizing, for each  $\vartheta \in (0, \pi/2)$ , the following objective function:

$$\sum_{n=0}^{N_B-1} \exp\left(-\frac{u\gamma}{\beta \sin^2 \vartheta} \text{SINR}_n\right). \quad (2.22)$$

It can be proven that (2.22), as a function of  $\xi_n$ , is a convex increasing function in the range  $\xi_n < u\gamma/(2\beta \sin^2 \vartheta)$ ; indeed, the first and second derivatives of (2.22) with respect to  $\xi_n$  are both positive, provided that  $\xi_n < u\gamma/(2\beta \sin^2 \vartheta)$ , which represents a condition likely to be satisfied in the moderate-to-high SNR region, i.e., when  $\gamma \gg 1$ .

Thus, by applying the Jensen's inequality and relying on the definition of  $\xi_n$ , eq. (2.22) can be lower-bounded as follows:

$$\begin{aligned} \sum_{n=0}^{N_B-1} \exp\left(-\frac{u\gamma}{\beta \sin^2 \vartheta} \text{SINR}_n\right) &\geq \exp\left(-\frac{u\gamma}{\beta \sin^2 \vartheta} \frac{1}{\sum_{n=0}^{N_B-1} \xi_n}\right) \\ &= \exp\left\{-\frac{u\gamma/(\beta \sin^2 \vartheta)}{\text{tr}[(\mathbf{C}^H \mathbf{C})^{-1}]}\right\} \end{aligned} \quad (2.23)$$

where  $\text{tr}[(\mathbf{C}^H \mathbf{C})^{-1}] = \sum_{n=0}^{N_B-1} \xi_n$ , with  $\text{tr}(\cdot)$  denoting the matrix trace operator.

Optimal precoding and relaying matrices can be obtained by minimizing the lower bound (2.23) or, equivalently, the quantity  $\text{tr}[(\mathbf{C}^H \mathbf{C})^{-1}]$ . Ultimately, let

$$\tilde{\mathbf{F}} \triangleq \text{diag}(c_1 \mathbf{F}_1, c_2 \mathbf{F}_2, \dots, c_{N_C} \mathbf{F}_{N_C}) \in \mathbb{C}^{(N_C N_R) \times (N_C N_R)}, \quad (2.24)$$

where  $c_i \triangleq \sqrt{\alpha_i} \sigma_{h,i} \sigma_{g,i}, \forall i \in \{1, 2, \dots, N_C\}$ , and

$$\mathbf{B} \triangleq \mathbf{G} \tilde{\mathbf{F}} \in \mathbb{C}^{(N_D) \times (N_C N_R)}, \quad (2.25)$$

we can formulate the joint design problem as follows

$$\min_{\mathbf{F}_0, \mathbf{B}} f_0(\mathbf{F}_0, \mathbf{B}) \quad (2.26)$$

$$\text{s.t.} \quad \text{tr}(\mathbf{F}_0^H \mathbf{F}_0) = 1 \quad (2.27)$$

$$\text{tr}(\mathbf{B}^H \mathbf{B}) = 1 \quad (2.28)$$

where  $f_0(\mathbf{F}_0, \mathbf{B}) \triangleq \text{tr}[(\mathbf{F}_0^H \mathbf{H}^H \mathbf{B}^H \mathbf{B} \mathbf{H} \mathbf{F}_0)^{-1}]$ , eq. (2.27) is the transmit power constraint at the source, while (2.28) represents the power constraint at the output of the overall forward channel  $\mathbf{G}$ .

Since it can be readily proven that the objective function  $f_0$  in (2.26) is Schur-concave [81], the solution of the problem (2.26), subject to constraints (2.27) and (2.28), is obtained [82] by parameterizing  $\mathbf{F}_0$  and  $\mathbf{B}$  in terms of SVD of the overall backward channel matrix  $\mathbf{H} = \mathbf{U} \mathbf{\Lambda} \mathbf{V}^H$ , that is,

$$\mathbf{F}_{0,\text{opt}} = \mathbf{V}_1 \mathbf{\Sigma} \quad \text{and} \quad \mathbf{B}_{\text{opt}} = \mathbf{\Delta} \mathbf{U}_1^H \quad (2.29)$$

where  $\mathbf{V}_1 \in \mathbb{C}^{N_S \times L}$  has as columns the right eigenvectors of  $\mathbf{H}$  corresponding to its largest  $L \triangleq \min\{N_B, \text{rank}(\mathbf{H})\}$  eigenvalues in increasing order,  $\mathbf{\Sigma} = [\text{diag}\{\sigma_\ell\}, \mathbf{O}_{L \times (N_B - L)}] \in \mathbb{C}^{L \times N_B}$ , with  $\sigma_\ell \in \mathbb{R}$ , for  $\ell \in \{0, 1, \dots, L-1\}$ ,  $\mathbf{U}_1 \in \mathbb{C}^{N_C N_R \times L}$  collects the left eigenvectors of  $\mathbf{H}$  corresponding to its largest  $L$  eigenvalues, and  $\mathbf{\Delta} \triangleq [\text{diag}\{\delta_\ell\}, \mathbf{O}_{(N_D - L) \times L}]^T \in \mathbb{C}^{N_D \times L}$  is defined as  $\mathbf{\Sigma}$ .

Recalling the definitions (2.24) and (2.25) which provide

$$\mathbf{B} \triangleq \mathbf{G} \tilde{\mathbf{F}} = [c_1 \mathbf{G}_1 \mathbf{F}_1 \quad c_2 \mathbf{G}_2 \mathbf{F}_2 \quad \dots \quad c_{N_C} \mathbf{G}_{N_C} \mathbf{F}_{N_C}],$$

and by partitioning  $\mathbf{B}_{\text{opt}} = [\mathbf{B}_{1,\text{opt}} \quad \mathbf{B}_{2,\text{opt}} \quad \dots \quad \mathbf{B}_{N_C,\text{opt}}]$ , one has that the optimal  $i$ th relaying matrix, for  $i \in \{1, 2, \dots, N_C\}$ , is given by  $\mathbf{F}_{i,\text{opt}} =$

$[1/(\sqrt{\alpha_i} \sigma_{h,i} \sigma_{g,i})] \mathbf{G}_i^\dagger \mathbf{B}_{i,\text{opt}}$ , provided that  $\mathbf{G}_i$  is full-row rank, i.e.,  $N_R \geq N_D$  and  $\text{rank}(\mathbf{G}_i) = N_D$ . As it is apparent from (2.29), the two solutions  $\mathbf{F}_{0,\text{opt}}$  and  $\mathbf{B}_{\text{opt}}$  jointly diagonalize the overall dual-hop MIMO channel  $\mathbf{C}$ .

At this point, substituting (2.29) into (2.26)-(2.28), the optimization problem becomes

$$\min_{\{z_\ell\}, \{w_\ell\}} \sum_{\ell=0}^{L-1} \frac{1}{z_\ell w_\ell \lambda_\ell^2} \quad (2.30)$$

$$\text{s.to} \quad \sum_{\ell=0}^{L-1} z_\ell = 1, \quad z_\ell > 0 \quad (2.31)$$

$$\sum_{\ell=0}^{L-1} w_\ell = 1, \quad w_\ell > 0 \quad (2.32)$$

where, for simplicity of notation, we defined  $z_\ell \triangleq \sigma_\ell^2$  and  $w_\ell \triangleq \delta_\ell^2$ . The optimization problem is convex, since the object function is convex and the constraints are linear. Moreover, for symmetry considerations, it turns out that  $z_\ell = w_\ell$ , for  $\ell \in \{0, 1, \dots, L-1\}$ . Hence, problem (2.30) admits the following closed-form solution

$$z_\ell = w_\ell = (2\mu^{-1} \lambda_\ell^{-2})^{1/3} \quad \ell \in \{0, 1, \dots, L-1\} \quad (2.33)$$

where  $\mu$  must be chosen to satisfy the power constraint (2.31) or (2.32).

### 2.5.3 Statistical-only CSI

In this case, we suppose to be unaware of the instantaneous MIMO channel state and to have only statistical knowledge of all the backward and forward channels. In order to derive an upper bound on the *average* performance of the considered cooperative scheme, relying on the approximation (2.20), we start by keeping the second-hop channel matrix  $\mathbf{G}$  fixed and evaluate the conditioned SEP by averaging (2.17) over the first-hop channel matrix  $\mathbf{H}$ , thus yielding  $P_{\text{coop},n}(e | \mathbf{G}) \triangleq \mathbb{E}_{\mathbf{H}} [\text{Pr}(E_n | \mathbf{G}, \mathbf{H})]$ . To this aim, we provide the following theorem:

**Theorem 2.** *Let  $N_C N_R \geq N_D$ ,  $1 < N_B \leq \min(N_S, N_D)$ , and  $D \triangleq N_D - N_B + 1$ . Assume that  $\{\mathbf{F}_i\}_{i=0}^{N_C}$  do not depend on the underlying*

channel coefficients. In the high-SNR region, i.e., for  $\gamma \gg 1$ , one has

$$P_{coop,n}(e | \mathbf{G}) \lesssim b \left( \frac{u\gamma}{\beta} \right)^{-D} \{(\mathbf{F}_0^H \mathbf{F}_0)^{-1}\}_{nn}^D \frac{\text{tr}^{N_B-1}(\tilde{\mathbf{G}} \tilde{\mathbf{F}} \tilde{\mathbf{F}}^H \tilde{\mathbf{G}}^H)}{\det(\tilde{\mathbf{G}} \tilde{\mathbf{F}} \tilde{\mathbf{F}}^H \tilde{\mathbf{G}}^H)} \quad (2.34)$$

where  $\tilde{\mathbf{G}} \triangleq \mathbf{G} [\text{diag}(\sigma_{g,1}^{-1}, \sigma_{g,2}^{-1}, \dots, \sigma_{g,N_C}^{-1}) \otimes \mathbf{I}_{N_R}] \in \mathbb{C}^{N_D \times (N_C N_R)}$ , with the second-hop matrix  $\mathbf{G}$  and  $\tilde{\mathbf{F}}$  already defined.

**Proof.** See Appendix 2.

Theorem 2 shows the impact of the precoding matrix  $\mathbf{F}_0$  and the forwarding matrices  $\{\mathbf{F}_i\}_{i=1}^{N_C}$  on the system performance in the high-SNR regime, given  $\mathbf{G}$ . It is worth noting that, for high SNR values, the scaling factor  $\alpha_i = \gamma P_i / (1 + \gamma \sigma_{h,i}^2)$  can be approximated as  $\alpha_i \approx P_i / \sigma_{h,i}^2$ , i.e., it becomes independent of  $\gamma$ ; consequently, the diversity order of the system is equal to  $D = N_D - N_B + 1$ . It is apparent that the diversity order does not depend on the choice of the matrices  $\{\mathbf{F}_i\}_{i=0}^{N_C}$ : this result is the consequence of the fact that the precoding and forwarding matrices are channel-independent by assumption.

At this point, according to (2.13), we can average (2.34) with respect to the second-hop channel matrix  $\mathbf{G}$ . In this regard, the following Lemma holds.

**Lemma 2.** *It results that*

$$\mathbb{E}_{\tilde{\mathbf{G}}} \left[ \frac{\text{tr}^{N_B-1}(\tilde{\mathbf{G}} \tilde{\mathbf{F}} \tilde{\mathbf{F}}^H \tilde{\mathbf{G}}^H)}{\det(\tilde{\mathbf{G}} \tilde{\mathbf{F}} \tilde{\mathbf{F}}^H \tilde{\mathbf{G}}^H)} \right] \leq \frac{\text{tr}^{N_B-1}(\tilde{\mathbf{F}} \tilde{\mathbf{F}}^H)}{\left[ \prod_{p=1}^{N_D} \lambda_p(\tilde{\mathbf{F}} \tilde{\mathbf{F}}^H) \right]} \times \mathbb{E}_{\tilde{\mathbf{G}}} \left[ \frac{\text{tr}^{N_B-1}(\tilde{\mathbf{G}} \tilde{\mathbf{G}}^H)}{\lambda_1^{N_D}(\tilde{\mathbf{G}} \tilde{\mathbf{G}}^H)} \right] \quad (2.35)$$

where  $\lambda_1(\tilde{\mathbf{G}} \tilde{\mathbf{G}}^H) \leq \lambda_2(\tilde{\mathbf{G}} \tilde{\mathbf{G}}^H) \leq \dots \leq \lambda_{N_D}(\tilde{\mathbf{G}} \tilde{\mathbf{G}}^H)$  and  $\lambda_1(\tilde{\mathbf{F}} \tilde{\mathbf{F}}^H) \leq \lambda_2(\tilde{\mathbf{F}} \tilde{\mathbf{F}}^H) \leq \dots \leq \lambda_{N_C N_R}(\tilde{\mathbf{F}} \tilde{\mathbf{F}}^H)$  are the ordered eigenvalues of  $\tilde{\mathbf{G}} \tilde{\mathbf{G}}^H$  and  $\tilde{\mathbf{F}} \tilde{\mathbf{F}}^H$ , respectively.

**Proof.** See Appendix D.

Closed-form evaluation of the ensemble average in (2.35) is cumbersome. An approximated upper bound can be obtained by observing that  $\text{tr}(\tilde{\mathbf{G}} \tilde{\mathbf{G}}^H) = \sum_{p=1}^{N_D} \lambda_p(\tilde{\mathbf{G}} \tilde{\mathbf{G}}^H) \leq N_D \lambda_{N_D}(\tilde{\mathbf{G}} \tilde{\mathbf{G}}^H)$  and using the

fact [83, 84] that, if  $N_D/(N_C N_R) \rightarrow \chi \in (0, 1)$  for  $N_C N_R, N_D \rightarrow +\infty$ , then the smallest and largest eigenvalues of  $(\tilde{\mathbf{G}} \tilde{\mathbf{G}}^H)/(N_C N_R)$  converge almost surely to  $(1 - \sqrt{\chi})^2$  and  $(1 + \sqrt{\chi})^2$ , respectively.<sup>8</sup> Consequently, accounting for (2.34) and (2.35), one gets the upper bound

$$\begin{aligned} P_{\text{coop},n}(e) &\lesssim b \left( \frac{u \gamma N_C N_R}{\beta} \right)^{-D} \frac{\left[ \sqrt{N_D} \left( 1 + \sqrt{\frac{N_D}{N_C N_R}} \right) \right]^{2(N_B-1)}}{\left( 1 - \sqrt{\frac{N_D}{N_C N_R}} \right)^{N_D}} \\ &\times \{(\mathbf{F}_0^H \mathbf{F}_0)^{-1}\}_{nn}^D \frac{\text{tr}^{N_B-1}(\mathbf{F} \mathbf{F}^H)}{\left[ \prod_{p=1}^{N_D} \lambda_p(\mathbf{F} \mathbf{F}^H) \right]} \end{aligned} \quad (2.36)$$

which approximatively holds for  $N_C N_R, N_D \gg 1$ .

One can conclude that the choice of  $\{\mathbf{F}_i\}_{i=0}^{N_C}$  strongly impacts on the coding gain of the system and their design heavily depends on the available CSI in the network.

Once that a bound on the SEP has been derived, by substituting (2.36) into (2.14) and neglecting the multiplicative constant terms, we observe that the synthesis of the precoding  $\mathbf{F}_0$  and forwarding  $\{\mathbf{F}_i\}_{i=1}^{N_C}$  matrices can be carried out by minimizing the function

$$\frac{\text{tr}^{N_B-1}(\mathbf{F} \mathbf{F}^H)}{\left[ \prod_{p=1}^{N_D} \lambda_p(\mathbf{F} \mathbf{F}^H) \right]} \sum_{n=1}^{N_B} \{(\mathbf{F}_0^H \mathbf{F}_0)^{-1}\}_{nn}^D \quad (2.37)$$

under suitable constraints, whose expressions will be given later.

The relation (2.37) suggests that the precoding matrix  $\mathbf{F}_0$  can be optimized independently of  $\{\mathbf{F}_i\}_{i=1}^{N_C}$ . Focusing, as first step, on the synthesis of the precoding matrix, we choose  $\mathbf{F}_0$  as the result of the following constrained optimization problem

$$\mathbf{F}_{0,\text{opt}} \triangleq \arg \min_{\mathbf{F}_0} \sum_{n=1}^{N_B} \{(\mathbf{F}_0^H \mathbf{F}_0)^{-1}\}_{nn}^D \quad (2.38)$$

$$\text{s.to } \text{tr}(\mathbf{F}_0^H \mathbf{F}_0) = 1 \quad (2.39)$$

where (2.39) is the transmit power constraint at the source.

---

<sup>8</sup>Only real-valued Wishart matrices are considered in [83] and [84], but the proofs can easily be generalized to the complex case.

Since the diversity order  $D$  is greater than or equal to 1, let  $x_n \triangleq \{(\mathbf{F}_0^H \mathbf{F}_0)^{-1}\}_{nm}$ , the power function  $x_n^D$  is convex on  $\mathbb{R}_{++}$  and, thus, the function  $\sum_{n=1}^{N_B} x_n^D$  is Schur-convex [81]. It follows [81] that the optimal solution  $\mathbf{F}_{0,\text{opt}}$  of rank  $N_B$  admits the following diagonalizing structure:

$$\mathbf{F}_{0,\text{opt}} = \mathbf{U} \boldsymbol{\Sigma}_{\text{opt}} \mathbf{V}^H \quad (2.40)$$

where  $\mathbf{U} \in \mathbb{C}^{N_S \times N_B}$  is an arbitrary semiunitary (i.e.,  $\mathbf{U}^H \mathbf{U} = \mathbf{I}_{N_B}$ ) matrix,  $\boldsymbol{\Sigma}_{\text{opt}} \triangleq \text{diag}(\sigma_{\text{opt},1}, \sigma_{\text{opt},2}, \dots, \sigma_{\text{opt},N_B}) \in \mathbb{C}^{N_B \times N_B}$  has zero elements, except along the main diagonal, whereas  $\mathbf{V} \in \mathbb{C}^{N_B \times N_B}$  is an unitary (i.e.,  $\mathbf{V}^H \mathbf{V} = \mathbf{V} \mathbf{V}^H = \mathbf{I}_{N_B}$ ) rotation matrix such that  $(\mathbf{F}_0^H \mathbf{F}_0)^{-1}$  has identical diagonal elements [81]. This rotation can be computed using the algorithm of [85, 86] or, conveniently, with the DFT matrix or the Hadamard matrix, when  $N_B$  is a power of two [74]. At this point, by introducing the row-wise partition  $\mathbf{V} = [\mathbf{v}_1, \mathbf{v}_2, \dots, \mathbf{v}_{N_B}]^H$ , with  $\mathbf{v}_n = [v_{1,n}, v_{2,n}, \dots, v_{N_B,n}]^T$ , the optimization problem (2.38) in convex form can be expressed as

$$\{\sigma_{\text{opt},i}\} \triangleq \min_{\{\sigma_i\}} \sum_{n=1}^{N_B} \left( \sum_{i=1}^{N_B} \frac{|v_{i,n}|^2}{\sigma_i^2} \right)^D \quad (2.41)$$

$$\text{s.to} \quad \sum_{i=1}^{N_B} \sigma_i^2 = 1 \quad (2.42)$$

which can be efficiently solved using the interior-point method [76].

Now, let us consider the optimization of the forwarding matrices  $\{\mathbf{F}_i\}_{i=1}^{N_C}$ ; relying on (2.37) and accounting for the block diagonal structure of  $\tilde{\mathbf{F}}$ , we can firstly observe that

$$\begin{aligned} \frac{\text{tr}^{N_B-1}(\tilde{\mathbf{F}} \tilde{\mathbf{F}}^H)}{\left[ \prod_{p=1}^{N_D} \lambda_p(\tilde{\mathbf{F}} \tilde{\mathbf{F}}^H) \right]} &= \frac{\left[ \sum_{i=1}^{N_C} \text{tr}(\alpha_i \sigma_{h,i} \sigma_{g,i} \mathbf{F}_i \mathbf{F}_i^H) \right]^{N_B-1}}{\left[ \prod_{p=1}^{N_D} \lambda_p(\tilde{\mathbf{F}} \tilde{\mathbf{F}}^H) \right]} \quad (2.43) \\ &\leq (\alpha_{\max} \sigma_{h,\max} \sigma_{g,\max})^{N_B-1} \frac{\left[ \sum_{i=1}^{N_C} \text{tr}(\mathbf{F}_i \mathbf{F}_i^H) \right]^{N_B-1}}{\left[ \prod_{p=1}^{N_D} \lambda_p(\tilde{\mathbf{F}} \tilde{\mathbf{F}}^H) \right]} \\ &\leq (\alpha_{\max} \sigma_{h,\max} \sigma_{g,\max})^{N_B-1} \frac{\left( \sum_{m=1}^{N_C N_R} \lambda_m \right)^{N_B-1}}{\prod_{i=m}^{N_D} \lambda_m} \end{aligned}$$

where  $\{\lambda_m\}_{m=1}^{N_C N_R}$  represent the ordered (in increasing sense) eigenvalues of matrices  $\{\mathbf{F}_i \mathbf{F}_i^H\}_{i=1}^{N_C}$ . Consequently, the eigenvalues of the forwarding matrices  $\{\mathbf{F}_i\}_{i=1}^{N_C}$  can be optimally chosen as the result of the following constrained minimization problem:

$$\min_{\{\lambda_m\}} f_0(\lambda_1, \lambda_2, \dots, \lambda_{N_C N_R}) \triangleq \frac{\left(\sum_{m=1}^{N_C N_R} \lambda_m\right)^{N_B-1}}{\prod_{m=1}^{N_D} \lambda_m}, \quad \text{s.to } \sum_{m=1}^{N_C N_R} \lambda_m = 1. \quad (2.44)$$

It can be easily proven that  $f_0(\lambda_1, \lambda_2, \dots, \lambda_{N_C N_R})$  is a log-convex [76] function on  $\mathbb{R}_{++}^{N_C N_R}$  for  $N_B = 1$ ; for  $N_B > 1$ , after calculating the partial second-order derivatives of  $\log[f_0(\lambda_1, \lambda_2, \dots, \lambda_{N_C N_R})]$  with respect to  $\lambda_m$ , for  $m = 1, 2, \dots, N_C N_R$ , by straightforward manipulations, it results that  $f_0(\lambda_1, \lambda_2, \dots, \lambda_{N_C N_R})$  is log-convex on  $\mathbb{R}_{++}^{N_C N_R}$  if  $(\sum_{m=1}^{N_C N_R} \lambda_m)/\lambda_{\max} > (N_B - 1)$ , where  $\lambda_{\max}$  denotes the maximum eigenvalue of  $\{\mathbf{F}_i \mathbf{F}_i^H\}_{i=1}^{N_C}$ . Therefore, minimization of the objective function (2.44) is tantamount to the following convex problem

$$\{\lambda_{\text{opt},m}\} \triangleq \min_{\{\lambda_m\}} \log \left[ \frac{\left(\sum_{m=1}^{N_C N_R} \lambda_m\right)^{N_B-1}}{\prod_{m=1}^{N_D} \lambda_m} \right] \quad (2.45)$$

where  $\lambda_m > 0$  obeys  $\sum_{m=1}^{N_C N_R} \lambda_m = 1$ , whose solution can be numerically computed through the interior-point algorithm. Ultimately, each optimal forwarding matrix  $\mathbf{F}_{\text{opt},i}$  can be expressed as

$$\mathbf{F}_{\text{opt},i} = \mathbf{W}_i \mathbf{\Lambda}_{\text{opt},i} \mathbf{Q}_i^H \quad (2.46)$$

where  $\mathbf{W}_i \in \mathbb{C}^{N_R \times N_R}$  and  $\mathbf{Q}_i \in \mathbb{C}^{N_R \times N_R}$  are arbitrary unitary matrices, whereas  $\mathbf{\Lambda}_{\text{opt},i} \triangleq \text{diag}(\lambda_{\text{opt},(i-1)N_R+1}^{1/2}, \dots, \lambda_{\text{opt},iN_R}^{1/2})$ , for  $i = 1, 2, \dots, N_C$ .

#### 2.5.4 Numerical results

In this subsection we present Monte Carlo numerical results aimed at assessing the performance of the proposed design procedures. We consider a network configuration, encompassing a source-destination pair spaced by a distance  $d_{SD} = 1$ , plus  $N_C$  relaying nodes, which are randomly and independently distributed in a circle of radius  $r = 0.1$ , positioned on the line joining the source to the destination. Source, destination, and relays

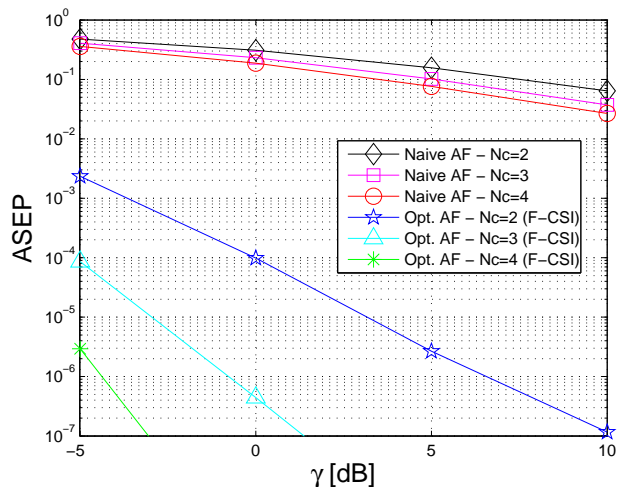


Figure 2.9: ASEP vs SNR for Naive and F-CSI cases.

are equipped with  $N_S = 2$ ,  $N_D = 2$ , and  $N_R = 2$  antennas, respectively. The number of symbols-per-block is  $N_B = 2$ , the number of OFDM subcarriers is  $M = 32$ , and the subcarrier modulation is Gray-labeled 4-QAM (i.e.,  $Q = 4$ ). Both the first-hop and second-hop MIMO channels are generated according to assumptions **(a3)** and **(a4)** (see the assumptions section), with  $\sigma_{h,i}^2 \triangleq (d_{SD}/d_{SR_i})^\eta$  and  $\sigma_{g,i}^2 \triangleq (d_{SD}/d_{R_iD})^\eta$ , where  $d_{SD}$ ,  $d_{SR_i}$ , and  $d_{R_iD}$  are the distance between the source and the destination, the source and the  $i$ th relay, and the  $i$ th relay and the destination, respectively, whereas  $\eta = 3$  is the path-loss exponent. All the relays transmit with the same power  $P_i = 1$ , for  $i \in \{1, 2, \dots, N_C\}$ .<sup>9</sup> As performance measure we report the average SEP (ASEP), obtained through Monte Carlo simulation. In particular, we carry out  $10^6$  independent Monte Carlo runs, with each run employing a different configuration of relays' positions and a different set of fading channels.

In Fig. 2.9 we report the obtained ASEP for the optimized AF protocol, in the case of full instantaneous CSI (F-CSI), as a function of the SNR  $\gamma$  ranging from  $-5$  to  $10$  dB. The curves are parameterized with respect to three different values of the number of relays, i.e.,  $N_C \in \{2, 3, 4\}$ , which are distributed in a circle positioned on the line joining the source

<sup>9</sup>The issue of power optimization, although interesting, is outside the scope of this contribution.

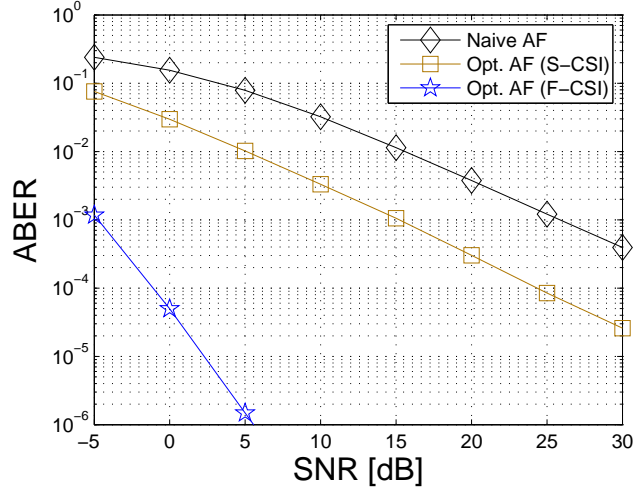


Figure 2.10: ASEP vs SNR for Naive, S-CSI and F-CSI cases ( $N_C = 2$ ).

to the destination at distance  $d_{SC} = 0.2$  from the source. The performance of the proposed technique is compared with that of the “naive” AF approach [40, 54], wherein no precoding is employed at the source (i.e.,  $\mathbf{F}_0 = \mathbf{I}_{N_S}$ ) and the relaying matrix  $\mathbf{F}_i$  at the  $i$ th relay terminal simply forwards a scaled version of its received signal (i.e.,  $\mathbf{F}_i = \sqrt{\alpha_i} \mathbf{I}_{N_R}$ ). Results show that tremendous performance gains can be obtained, at the price of an increased amount of a priori information regarding the forward and backward channels. In particular, from Fig. 2.9 it is evident that, as the number  $N_C$  of cooperating relays increases, the optimized AF solution allows one to capture a remarkable performance improvement not only in terms of coding gain, but also in terms of diversity gain. On the contrary, as  $N_C$  grows, the “naive” AF approach exhibits only a slight rise in the coding gain, ensuring a diversity order  $D = N_D - N_B + 1$ , irrespective of the number of cooperating relays [54].

In Fig. 2.10 the ASEP is reported, as a function of the SNR (ranging from  $-5$  to  $30$  dB), for the naive, Statistical CSI (S-CSI), and F-CSI cases. Here,  $N_C = 2$  relays are distributed in a circle positioned on the line joining the source to the destination at distance  $d_{SC} = 0.2612$  from the source. Fig. 2.10 shows that also the performance improvement, with respect to the naive approach, achieved in the case of system optimized on a S-CSI basis is considerable. For an average SEP equal to  $10^{-3}$ ,

in fact, the S-CSI design provides a gain of approximately 10 dB with respect to the naive one. However, unlike the F-CSI design, the S-CSI approach provides, with respect to the naive case, only a performance improvement in terms of coding gain but not in terms of diversity order which, even in this case, turns out to be equal to  $N_D - N_B + 1$ .

It is worth noting that the performance improvements shown in Fig. 2.9 and Fig. 2.10 come at a certain price. Specifically, the F-CSI design can be considered only when full instantaneous CSI is available both at the source and the relays nodes. This implies that a huge amount of overhead, related to the training and feedback sequences, has to be accepted in order to perform the channel estimation. In this regard, it is useful to highlight that channel estimation is performed frequently and, consequently, the amount of overhead (per unit time) is directly proportional to the channel time variability. The S-CSI design, instead, provides performance not comparable to that of the F-CSI design but, on the other hand, it requires only a statistical knowledge of the involved channels (i.e., a path loss estimation has to be carried out), to achieve a remarkable improvement with respect to the naive approach.

## 2.6 Conclusions

In this chapter some results related to the MIMO cooperative multiple-relay systems have been presented. Firstly, an accurate approximation of the average SEP in the high-SNR regime has been obtained for a spatially multiplexed dual-hop MIMO network, with multiple AF nonorthogonal relays and linear ZF equalization at the destination. Moreover, the performance gain of the cooperative scheme over direct transmission has been assessed and, with reference to a relaying cluster, have been derived also simple formulas that allow to optimally place the relays. Then, a tight approximation for the SEP of a similar system, but in the case of MMSE equalization at the destination, has been presented without imposing any restriction on the number of relays or their positions. Finally, a framework to optimize precoding and relaying matrices in the reference system has been discussed. The design was based on approximate minimization of the average (over all spatial streams) SEP and can be expressed in closed form. Since the proposed design requires full CSI at the source and the relays, ongoing research is focused on simplified optimization procedures, where the amount of required CSI is relaxed.



## Chapter 3

# Design of cooperative multiple-relay communications over frequency selective channels corrupted by non-Gaussian noise

This chapter deals with the synthesis of receiver techniques, in cooperative multiple-relay systems, aimed at mitigating the impulsive noise, which may represent one of the predominant cause of system performance degradation. At first, we consider the case of a direct communication link between the source and destination. In particular, a SISO OFDM system employing non-linear blanking preprocessing, with the aim of mitigating the impulsive noise effects, will be considered and the design of a new equalizer will be presented. Specifically, it will be shown that, by exploiting redundancy in the OFDM signal that arises from the presence of virtual carriers (a solution adopted in several multicarrier standards), it is possible to design frequency-domain linear FIR equalizers for channels affected by impulsive noise (IN), which are able to compensate for

the intercarrier interference (ICI) introduced by a blanking nonlinearity.<sup>1</sup> In particular, a sufficient condition ensuring the existence of such a FIR ICI-free solution is derived. Moreover, it is shown that, with respect to conventional ZF receivers (with or without blanking), a performance gain can be obtained for SNR values of practical interest, with an affordable increase in computational complexity.

Then, a cooperative two-relay OFDM system employing space-time block coding will be presented to show the beneficial effects of space and time diversity in further mitigating the impulsive noise.

### 3.1 Introduction

Transceivers based on OFDM have been widely adopted in several wired and wireless standards, including digital subscriber lines [87] and power line communications [88], digital audio [89] and video broadcasting [90], IEEE 802.11 [91] and 802.16 [92], and 3G/4G long term evolution [93]. Such a success is mainly due to the capability of OFDM transceivers to efficiently equalize FIR frequency-selective channels [77]. Indeed, the use of FFT algorithms to perform DFT and its inverse (IDFT), coupled with the insertion of a CP, allows one to equalize the FIR channel by means of simple CP removal followed by one-tap frequency-domain equalization (FEQ), provided that the CP length exceeds channel dispersion.

In addition to AWGN and various transceiver implementation losses<sup>2</sup>, potential sources of performance degradation for OFDM systems operating over linear time-invariant channels include narrowband interference (NBI) and IN. Whereas NBI typically affects only a subset of subcarriers and can be rejected, e.g., by adding suitable constraints to the conventional ZF solution [94–105], *asynchronous* non-Gaussian IN [106–109], characterized by impulses occurring at the DFT input of the receiver with random arrivals, short duration, and high power, might corrupt *all* the subcarriers within an OFDM symbol and, hence, is much more difficult to counteract.<sup>3</sup> This fact has recently motivated a vast bulk of

---

<sup>1</sup>The proposed approach can be extended to other memoryless nonlinearities [18], e.g., clipping or combination of blanking and clipping.

<sup>2</sup>Including time and carrier frequency offsets between the transmitter and the receiver, analog front-end in-phase/quadrature-phase (I/Q) imbalances, and insufficient CP length.

<sup>3</sup>Another type of non-Gaussian IN consists of impulses of longer duration that occur periodically in time (so-called *periodic* IN) [110].

research regarding IN characterization and mitigation in OFDM systems (see, e.g., [18, 39, 111–117]).

A simple strategy to mitigate IN in OFDM systems consists of using at the receiver, before the DFT, a memoryless nonlinearity preprocessor (e.g., clipping, blanking, or a combination thereof) [18, 111]. However, since blanking/clipping is a nonlinear sample-by-sample operation in the time-domain, it distorts the signal constellation and, even worse, destroys orthogonality among OFDM subcarriers, thus resulting into ICI in the frequency-domain. To overcome such a problem, iterative cancellation techniques have been proposed in [112, 113], which nevertheless require *ad hoc* adjustments to avoid slow convergence. An alternative approach [116] is to introduce time diversity at the transmitter by interleaving multiple OFDM symbols after the IDFT and performing symbol-by-symbol blanking at the receiver. In this case, even though linear FIR equalization strategies, e.g., ZF or MMSE ones, can be used, channel estimation and synchronization must be acquired *before* deinterleaving. On the other hand, instead of employing nonlinear preprocessing at the receiver, it is possible to resort to advanced IN estimation and cancellation methods [114, 117], which exploit the sparsity features of noise in the time-domain. However, also in these cases, the resulting algorithms are iterative and, when compared to the conventional OFDM receiver, a significant computational burden is added.

### 3.2 Asynchronous Middleton Class A model

In this section it will be briefly described the impulsive noise model considered throughout the entire chapter. Specifically, the reference model is the well-known asynchronous Middleton Class A (MCA) model [106, 108], which will be employed in the numerical performance analysis. A MCA noise sample can be expressed as a complex RV  $x = g + i$ , where  $g$  is zero-mean circular symmetric complex Gaussian thermal noise with variance  $\sigma_g^2$ , i.e.,  $g \in \mathcal{CN}(0, \sigma_g^2)$ , whereas  $i$  models the non-Gaussian impulse noise with variance  $\sigma_i^2$ . The probability density function of  $x$  can be expressed as

$$p_x(z) = \sum_{n=0}^{+\infty} \alpha_n p_{x|n}(z|n),$$

i.e., as a weighted sum of conditionally-Gaussian probability density functions

$$p_{x|n}(z|n) \triangleq \pi^{-1} \sigma_n^{-2} \exp(-|z|^2/\sigma_n^2); z \in \mathbb{C},$$

where  $\alpha_n \triangleq e^{-\lambda} \lambda^n/n!$  is the probability that  $n$  noise pulses simultaneously occur. For any given  $n \in \mathbb{N}$ , the parameter  $\sigma_n^2$  represents the conditional variance of  $x$ , which is given by  $\sigma_n^2 = \sigma^2 \beta_n$ , where  $\sigma^2 \triangleq \sigma_g^2 + \sigma_i^2$  is the variance of  $x$ , whereas  $\beta_n \triangleq (n \lambda^{-1} + \Gamma)/(1 + \Gamma)$ , with  $\lambda > 0$  the *impulsive index* and  $\Gamma \triangleq \sigma_g^2/\sigma_i^2 > 0$  the *Gaussian ratio*. The two parameters  $\lambda$  and  $\Gamma$  control the degree of impulsiveness of the noise: for  $\lambda \ll 1$ , the noise becomes more and more impulsive; for  $\lambda \geq 1$ , the noise tends to be Gaussian. Similarly, for small values of  $\Gamma$ , the noise becomes more impulsive, while it tends to be Gaussian for large values of  $\Gamma$ . Typically, it is assumed that  $\Gamma \ll 1$  (see, e.g., [112]).

### 3.3 Non-cooperative communications over non-Gaussian channels

This contribution deals with the problem of equalizing FIR channels in OFDM systems, which employ at the receiver a blanking nonlinearity to mitigate impulsive noise. By exploiting the frequency redundancy associated with the presence of OFDM virtual carriers, it is designed a frequency-domain linear FIR equalizer that compensates for the ICI generated by nonlinear preprocessing. Monte Carlo computer simulations, carried out assuming a MCA model for the IN, allows one to assess the error probability performance of the proposed equalizer.

#### 3.3.1 OFDM system model

We consider a single-user OFDM system employing  $M$  subcarriers,  $M_{\text{uc}}$  of which are utilized, whereas the remaining  $M_{\text{vc}} \triangleq M - M_{\text{uc}} > 0$  ones are virtual carriers (VCs). The discrete-time channel between the transmitter and receiver is modeled as a causal FIR filter with impulse response  $h(n)$  ( $n \in \mathbb{Z}$ ), whose order  $L_h$  does not exceed the CP length  $L_{\text{cp}}$ , with  $h(0), h(L_h) \neq 0$ . Perfect symbol and carrier-frequency synchronization between the transmitter and receiver is assumed, and channel state information is known only at the receiver via training, but is unknown at

the transmitter. Let  $\mathbf{s} \in \mathbb{C}^{M_{uc}}$  be the data block to be transmitted<sup>4</sup> and satisfying assumption **(a1)** (see the assumptions in Table ??). Let  $\mathcal{J}_{uc} \triangleq \{q_0, q_1, \dots, q_{M_{uc}-1}\} \subset \mathcal{J} \triangleq \{0, 1, \dots, M-1\}$  collect all the indices of the used subcarriers, the symbol block  $\mathbf{s}$  is first processed by the full-column rank matrix  $\mathbf{\Theta} \in \mathbb{R}^{M \times M_{uc}}$ , which inserts the VCs in the arbitrary positions  $\mathcal{J}_{vc} \triangleq \mathcal{J} - \mathcal{J}_{uc}$ . By construction, it results that  $\mathbb{E}[\|\mathbf{\Theta} \mathbf{s}\|^2] = 1$ . Before being transmitted, the entries of  $\mathbf{\Theta} \mathbf{s} \in \mathbb{C}^M$  are subject to conventional OFDM processing, encompassing  $M$ -point IDFT followed by CP insertion. At the receiver, after discarding the CP, the time-domain block can be written [77] as

$$\mathbf{r} = \mathbf{H} \mathbf{W}_{\text{idft}} \mathbf{\Theta} \mathbf{s} + \mathbf{w} \tag{3.1}$$

where  $\mathbf{H} \in \mathbb{C}^{M \times M}$  is a circulant matrix, whose first column is represented by  $[h(0), \dots, h(L_h), 0, \dots, 0]^T$ ,  $\mathbf{W}_{\text{idft}} \in \mathbb{C}^{M \times M}$  is the unitary symmetric IDFT matrix,<sup>5</sup> and  $\mathbf{w} \in \mathbb{C}^M$  models the additive noise. With regard to the additive noise, it is assumed that  $\mathbf{w} \triangleq [w_0, w_1, \dots, w_{M-1}]^T$  is independent of  $\mathbf{s}$  and its elements are i.i.d. zero-mean RVs with variance  $\sigma^2 \triangleq \mathbb{E}[|w_m|^2]$ , modeled e.g. as MCA RVs with parameters  $\Gamma$  and  $\lambda$ .

By resorting to standard eigenstructure concepts [74], one has  $\mathbf{H} = \mathbf{W}_{\text{idft}} \mathbf{H} \mathbf{W}_{\text{dft}}$  in (3.1), where the diagonal entries of

$$\mathbf{H} \triangleq \text{diag}(H_0, H_1, \dots, H_{M-1}) \tag{3.2}$$

are the values of the transfer function  $H(z) \triangleq \sum_{n=0}^{L_h} h(n) z^{-n}$  evaluated at the subcarriers  $z_m \triangleq \exp[j(2\pi/M)m]$ , i.e.,  $H_m = H(z_m)$ ,  $\forall m \in \mathcal{J}$ . It is assumed, here, that the channel transfer function  $H(z)$  has no zero on the used subcarriers, i.e.,  $H_m \neq 0 \forall m \in \mathcal{J}_{uc}$ .

### 3.3.2 ICI analysis of sample-by-sample blanking

To mitigate the adverse effects of IN, a common strategy is to use sample-by-sample blanking preprocessing [18, 111] in the time-domain, before the conventional OFDM equalizer (i.e., before DFT and FEQ), aimed at discarding those samples of  $\mathbf{r}$  that are most contaminated by IN.

Let  $r_m$  be the  $m$ th ( $m \in \mathcal{J}$ ) sample of  $\mathbf{r}$  and  $\xi > 0$  denote a suitable threshold, the output of the blanking nonlinearity is  $\tilde{y}_m = r_m$

---

<sup>4</sup>Since all the considered processing is on a symbol-by-symbol basis, for the sake of notation simplicity, we avoid indicating the functional dependence on the symbol interval index.

<sup>5</sup>Its inverse  $\mathbf{W}_{\text{dft}} \triangleq \mathbf{W}_{\text{idft}}^{-1} = \mathbf{W}_{\text{idft}}^*$  is the DFT matrix.

if  $|r_m| \leq \xi$ ,  $\tilde{y}_m = 0$  otherwise. Let  $\mathcal{B} \triangleq \{m \in \mathcal{J} : |r_m| > \xi\} = \{m_1, m_2, \dots, m_{|\mathcal{B}|}\}$  denote the subset collecting all the indices of the blanked entries of  $\mathbf{r}$ ; the complement of  $\mathcal{B}$  with respect to  $\mathcal{J}$  is denoted by  $\overline{\mathcal{B}} = \{\overline{m}_1, \overline{m}_2, \dots, \overline{m}_{|\overline{\mathcal{B}}|}\}$ . The input-output relationship of the blanking preprocessor is  $\tilde{\mathbf{y}} \triangleq [\tilde{y}_0, \tilde{y}_1, \dots, \tilde{y}_{M-1}]^T = (\mathbf{I}_M - \mathbf{B}) \mathbf{r}$ , where  $\mathbf{B} \triangleq \text{diag}(b_0, b_1, \dots, b_{M-1})$ , with  $b_m = 1$  for  $m \in \mathcal{B}$ ,  $b_m = 0$  otherwise.

Taking into account (3.1) and the eigenstructure of  $\mathbf{H}$ , after DFT one obtains the frequency-domain block  $\mathbf{y} \triangleq \mathbf{W}_{\text{dft}} \tilde{\mathbf{y}} = \mathbf{C} \mathcal{H} \Theta \mathbf{s} + \mathbf{v}$ , where  $\mathbf{C} \triangleq \mathbf{W}_{\text{dft}} (\mathbf{I}_M - \mathbf{B}) \mathbf{W}_{\text{idft}} \in \mathbb{C}^{M \times M}$  and  $\mathbf{v} \triangleq \mathbf{W}_{\text{dft}} (\mathbf{I}_M - \mathbf{B}) \mathbf{w} \in \mathbb{C}^M$ . It can be verified that  $\mathbf{C}$  is a circulant matrix, whose diagonal entries  $\{\mathbf{C}\}_{m,m}$  for each  $m \in \mathcal{J}$  are equal to  $\{\mathbf{C}\}_{m,m} = 1 - |\mathcal{B}|/M = 1 - (M - |\overline{\mathcal{B}}|)/M = |\overline{\mathcal{B}}|/M$ , where  $|\mathcal{B}|$  and  $|\overline{\mathcal{B}}|$  denote the cardinality of  $\mathcal{B}$  and  $\overline{\mathcal{B}}$ , respectively. Consequently, vector  $\mathbf{y}$  can be rewritten as

$$\mathbf{y} = \underbrace{\frac{|\overline{\mathcal{B}}|}{M} \mathcal{H} \Theta \mathbf{s}}_{(a)} + \underbrace{\left( \mathbf{C} - \frac{|\overline{\mathcal{B}}|}{M} \mathbf{I}_M \right) \mathcal{H} \Theta \mathbf{s} + \mathbf{v}}_{(b)}. \quad (3.3)$$

The latter equation shows that the adverse effect of blanking is twofold [113]: (i) reduction of the signal amplitude by a factor  $|\overline{\mathcal{B}}|/M$ ; (ii) introduction of ICI, due to departure of  $\mathbf{C}$  from a scaled identity matrix. Indeed, if no entry of  $\mathbf{r}$  is blanked, then  $|\overline{\mathcal{B}}| = M$  and  $\mathbf{C} = \mathbf{I}_M$ . In Subsection 3.3.3, we show that these undesired effects of the nonlinearity can be compensated for by a frequency-domain linear FIR equalizer.

### 3.3.3 Frequency-domain FIR ICI-free equalization

Consider the problem of recovering the transmitted block  $\mathbf{s}$  from the blanking preprocessor output  $\mathbf{y}$  after DFT. To this purpose, we employ a frequency-domain linear FIR equalizer, defined by the input-output relationship  $\mathbf{x} = \mathbf{F} \mathbf{y}$ , with  $\mathbf{F} \in \mathbb{C}^{M_{\text{uc}} \times M}$ , followed by a minimum-distance decision device. The ICI-free condition leads to the matrix equation  $\mathbf{F} \mathbf{C} \mathcal{H} \Theta = \mathbf{I}_{M_{\text{uc}}}$ . Such an equation is consistent (i.e., it admits at least one solution) if and only if (iff)  $(\mathbf{C} \mathcal{H} \Theta)^- (\mathbf{C} \mathcal{H} \Theta) = \mathbf{I}_{M_{\text{uc}}}$ , with  $(\cdot)^-$  denoting the generalized (1)-inverse [79]. This condition is fulfilled<sup>6</sup> if

<sup>6</sup> Also the performance of the MMSE equalizer depends on the existence of ICI-free solutions: if  $\text{rank}(\mathbf{C} \mathcal{H} \Theta) \neq M_{\text{uc}}$ , the error probability performance curve of the MMSE equalizer exhibits a floor when  $\sigma^2 \rightarrow 0$  [118, 119].

$\mathbf{C}\mathcal{H}\Theta$  is full-column rank, i.e.,  $\text{rank}(\mathbf{C}\mathcal{H}\Theta) = M_{\text{uc}}$ . Under this assumption, the *minimal norm* [79] solution of  $\mathbf{F}\mathbf{C}\mathcal{H}\Theta = \mathbf{I}_{M_{\text{uc}}}$  is given by  $\mathbf{F}_{\text{ICI-free}} = (\mathbf{C}\mathcal{H}\Theta)^\dagger$ .

### Sufficient condition for the existence of ICI-free solutions

We investigate whether  $\text{rank}(\mathbf{C}\mathcal{H}\Theta) = M_{\text{uc}}$  is satisfied, which is a sufficient condition for the existence of ICI-free solutions. To this aim, we provide the following Theorem.

**Theorem 3** (Existence of ICI-free solutions). *The matrix  $\mathbf{C}\mathcal{H}\Theta$  is full-column rank iff  $[\mathcal{H}\Theta, \mathbf{W}_{\text{dft}}\Psi] \in \mathbb{C}^{M \times (M_{\text{uc}} + |\mathcal{B}|)}$  is full-column rank, where  $\Psi \triangleq [\mathbf{1}_{m_1}, \mathbf{1}_{m_2}, \dots, \mathbf{1}_{m_{|\mathcal{B}|}}] \in \mathbb{R}^{M \times |\mathcal{B}|}$ , with  $\mathbf{1}_m \in \mathbb{R}^M$  denoting the  $(m+1)$ th column of  $\mathbf{I}_M$ .*

**Proof.** See App. E.

Some remarks are now in order. First, perfect ICI suppression may not be achieved, i.e.,  $\mathbf{C}\mathcal{H}\Theta$  might not be full-column rank, even if the channel transfer function  $H(z)$  has no zero on the used subcarriers [see assumption **(a3)**]. This is due to the fact that the blanking preprocessor introduces ICI in the frequency-domain signal. Only when no entry of  $\mathbf{r}$  is blanked, assumption **(a3)** is sufficient for ensuring the existence of ICI-free solutions. Second, the fact that some entries of  $\mathbf{r}$  are blanked does not prevent perfect ICI compensation. This result stems from the fact that the blanking preprocessor operates in the time-domain (i.e., before the DFT), where each entry of  $\mathbf{r}$  is a (noisy) linear combination of all the entries of  $\mathbf{s}$ . Therefore, if the  $(m_i)$ -th sample is blanked, i.e.,  $b_{m_i} = 1$ , the vector  $\mathbf{s}$  can still be recovered from the other entries of  $\mathbf{r}$ . Third, condition  $\text{rank}(\mathbf{C}\mathcal{H}\Theta) = M_{\text{uc}}$  amounts to  $\text{rank}([\mathcal{H}\Theta, \mathbf{W}_{\text{dft}}\Psi]) = M_{\text{uc}} + |\mathcal{B}|$ , which necessarily requires that  $M \geq M_{\text{uc}} + |\mathcal{B}|$  or, equivalently,  $M_{\text{vc}} \geq |\mathcal{B}|$ . Thus, the number  $M_{\text{vc}}$  of VCs also represents the maximum number of entries of  $\mathbf{r}$  that can be blanked without preventing perfect ICI compensation.

Finally, Theorem 3 does not allow one to determine the threshold  $\xi$  (or, equivalently, the blanking subset  $\mathcal{B}$ ), whose choice nevertheless affects the symbol-error-rate (SER) performance of the receiver. Since closed-form analytical evaluation of SER as a function of  $\xi$  is a challenging problem<sup>7</sup>, we explore the impact of  $\xi$  on SER performance and discuss its choice in Subsection 3.3.4 by numerical experiments.

<sup>7</sup> In principle, following [18, 111], one may choose  $\xi$  so as to maximize the signal-

### Computational complexity

The computational complexity of the  $\mathbf{F}_{\text{ICI-free}}$  equalizer is dominated by calculation of the Moore-Penrose generalized inverse of  $\mathbf{C}\mathcal{H}\Theta$ . To evaluate such a complexity, observe that the matrix  $\mathbf{C}\mathcal{H}\Theta$  is obtained from  $\mathbf{C}\mathcal{H} = [\zeta_0, \zeta_1, \dots, \zeta_{M-1}]$  by picking its columns  $\zeta_q \in \mathbb{C}^M$  located on the used subcarrier positions, i.e., for  $q \in \mathcal{J}_{\text{uc}}$ . It results that  $\zeta_q = H_q \sum_{\bar{m} \in \bar{\mathcal{B}}} z_{q\bar{m}} \chi_{\bar{m}}$ , where  $\chi_{\bar{m}} \triangleq (1/M)[1, z_{\bar{m}}, z_{2\bar{m}} \dots, z_{(M-1)\bar{m}}]^H \in \mathbb{C}^M$ . Let  $\mathbf{e}_q \triangleq [z_{q\bar{m}_1}, z_{q\bar{m}_2} \dots, z_{q\bar{m}_{|\bar{\mathcal{B}}|}}]^T \in \mathbb{C}^{|\bar{\mathcal{B}}|}$ , one has  $\mathbf{C}\mathcal{H}\Theta = \mathbf{\Omega}\mathbf{E}\mathcal{H}_{\text{uc}}$ , with  $\mathbf{\Omega} \triangleq [\chi_{\bar{m}_1}, \chi_{\bar{m}_2}, \dots, \chi_{\bar{m}_{|\bar{\mathcal{B}}|}}] \in \mathbb{C}^{M \times |\bar{\mathcal{B}}|}$ ,  $\mathbf{E} \triangleq [\mathbf{e}_{q_0}, \mathbf{e}_{q_1}, \dots, \mathbf{e}_{q_{M_{\text{uc}}-1}}] \in \mathbb{C}^{|\bar{\mathcal{B}}| \times M_{\text{uc}}}$ , and  $\mathcal{H}_{\text{uc}} \triangleq \text{diag}(H_{q_0}, H_{q_1}, \dots, H_{q_{M_{\text{uc}}-1}})$ . Since  $\mathcal{H}_{\text{uc}}$  is non-singular by virtue of assumption **(a3)** and  $\mathbf{\Omega}\mathbf{E}$  is full-column rank by construction, i.e.,  $\text{rank}(\mathbf{\Omega}\mathbf{E}) = M_{\text{uc}}$ , it results [79] that  $\mathbf{F}_{\text{ICI-free}} = \mathcal{H}_{\text{uc}}^{-1}(\mathbf{\Omega}\mathbf{E})^\dagger = M\mathcal{H}_{\text{uc}}^{-1}\mathbf{E}^\dagger\mathbf{\Omega}^H$ , where we additionally used the fact that  $\mathbf{\Omega}^H\mathbf{\Omega} = (1/M)\mathbf{I}_{|\bar{\mathcal{B}}|}$ . Compared to the conventional OFDM receiver, the increase in computational complexity for the proposed ICI-free equalizer is due to the calculus of  $\mathbf{E}^\dagger$ . It can be verified that  $\mathbf{E}$  is a polynomial Vandermonde matrix [120] with basis polynomials  $P_j(x) = x^{q_j}$ , for  $x \in \mathbb{C}$  and  $j \in \{0, 1, \dots, M_{\text{uc}} - 1\}$ , and node points  $t_i = z_{m_i}$ , for  $j \in \{1, 2, \dots, |\bar{\mathcal{B}}|\}$ .<sup>8</sup> Thus, the matrix  $\mathbf{E}^\dagger$  can be calculated [120] by special fast or superfast algorithms in  $\mathcal{O}(M^2)$  or  $\mathcal{O}(M \log^2(M))$  floating point operations, respectively.

### 3.3.4 Numerical performance analysis

The average SER (ASER) performance of the proposed ICI-free receiver (referred to as “Blanking + ICI comp.”) was assessed by means of Monte Carlo computer simulations. As a comparison, we also evaluated the ASER performance of: (i) the receiver with blanking nonlinearity followed by conventional ZF equalization, i.e.,  $\mathbf{F}_{\text{zf}} = (\mathcal{H}\Theta)^\dagger$  (referred to as “Blanking”); (ii) the conventional OFDM receiver without any nonlinearity preprocessing and ZF equalization (referred to as “Conventional”). With reference to the proposed equalizer, according to Theorem 3, only the  $M_{\text{vc}}$  entries of  $\mathbf{r}$  with largest magnitudes are blanked if  $|\bar{\mathcal{B}}| > M_{\text{vc}}$ .

---

to-interference-plus-noise ratio (SINR) at the equalizer output, which is simpler to evaluate. However, since the IN is non-Gaussian, SINR maximization is no longer equivalent to SER minimization.

<sup>8</sup>According to Theorem 3, one has  $|\bar{\mathcal{B}}| \geq M_{\text{uc}}$  and  $\text{rank}(\mathbf{E}) = M_{\text{uc}}$ .

Regarding the simulation setup, we considered an OFDM system with  $M = 32$  subcarriers and a CP length  $L_{\text{cp}} = 8$ . The system employs  $M_{\text{vc}} = 8$  VCs, all located at the edges of the OFDM spectrum, and Gray-labeled 4-QAM signaling for the  $M_{\text{uc}} = 24$  utilized subcarriers.<sup>9</sup> The channel impulse response was chosen according to the channel model HiperLAN/2 A (see [121] for details). The MCA impulsive noise was generated by using a modified version of the Matlab toolbox in [122]. We considered a *highly-impulsive* noise scenario (i.e.,  $\lambda = 10^{-3}$ ,  $\Gamma = 10^{-1}$ ).

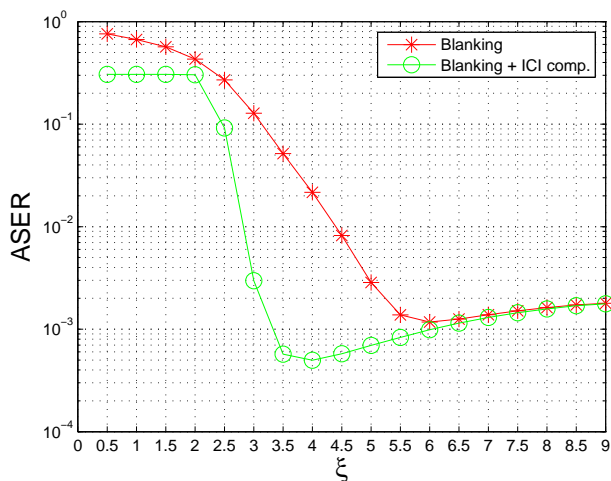


Figure 3.1: ASER vs  $\xi$  with SNR equal to 15 dB.

Fig. 3.1 and Fig 3.2 report the performance of the two receivers with blanking as a function of the threshold  $\xi$ , with  $\text{SNR} \triangleq 1/\sigma^2 \in \{15, 25\}$  dB. Results show that, as expected, the performance of both receivers depends on the value of the blanking threshold. However, the “Blanking + ICI comp.” receiver outperforms the “Blanking” one for all the considered values of  $\xi$ , except for very large values of  $\xi$  when the entries of  $\mathbf{r}$  are not blanked with high probability and, then, the ICI-free equalizer  $\mathbf{F}_{\text{ICI-free}}$  boils down to the conventional ZF equalization matrix  $\mathbf{F}_{\text{zf}}$ . The ASER performances of all the considered receivers are depicted in Fig. 3.3 as a function of the SNR. With regard to the receivers employing blanking, we chose the value of  $\xi$  minimizing the ASER, for each SNR value. It can be seen that, compared to the conventional OFDM

<sup>9</sup>We performed simulations using a 16-QAM constellation, whose ASER curves are not reported since they show trends similar to the 4-QAM case.

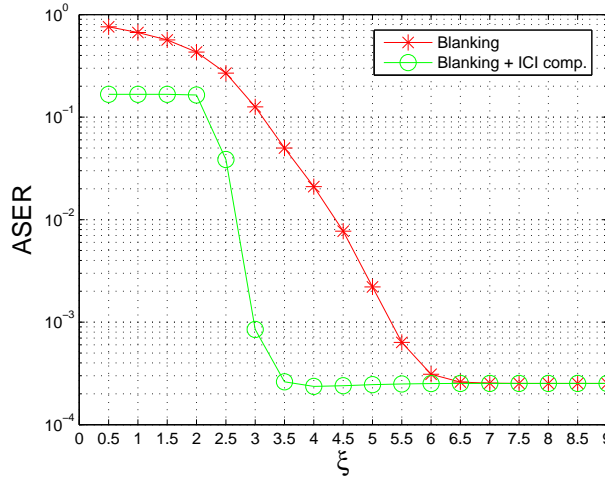


Figure 3.2: ASER vs  $\xi$  with SNR equal to 25 dB.

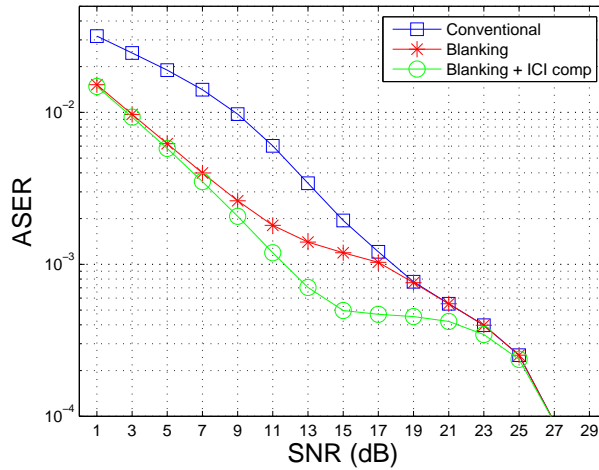


Figure 3.3: ASER vs SNR with  $\xi$  optimally chosen for each SNR value.

receiver, employing a blanking preprocessing allows one to remarkably improve performances, except for large values of the SNR, for which blanking becomes unlikely and, thus, all the three receivers tend to coincide. Remarkably, the “Blanking + ICI comp.” receiver outperforms the “Blanking” one for SNR values of practical interest, ranging from 10

to 20 dB. For instance, for an ASER value of  $10^{-3}$ , the “Blanking + ICI comp.” receiver ensures an SNR gain of about 6 dB with respect to the “Blanking” and “Conventional” ones.

### 3.4 Cooperative communications over non-Gaussian channels

In this section we consider a cooperative OFDM system, employing space-time block coding (STBC). As in the previous section, the destination performs a blanking preprocessing in order to mitigate the adverse effects of the impulsive noise. The goal is to show the impact of the considered distributed STBC (DSTBC) technique on the performance of the system under investigation, by comparison with those of the direct communication. To assess the gain obtained, Monte Carlo computer simulations have been carried out assuming an MCA model for the IN.

#### 3.4.1 Network model

The considered cooperative network refers to the general topology of Section 2.2 and, therefore, is composed by a source-destination pair and a certain number of relay nodes indexed by  $i \in \mathcal{I} \triangleq \{1, 2, \dots, N_C\}$ , where  $N_C \in \{2, 3\}$ . All the nodes are equipped with a single antenna and employ OFDM. Relays adopt the DF cooperative approach so that we assume perfect symbol recovery after the first hop and describe, therefore, only the processing carried out in the second (medium access - MAC) phase of the cooperative protocol. Once the relays have recovered the length- $M_{uc}$  OFDM symbols,  $\mathbf{s}_1$  and  $\mathbf{s}_2$ , transmitted by the source within two subsequent symbol intervals, they add to each symbol  $M_{vc}$  virtual carriers, thus obtaining  $\tilde{\mathbf{s}}_1 = \Theta \mathbf{s}_1$  and  $\tilde{\mathbf{s}}_2 = \Theta \mathbf{s}_2$ , where  $\Theta$  represents the VCs insertion matrix. These represent the OFDM *extended* symbols to be transmitted by the relay nodes, toward the destination, according to an Alamouti DSTBC scheme. In the following, we consider both the centralized and decentralized schemes for the Alamouti DSTBC implemented with  $N_C = 2$  and  $N_C = 3$  relay nodes over a number of time slots equal to  $T_{code}$ , which we refer to as *supersymbol interval*. In particular, we consider the  $2 \times 2$  configuration (i.e., the original Alamouti code over two transmit antennas and two transmission time slots), and the  $4 \times 3$  configuration of the Alamouti code (i.e., the generalized Alamouti code over three transmit antennas and four transmission time slots). Moreover, since the processing will be carried out on a supersymbol by supersymbol basis, the following discussion will be related to a generic time interval of duration  $T_{code}$  by omitting, for the sake notation simplicity, the supersymbol time index.

### Centralized scheme - $N_C = 2$

In the centralized case we assume that all the relays are aware of the symbol to be transmitted in the current time slot.

For  $N_C = 2$ , according to the original work of Alamouti [123], the considered space-time scheduling is reported in Table 3.1 whose code rate is  $R_{\text{code}} = 1$  and where  $T_{\text{code}} = 2$ .

Table 3.1: Space-time transmission scheduling for  $N_C = 2$

	Relay 1	Relay 2
<b>time slot 1</b>	$\tilde{s}_1$	$\tilde{s}_2$
<b>time slot 2</b>	$-\tilde{s}_2^*$	$\tilde{s}_1^*$

Consequently, the time-domain symbols received by the destination, within the supersymbol interval, assume the following form:

$$\begin{aligned}
 \text{(time slot 1)} \quad \mathbf{r}_1 &= \mathbf{G}_1 \mathbf{W}_{\text{idft}} \tilde{s}_1 + \mathbf{G}_2 \mathbf{W}_{\text{idft}} \tilde{s}_2 + \mathbf{w}_1 \\
 \text{(time slot 2)} \quad \mathbf{r}_2 &= \mathbf{G}_2 \mathbf{W}_{\text{idft}} \tilde{s}_1^* - \mathbf{G}_1 \mathbf{W}_{\text{idft}} \tilde{s}_2^* + \mathbf{w}_2 \quad (3.4)
 \end{aligned}$$

Then, according to the Alamouti combining scheme, one can write

$$\begin{aligned}
 \tilde{\mathbf{r}} &= \begin{bmatrix} \mathbf{r}_1 \\ \mathbf{r}_2^* \end{bmatrix} = \begin{bmatrix} \mathbf{G}_1 \mathbf{W}_{\text{idft}} \Theta & \mathbf{G}_2 \mathbf{W}_{\text{idft}} \Theta \\ \mathbf{G}_2^* \mathbf{W}_{\text{dft}} \Theta & -\mathbf{G}_1^* \mathbf{W}_{\text{dft}}^* \Theta \end{bmatrix} \begin{bmatrix} \mathbf{s}_1 \\ \mathbf{s}_2 \end{bmatrix} + \begin{bmatrix} \mathbf{w}_1 \\ \mathbf{w}_2^* \end{bmatrix} \\
 &= \begin{bmatrix} \mathbf{W}_{\text{idft}} \mathcal{G}_1 \Theta & \mathbf{W}_{\text{idft}} \mathcal{G}_2 \Theta \\ \mathbf{W}_{\text{dft}} \mathcal{G}_2^* \Theta & -\mathbf{W}_{\text{dft}} \mathcal{G}_1^* \Theta \end{bmatrix} \begin{bmatrix} \mathbf{s}_1 \\ \mathbf{s}_2 \end{bmatrix} + \begin{bmatrix} \mathbf{w}_1 \\ \mathbf{w}_2^* \end{bmatrix} \quad (3.5)
 \end{aligned}$$

where  $\mathcal{G}_i \triangleq \mathbf{W}_{\text{dft}} \mathbf{G}_i \mathbf{W}_{\text{idft}}$ ,  $\forall i \in \mathcal{I}_2 \triangleq \{1, 2\}$ . At this point, similarly to the direct link case previously treated, a blanking non-linear preprocessing is performed at the destination. Let  $\mathcal{J} \triangleq \{0, 1, \dots, M-1\}$ ,  $r_{t,m}$  be the  $m$ -th ( $m \in \mathcal{J}$ ) sample of  $\tilde{\mathbf{r}}$  associated to the  $t$ -th ( $t \in \mathcal{T}_2 \triangleq \{1, 2\}$ ) time slot and  $\xi > 0$  denote a suitable threshold, the output of the blanking nonlinearity,  $\forall t \in \mathcal{T}_2$  and  $\forall m \in \mathcal{J}$ , is

$$\tilde{y}_{t,m} = \begin{cases} r_{t,m} & \text{if } |r_{t,m}| \leq \xi \\ 0 & \text{otherwise} \end{cases} \quad (3.6)$$

Let  $\mathcal{B}_t \triangleq \{m \in \mathcal{J} : |r_{t,m}| > \xi\} = \{m_1, m_2, \dots, m_{|\mathcal{B}_t|}\}$  denote the subset collecting all the indices of the blanked entries of  $\mathbf{r}_t$ ,  $\forall t \in \mathcal{T}_2$ ; the complement of  $\mathcal{B}_t$  with respect to  $\mathcal{J}$  is denoted by  $\overline{\mathcal{B}}_t = \{\overline{m}_1, \overline{m}_2, \dots, \overline{m}_{|\overline{\mathcal{B}}_t|}\}$ .

The input-output relationship of the blanking preprocessor is

$$\tilde{\mathbf{y}} \triangleq [\tilde{y}_{1,0}, \tilde{y}_{1,1}, \dots, \tilde{y}_{1,M-1}, \tilde{y}_{2,0}, \dots, \tilde{y}_{2,M-1}]^T = (\mathbf{I}_{2M} - \mathbf{B}) \tilde{\mathbf{r}}, \quad (3.7)$$

where  $\mathbf{B} \triangleq \text{blkdiag}(\mathbf{B}_1, \mathbf{B}_2)$ ,  $\mathbf{B}_1 \triangleq \text{diag}(b_{1,0}, b_{1,1}, \dots, b_{1,M-1})$ , and  $\mathbf{B}_2 \triangleq \text{diag}(b_{2,0}, b_{2,1}, \dots, b_{2,M-1})$ , with  $b_{t,m} = 1$  for  $m \in \mathcal{B}_t$  and  $b_{t,m} = 0$  otherwise, for  $t \in \mathcal{T}_2$ . The output of the blanking non-linearity turns out to be

$$\tilde{\mathbf{y}} = (\mathbf{I}_{2M} - \mathbf{B}) \tilde{\mathbf{r}} = \begin{bmatrix} (\mathbf{I}_M - \mathbf{B}_1) \mathbf{r}_1 \\ (\mathbf{I}_M - \mathbf{B}_2) \mathbf{r}_2^* \end{bmatrix} \quad (3.8)$$

whose frequency-domain version is

$$\begin{aligned} \mathbf{y} &= \begin{bmatrix} \mathbf{W}_{\text{dft}} (\mathbf{I}_M - \mathbf{B}_1) \mathbf{r}_1 \\ \mathbf{W}_{\text{dft}}^* (\mathbf{I}_M - \mathbf{B}_2) \mathbf{r}_2^* \end{bmatrix} \\ &= \begin{bmatrix} \mathbf{C}_1 \mathcal{G}_1 \Theta & \mathbf{C}_1 \mathcal{G}_2 \Theta \\ \mathbf{C}_2 \mathcal{G}_2^* \Theta & -\mathbf{C}_2 \mathcal{G}_1^* \Theta \end{bmatrix} \begin{bmatrix} \mathbf{s}_1 \\ \mathbf{s}_2 \end{bmatrix} + \begin{bmatrix} \mathbf{v}_1 \\ \mathbf{v}_2 \end{bmatrix} \\ &\triangleq \mathbf{C}_{c2} \mathbf{s} + \mathbf{v}. \end{aligned} \quad (3.9)$$

where  $\mathbf{C}_1 \triangleq \mathbf{W}_{\text{dft}} (\mathbf{I}_M - \mathbf{B}_1) \mathbf{W}_{\text{idft}}$ ,  $\mathbf{C}_2 \triangleq \mathbf{W}_{\text{idft}} (\mathbf{I}_M - \mathbf{B}_2) \mathbf{W}_{\text{dft}}$ ,  $\mathbf{v}_1 \triangleq \mathbf{W}_{\text{dft}} (\mathbf{I}_M - \mathbf{B}_1) \mathbf{w}_1$ , and  $\mathbf{v}_2 \triangleq \mathbf{W}_{\text{idft}} (\mathbf{I}_M - \mathbf{B}_2) \mathbf{w}_1^*$ .

Finally, to recover the transmitted block  $\mathbf{s}$ , a ZF equalizer, followed by a minimum distance detector, can be considered if and only if the equivalent channel matrix  $\mathbf{C}_{c2}$  is full-column rank. Therefore, when  $\text{rank}(\mathbf{C}_{c2}) = 2M_{\text{uc}}$ , the ZF solution exists and the corresponding equalizer can be written as  $\mathbf{F}_{c2} = \mathbf{C}_{c2}^\dagger$ .

### Centralized scheme - $N_C = 3$

Now, we consider the case of  $N_C = 3$ , where  $R_{\text{code}} = 3/4$  and  $T_{\text{code}} = 3$ . The corresponding space-time scheduling is reported in Table 3.2

Table 3.2: Space-time transmission scheduling for  $N_C = 3$

	Relay 1	Relay 2	Relay 3
time slot 1	$\tilde{\mathbf{s}}_1$	$\tilde{\mathbf{s}}_2$	$\tilde{\mathbf{s}}_3$
time slot 2	$-\tilde{\mathbf{s}}_2^*$	$\tilde{\mathbf{s}}_1^*$	$\mathbf{0}$
time slot 3	$-\tilde{\mathbf{s}}_3^*$	$\mathbf{0}$	$\tilde{\mathbf{s}}_1^*$
time slot 4	$\mathbf{0}$	$-\tilde{\mathbf{s}}_3^*$	$\tilde{\mathbf{s}}_2^*$

and the time-domain symbols received by the destination, within the supersymbol interval, are the following:

$$\begin{aligned}
 (\text{time slot 1}) \quad \mathbf{r}_1 &= \mathbf{G}_1 \mathbf{W}_{\text{idft}} \tilde{\mathbf{s}}_1 + \mathbf{G}_2 \mathbf{W}_{\text{idft}} \tilde{\mathbf{s}}_2 + \mathbf{G}_3 \mathbf{W}_{\text{idft}} \tilde{\mathbf{s}}_3 + \mathbf{w}_1 \\
 (\text{time slot 2}) \quad \mathbf{r}_2 &= \mathbf{G}_2 \mathbf{W}_{\text{idft}} \tilde{\mathbf{s}}_1^* - \mathbf{G}_1 \mathbf{W}_{\text{idft}} \tilde{\mathbf{s}}_2^* + \mathbf{w}_2 \\
 (\text{time slot 3}) \quad \mathbf{r}_3 &= \mathbf{G}_3 \mathbf{W}_{\text{idft}} \tilde{\mathbf{s}}_1^* - \mathbf{G}_1 \mathbf{W}_{\text{idft}} \tilde{\mathbf{s}}_3^* + \mathbf{w}_3 \\
 (\text{time slot 4}) \quad \mathbf{r}_4 &= \mathbf{G}_3 \mathbf{W}_{\text{idft}} \tilde{\mathbf{s}}_2^* - \mathbf{G}_2 \mathbf{W}_{\text{idft}} \tilde{\mathbf{s}}_3^* + \mathbf{w}_4
 \end{aligned} \tag{3.10}$$

Moreover, similarly to the case for  $N_C = 2$ , the combined received block is

$$\begin{aligned}
 \tilde{\mathbf{r}} &= [\mathbf{r}_1^T \mathbf{r}_2^H \mathbf{r}_3^H \mathbf{r}_4^H]^T \\
 &= \begin{bmatrix} \mathbf{W}_{\text{idft}} \mathcal{G}_1 \Theta & \mathbf{W}_{\text{idft}} \mathcal{G}_2 \Theta & \mathbf{W}_{\text{idft}} \mathcal{G}_3 \Theta \\ \mathbf{W}_{\text{dft}} \mathcal{G}_2^* \Theta & -\mathbf{W}_{\text{dft}} \mathcal{G}_1^* \Theta & \mathbf{O} \\ \mathbf{W}_{\text{dft}} \mathcal{G}_3^* \Theta & \mathbf{O} & -\mathbf{W}_{\text{dft}} \mathcal{G}_1^* \Theta \\ \mathbf{O} & \mathbf{W}_{\text{dft}} \mathcal{G}_3^* \Theta & -\mathbf{W}_{\text{dft}} \mathcal{G}_2^* \Theta \end{bmatrix} \begin{bmatrix} \mathbf{s}_1 \\ \mathbf{s}_2 \\ \mathbf{s}_3 \end{bmatrix} + \begin{bmatrix} \mathbf{w}_1 \\ \mathbf{w}_2^* \\ \mathbf{w}_3^* \\ \mathbf{w}_4^* \end{bmatrix}
 \end{aligned} \tag{3.11}$$

where  $\mathcal{G}_i, \forall i \in \mathcal{I}_3 \triangleq \{1, 2, 3\}$ , are defined as in the case  $N_C = 2$ .

Finally, the frequency-domain output of the blanking preprocessor turns out to be

$$\begin{aligned}
 \mathbf{y} &= \begin{bmatrix} \mathbf{C}_1 \mathcal{G}_1 \Theta & \mathbf{C}_1 \mathcal{G}_2 \Theta & \mathbf{C}_3 \mathcal{G}_2 \Theta \\ \mathbf{C}_2 \mathcal{G}_2^* \Theta & -\mathbf{C}_2 \mathcal{G}_1^* \Theta & \mathbf{O} \\ \mathbf{C}_3 \mathcal{G}_3^* \Theta & \mathbf{O} & -\mathbf{C}_3 \mathcal{G}_1^* \Theta \\ \mathbf{O} & \mathbf{C}_4 \mathcal{G}_3^* \Theta & -\mathbf{C}_4 \mathcal{G}_2^* \Theta \end{bmatrix} \begin{bmatrix} \mathbf{s}_1 \\ \mathbf{s}_2 \\ \mathbf{s}_3 \end{bmatrix} + \begin{bmatrix} \mathbf{v}_1 \\ \mathbf{v}_2 \\ \mathbf{v}_3 \\ \mathbf{v}_4 \end{bmatrix} \\
 &\triangleq \mathbf{C}_{c3} \mathbf{s} + \mathbf{v}.
 \end{aligned} \tag{3.12}$$

where  $\mathbf{C}_1 \triangleq \mathbf{W}_{\text{dft}} (\mathbf{I}_M - \mathbf{B}_1) \mathbf{W}_{\text{idft}}$ ,  $\mathbf{v}_1 \triangleq \mathbf{W}_{\text{dft}} (\mathbf{I}_M - \mathbf{B}_1) \mathbf{w}_1$ ,  $\mathbf{C}_t \triangleq \mathbf{W}_{\text{idft}} (\mathbf{I}_M - \mathbf{B}_t) \mathbf{W}_{\text{dft}}$ , and  $\mathbf{v}_t \triangleq \mathbf{W}_{\text{idft}} (\mathbf{I}_M - \mathbf{B}_t) \mathbf{w}_t^*, \forall t \in \mathcal{T}_3 \triangleq \{2, 3, 4\}$ . In this case, by ensuring that  $\text{rank}(\mathbf{C}_{c3}) = 3M_{\text{uc}}$ , the ZF equalizers can be designed as  $\mathbf{F}_{c3} = \mathbf{C}_{c3}^\dagger$ .

### Decentralized scheme - $N_C = 2$

Let us consider the general case of a STBC over  $N_C$  relays and  $T_{\text{code}}$  time slots, and the corresponding generalized Alamouti code. With the decentralized scheme, each relay node transmits a vector whose generic  $t$ -th entry,  $\forall t \in \mathcal{T}_{\text{code}} \triangleq \{1, 2, \dots, T_{\text{code}}\}$ , turns out to be the linear combination of the symbols belonging to the  $t$ -th row of the code. Therefore,

the  $i$ -th relay node,  $\forall i \in \{1, 2, \dots, N_C\}$ , chooses its own  $N_C$  random coefficients, gathered in the vector  $\mathbf{a}_i \triangleq [a_{i,1}, a_{i,2} \dots a_{i,N_C}]^T$ , in a random and independent (from the other relay nodes) fashion. This way, unlike the centralized case, relays have not to be aware of the symbol to be transmitted in a specific time slot.

When  $N_C = 2$ , the distributed space-time scheduling turns out to be the result of the following processing flow

$$\begin{bmatrix} \tilde{s}_1 \\ \tilde{s}_2 \end{bmatrix} \longrightarrow \mathcal{A}_2 \triangleq \begin{bmatrix} \tilde{s}_1 & \tilde{s}_2 \\ -\tilde{s}_2^* & \tilde{s}_1^* \end{bmatrix} \quad (3.13)$$

$$\mathcal{A}_2 \longrightarrow \mathcal{A}_2 \begin{bmatrix} a_{i,1} \\ a_{i,2} \end{bmatrix} = \begin{bmatrix} a_{i,1} \tilde{s}_1 + a_{i,2} \tilde{s}_2 \\ -a_{i,1} \tilde{s}_2^* + a_{i,2} \tilde{s}_1^* \end{bmatrix}, \forall i \in \mathcal{I}_2, \quad (3.14)$$

where (3.13) indicates the application of the  $2 \times 2$  Alamouti DSTBC, while (3.14) corresponds to the randomization task which is the key mechanism to ensure a decentralized behavior. Similarly to the centralized case for  $N_C = 2$ , the time-domain symbols received by the destination, within the supersymbol interval, are the following:

$$\begin{aligned} \text{(time slot 1)} \quad \mathbf{r}_1 &= \mathbf{W}_{\text{idft}} \mathcal{G}_{1,d} \tilde{s}_1 + \mathbf{W}_{\text{idft}} \mathcal{G}_{2,d} \tilde{s}_2 + \mathbf{w}_1 \\ \text{(time slot 2)} \quad \mathbf{r}_2 &= \mathbf{W}_{\text{idft}} \mathcal{G}_{2,d} \tilde{s}_1^* - \mathbf{W}_{\text{idft}} \mathcal{G}_{1,d} \tilde{s}_2^* + \mathbf{w}_2 \end{aligned} \quad (3.15)$$

where  $\mathcal{G}_{1,d} \triangleq (a_{1,1} \mathcal{G}_1 + a_{2,1} \mathcal{G}_2)$  and  $\mathcal{G}_{2,d} \triangleq (a_{1,2} \mathcal{G}_1 + a_{2,2} \mathcal{G}_2)$ . Consequently, the combined time-domain received signal can be written as

$$\begin{aligned} \tilde{\mathbf{r}} &= [\mathbf{r}_1^T \mathbf{r}_2^H]^T \\ &= \begin{bmatrix} \mathbf{W}_{\text{idft}} \mathcal{G}_{1,d} \Theta & \mathbf{W}_{\text{idft}} \mathcal{G}_{2,d} \Theta \\ \mathbf{W}_{\text{dft}} \mathcal{G}_{2,d}^* \Theta & -\mathbf{W}_{\text{dft}} \mathcal{G}_{1,d}^* \Theta \end{bmatrix} \begin{bmatrix} \mathbf{s}_1 \\ \mathbf{s}_2 \end{bmatrix} + \begin{bmatrix} \mathbf{w}_1 \\ \mathbf{w}_2^* \end{bmatrix}, \end{aligned} \quad (3.16)$$

while the frequency-domain output of the non-linear blanking processor is

$$\begin{aligned} \mathbf{y} &= \begin{bmatrix} \mathbf{W}_{\text{dft}} (\mathbf{I}_M - \mathbf{B}_1) \mathbf{r}_1 \\ \mathbf{W}_{\text{dft}}^* (\mathbf{I}_M - \mathbf{B}_2) \mathbf{r}_2^* \end{bmatrix} \\ &= \begin{bmatrix} \mathbf{C}_1 \mathcal{G}_{1,d} \Theta & \mathbf{C}_1 \mathcal{G}_{2,d} \Theta \\ \mathbf{C}_2 \mathcal{G}_{2,d}^* \Theta & -\mathbf{C}_2 \mathcal{G}_{1,d}^* \Theta \end{bmatrix} \begin{bmatrix} \mathbf{s}_1 \\ \mathbf{s}_2 \end{bmatrix} + \begin{bmatrix} \mathbf{v}_1 \\ \mathbf{v}_2 \end{bmatrix} \\ &\triangleq \mathbf{C}_{d2} \mathbf{s} + \mathbf{v}, \end{aligned} \quad (3.17)$$

with  $\mathbf{C}_1$ ,  $\mathbf{C}_2$ ,  $\mathbf{v}_1$ , and  $\mathbf{v}_2$  already defined. In this case,  $\text{rank}(\mathbf{C}_{d2}) = 2 M_{\text{uc}}$  implies  $\mathbf{F}_{d2} = \mathbf{C}_{d2}^\dagger$ .

**Decentralized scheme -  $N_C = 3$** 

When  $N_C = 3$ , the distributed space-time scheduling turns out to be the result of the following processing flow

$$\begin{bmatrix} \tilde{\mathbf{s}}_1 \\ \tilde{\mathbf{s}}_2 \\ \tilde{\mathbf{s}}_3 \end{bmatrix} \rightarrow \mathcal{A}_3 \triangleq \begin{bmatrix} \tilde{\mathbf{s}}_1 & \tilde{\mathbf{s}}_2 & \tilde{\mathbf{s}}_3 \\ -\tilde{\mathbf{s}}_2^* & \tilde{\mathbf{s}}_1^* & \mathbf{0} \\ -\tilde{\mathbf{s}}_3^* & \mathbf{0} & \tilde{\mathbf{s}}_1^* \\ \mathbf{0} & -\tilde{\mathbf{s}}_3^* & \tilde{\mathbf{s}}_2^* \end{bmatrix} \quad (3.18)$$

$$\mathcal{A}_3 \rightarrow \mathcal{A}_3 \begin{bmatrix} a_{i,1} \\ a_{i,2} \\ a_{i,3} \end{bmatrix} = \begin{bmatrix} \sum_{j=1}^{N_C} a_{i,j} \tilde{\mathbf{s}}_j \\ -a_{i,1} \tilde{\mathbf{s}}_2^* + a_{i,2} \tilde{\mathbf{s}}_1^* \\ -a_{i,1} \tilde{\mathbf{s}}_3^* + a_{i,3} \tilde{\mathbf{s}}_1^* \\ -a_{i,2} \tilde{\mathbf{s}}_3^* + a_{i,3} \tilde{\mathbf{s}}_2^* \end{bmatrix}, \forall i \in \mathcal{I}_3, \quad (3.19)$$

where (3.18) indicates the application of the  $4 \times 3$  Alamouti DSTBC, while (3.19) corresponds to the randomization task. Similarly to the case for  $N_C = 2$ , the combined received signal can be written as

$$\begin{aligned} \tilde{\mathbf{r}} &= [\mathbf{r}_1^T \mathbf{r}_2^H \mathbf{r}_3^H \mathbf{r}_4^H]^T \\ &= \begin{bmatrix} \mathbf{W}_{\text{idft}} \mathcal{G}_{1,d} \Theta & \mathbf{W}_{\text{idft}} \mathcal{G}_{2,d} \Theta & \mathbf{W}_{\text{idft}} \mathcal{G}_{3,d} \Theta \\ \mathbf{W}_{\text{dft}} \mathcal{G}_{2,d}^* \Theta & -\mathbf{W}_{\text{dft}} \mathcal{G}_{1,d}^* \Theta & \mathbf{0} \\ \mathbf{W}_{\text{dft}} \mathcal{G}_{3,d}^* \Theta & \mathbf{0} & -\mathbf{W}_{\text{dft}} \mathcal{G}_{1,d}^* \Theta \\ \mathbf{0} & \mathbf{W}_{\text{dft}} \mathcal{G}_{3,d}^* \Theta & -\mathbf{W}_{\text{dft}} \mathcal{G}_{2,d}^* \Theta \end{bmatrix} \begin{bmatrix} \mathbf{s}_1 \\ \mathbf{s}_2 \\ \mathbf{s}_3 \end{bmatrix} \\ &+ [\mathbf{w}_1^T \mathbf{w}_2^H \mathbf{w}_3^H \mathbf{w}_4^H]^T, \end{aligned} \quad (3.20)$$

where  $\mathcal{G}_{i,d} \triangleq \sum_{j=1}^{N_C} a_{j,i} \mathcal{G}_j$ ,  $\forall i \in \mathcal{I}_3$ , while the frequency-domain output of the non-linear blanking preprocessor is

$$\begin{aligned} \mathbf{y} &= \begin{bmatrix} \mathbf{C}_1 \mathcal{G}_{1,d} \Theta & \mathbf{C}_1 \mathcal{G}_{2,d} \Theta & \mathbf{C}_1 \mathcal{G}_{3,d} \Theta \\ \mathbf{C}_2 \mathcal{G}_{2,d}^* \Theta & -\mathbf{C}_2 \mathcal{G}_{1,d}^* \Theta & \mathbf{0} \\ \mathbf{C}_3 \mathcal{G}_{3,d}^* \Theta & \mathbf{0} & -\mathbf{C}_3 \mathcal{G}_{1,d}^* \Theta \\ \mathbf{0} & \mathbf{C}_4 \mathcal{G}_{3,d}^* \Theta & -\mathbf{C}_4 \mathcal{G}_{2,d}^* \Theta \end{bmatrix} \begin{bmatrix} \mathbf{s}_1 \\ \mathbf{s}_2 \\ \mathbf{s}_3 \end{bmatrix} + \begin{bmatrix} \mathbf{v}_1 \\ \mathbf{v}_2 \\ \mathbf{v}_3 \\ \mathbf{v}_4 \end{bmatrix} \\ &\triangleq \mathcal{C}_{d3} \mathbf{s} + \mathbf{v}, \end{aligned} \quad (3.21)$$

with  $\mathbf{C}_1$ ,  $\mathbf{v}_1$ ,  $\mathbf{C}_t$ , and  $\mathbf{v}_t$ ,  $\forall t \in \mathcal{T}_3$ , already defined. Finally, in this case,  $\text{rank}(\mathcal{C}_{d3}) = 3 M_{\text{uc}}$  implies  $\mathbf{F}_{d3} = \mathcal{C}_{d3}^\dagger$ .

### 3.4.2 Numerical results

In this section numerical results, obtained by Monte Carlo computer simulations, aimed at showing the effect of joint cooperative transmission and DSTBC onto IN mitigation in OFDM systems are presented. We consider the topology of Fig. 2.1 where each node is equipped with

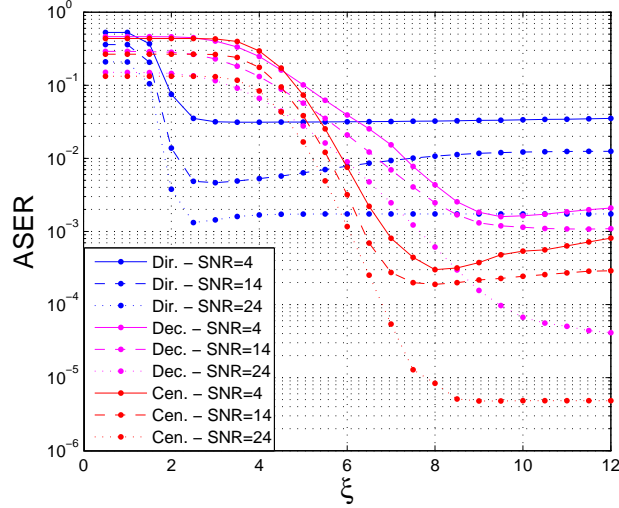


Figure 3.4: ASER vs  $\xi$  for  $\text{SNR} \in \{4, 14, 24\}$  dB ( $N_C=2$  - HI).

a single antenna and the relay nodes, whose number is  $N_C \in \{2, 3\}$ , are randomly and independently distributed in a circle centered along the line joining source and destination (where  $d_{SD} = 1$ ), at a normalized distance  $d_{SC} = 0.2612$  from the source. The entries of  $\mathbf{G}_i$ , which is statistically independent of  $\mathbf{G}_l$ , for  $l \neq i$ , are i.i.d. ZMCSCG random variables with variance  $\sigma_{g,i}^2 \triangleq (d_{SD}/d_{R_iD})^\eta$ , which depends on the average path loss associated to the link between the  $i$ -th relay node and destination, where  $d_{SD}$  and  $d_{R_iD}$  are the distance between the source and destination, and the  $i$ th relay and destination, respectively. The OFDM system employs  $M = 32$  subcarriers,  $M_{uc} = 24$  of which are loaded while the remaining  $M_{vc} = 8$  represent the so called virtual carriers. With regard to the impulsive noise, as in the overall chapter, the MCA noise model has been considered in the simulations. At the destination, a ZF equalizer, followed by a minimum distance detector is considered in order to recover the transmitted blocks. The existence of the ZF equalizers is ensured by

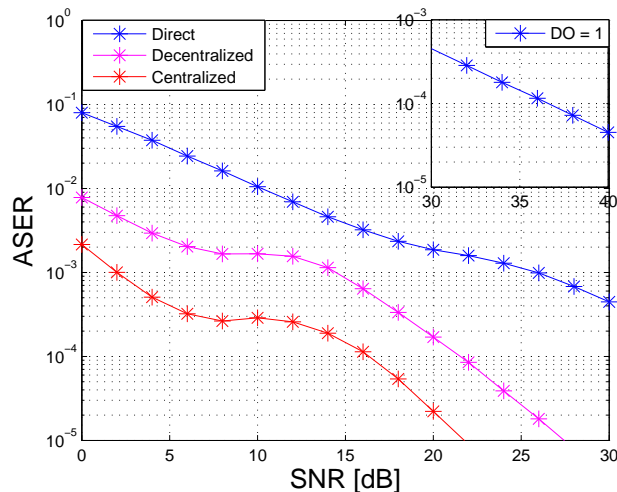


Figure 3.5: ASER vs SNR ( $N_C=2$  - HI).

condition  $M_{uc} \geq |\mathcal{B}|$  for each OFDM symbol (see Subsec. 3.3.3).

Fig. 3.5 shows the performance, in terms of ASER as a function of the SNR  $\triangleq 1/\sigma^2$ , for  $N_C = 2$  and in a highly-impulsive scenario ( $\lambda = 10^{-3}$  and  $\Gamma = 10^{-1}$ ), referred to as “HI”. Performance evaluation has been carried out for the three considered approaches, i.e., direct transmission, cooperative centralized and cooperative decentralized, employing the respective optimal (in the minimum ASER sense) blanking thresholds. As in the previous section, these optimal values have been numerically determined by assessing the performance, for each SNR value, as a function of the threshold (see the partial results in Fig. 3.4). From Fig. 3.5 it results that the joint employment of cooperation and DSTBC improves remarkably the performance with respect to the direct communication, in terms of both coding gain and diversity order. Specifically, the performance of the direct transmission, which is characterized by a diversity order of 1 (see the additional high-SNR trend shown within the box placed at the upper-right side of Fig. 3.5), turns out to be overwhelmed approximately by 10 dB and 22 dB, respectively, from those of the decentralized and centralized systems which, in their turn, show a diversity order of 2, typical of the original Alamouti transmit diversity scheme with two transmit antennas and one receive antenna.

Fig. 3.6 shows the performance of the three approaches, in terms

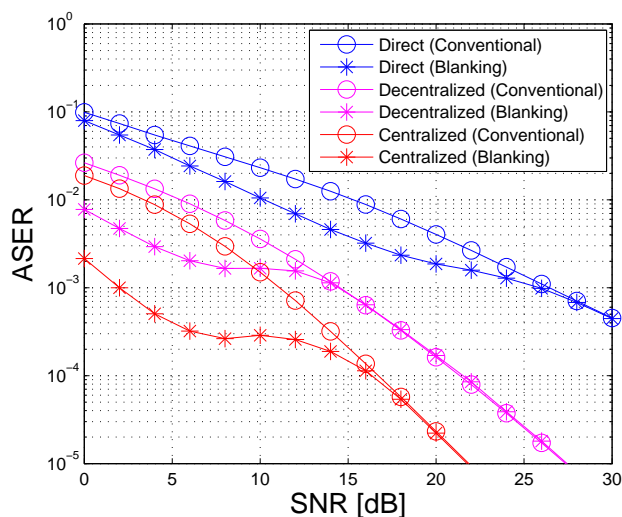


Figure 3.6: ASER vs SNR with and without blanking ( $N_C=2$  - HI).

of ASER as a function of the SNR, in the case of both conventional and blanking processing at the destination. Even in this case, a highly-impulsive scenario ( $\lambda = 10^{-3}$  and  $\Gamma = 10^{-1}$ ) and  $N_C = 2$  relay nodes are considered. As already seen in the previous section with regard to the direct case only, we observe that, even when a cooperative approach is employed, the introduction of a blanking nonlinearity provides a considerable performance improvement, with respect to the conventional OFDM processing, except for very large SNR values. In fact, for high-SNR increasing values, blanking becomes increasingly unlikely until a SNR value at which the two receivers, with and without blanking, provide the same performance (i.e., no time-domain sample turns out to be above the optimal blanking threshold). In particular, the gain provided by blanking preprocessing in both the cooperative cases turns out to be greater than that observed in the direct case whose gain, on the other hand, is spread over a wider SNR range. From Fig. 3.6 it can be seen also that the direct approach, employing blanking preprocessing, turns out to be outperformed by the DSTBC approach without blanking, both in the centralized and in the decentralized cases.

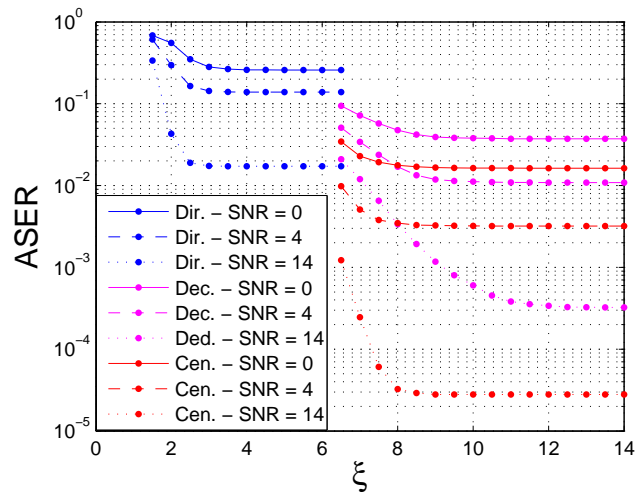
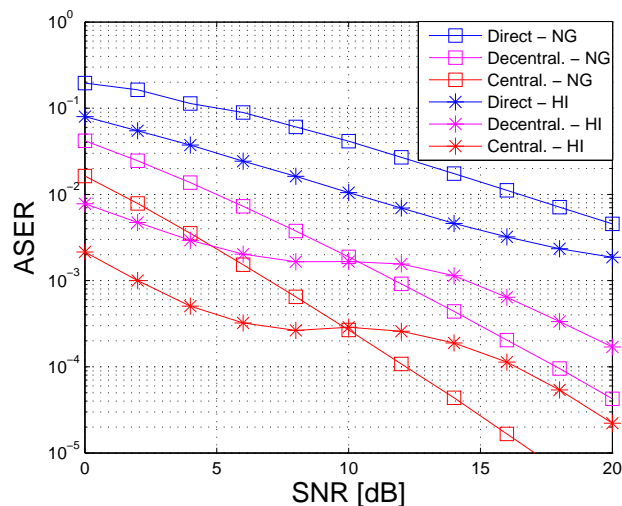
Figure 3.7: ASER vs  $\xi$  for  $\text{SNR} \in \{0, 4, 14\}$  dB ( $N_C=2$  - NG).Figure 3.8: ASER vs SNR ( $N_C=2$  - NG/HI).

Fig. 3.8 shows the performance comparison, in terms of ASER as a function of the  $\text{SNR} \triangleq 1/\sigma^2$  and for  $N_C = 2$ , between the near-Gaussian ( $\lambda = 10^{-1}$  and  $\Gamma = 10^{-1}$ ), referred to as “NG”, and highly-impulsive scenarios. Performance evaluation has been carried out by considering the optimal blanking thresholds (see the partial results for near-Gaussian

scenario in Fig. 3.7). Although the considerations made for the highly-impulsive scenario hold also for the near-Gaussian one, Fig. 3.8 suggests a further observation. Specifically, unlike the highly-impulsive case, in the near-Gaussian one the finite-SNR diversity order turns out to be approximately monotonically increasing as the SNR grows, until it reaches its asymptotic value for high-SNR values.

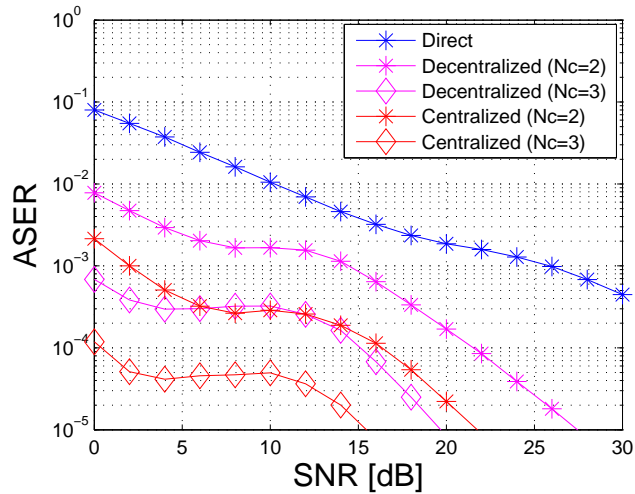


Figure 3.9: ASER vs SNR ( $N_C \in \{2, 3\}$  - HI).

Finally, Fig. 3.9 reports the ASER, as a function of the SNR, for all the considered schemes and for a highly-impulsive scenario. With regard to the cooperative schemes, simulation results for  $N_C = 2$  and  $N_C = 3$  are shown. From Fig. 3.9 it is apparent that, when  $N_C = 3$ , a remarkable performance improvement can be obtained, mainly in terms of coding gain, with respect to both the direct link case and the cooperative one with  $N_C = 2$ .

### 3.5 Conclusions

By exploiting the redundancy arising from the insertion of VCs in the OFDM signal, we have shown that closed-form FIR ICI-free compensation in OFDM receivers, which employ blanking nonlinearity processing to counteract IN, is still feasible. In this case, significant performance

gains can be obtained with a minor modification of the conventional ZF equalizer.

Then, we have considered an OFDM system in impulsive noise employing distributed space-time block coding, in order to obtain space and time diversity gains. Results of Monte Carlo computer simulations have shown that, irrespective of whether the blanking preprocessing is considered or not, a remarkable performance improvement, that is increasing in the number  $N_C$  of relay nodes, can be achieved with respect to the direct transmission.



## Chapter 4

# Virtual machine migration in Software-Defined future networks

This chapter addresses the potential impact of emerging technologies, like software defined networking (SDN) and network virtualization (NV), on future network evolution. It is argued that the above mentioned technologies could bring a significant disruption at the edge networks, where it will be possible to develop distributed clouds of virtual resources running on standard hardware. This contribution deals with a key technical challenge behind this vision: the capability of dynamically moving virtual machines (VMs), which run network services, functions, and users applications, among edge networks across wide area interconnections. Specifically, we focus on the problem of live migrating the memory state of a single VM between two physical machines, which are located at the edge and are inter-connected by a wide area network (WAN). With reference to a pre-copy mechanism, aimed at iteratively transferring the memory content to the destination machine, we develop a simplified mathematical model that unveils the dependence of the total migration time and downtime of the VM memory transfer on the main WAN parameters, such as capacity, buffering, and propagation delay. Numerical results obtained by Matlab simulations are presented to demonstrate the feasibility of live VM migration across WANs and the directions of research and development activities.

## 4.1 Introduction

Information and communications technologies are progressing at an impressive rate: processing is still following Moore's law, doubling in capability roughly every 18 months; storage capacity on a given chip is doubling every 12 months, driving a steady increase in connectivity demand for network access; optical bandwidth is doubling every 9 months, both by increasing the capacity of a single-wavelength fiber, and by transmitting multiple wavelengths on a single fiber. These progresses, and the down-spiralling of costs, are expected to have a dramatic impact on the evolution of network architectures: future networks (Fig. 4.1) are likely to become less hierarchical and based on optical core infrastructures (with a limited number and types of large nodes), which interconnect (by optical and/or radio links) different local areas, and are populated, at the edge (i.e., in a range of few meters around users) with a sheer number of heterogeneous nodes. The edge, toward which the process of "intelligence" migration is already in act, will become the business area where a new galaxy of ecosystems will be created.

In this scenario, the role of software will represent the true challenge: indeed, future networks will rely more and more on software, which will accelerate the pace of innovation (as it is doing continuously in the computing and storage domains). Already today, advances in resource virtualization are driving the deployment, on the same physical infrastructure, of diverse coexisting and isolated virtual networks of resources, which allows one to best fit, in a dynamical manner, a variety of service demands, similarly to having different operating systems (e.g., Windows, iOS, and Linux) on the same laptop. This has multiple advantages: for example, the crash, or the misuse, of a virtual resource is confined within a virtual network (e.g., by applying fault recovery policies enforced by self-healing capabilities), having no impact on other virtual networks; it is possible to implement, in each virtual network, specific procedures and policies (e.g., to optimize the usage of allocated resources according to service level agreements, SLA); the use of physical resources can be optimized, etc.

*Software defined networking* (SDN) [6, 14] can be seen as a further step in the direction of decoupling hardware from software: in particular, in an SDN architecture, control and data planes are decoupled, so that the network infrastructure is abstracted from business applications. The SDN paradigm should not be confused with *network virtualization*

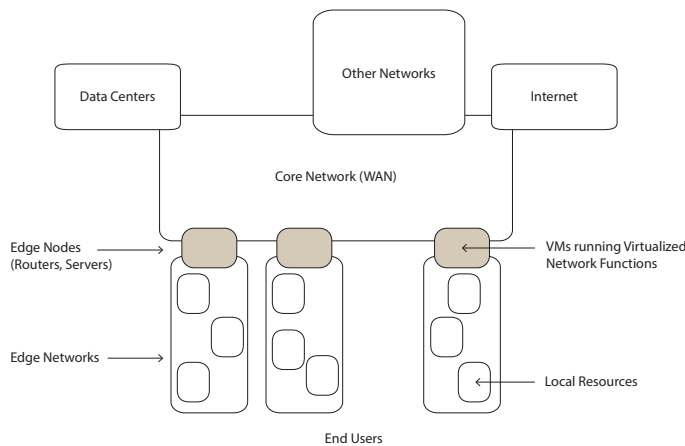


Figure 4.1: Edge networks scenario.

(NV) [124], even if the two concepts could intersect with interesting possibilities: indeed, NV is the second most-important trend allowing the setup of virtual networks by connecting virtual IT and networking resources. The above mentioned technologies are expected to bring about both programmability and flexibility: for example, it will be possible to build, on the same physical infrastructure, multiple overlay networks offering different services. On the other hand, this evolution is also determining an increase in design and management complexity: future networks are likely to exhibit the characteristics of complex systems, consisting of many diverse and autonomous, but interrelated, software and hardware components. Traditional management and control approaches will no longer be applicable: networks should be able to self-adapt and self-configure themselves (with limited human intervention). These capabilities can be achieved by introducing *autonomics* and *cognition* as a transformative software technology.

NV also enables live migration [125], i.e., a whole virtual machine (VM) can be moved between different physical machines (PMs) without disconnecting the client or application. Such a technology has already been proven to be a very effective tool in local area networks (LANs), i.e., when the VMs and the PMs are located within the same data center, to achieve the goals of server consolidation, load balancing, and hotspot mitigation.

In a cloud-based edge scenario, data centers can be spread over

wide areas and, thus, the need for migrating VMs over WANs arises. Compared to LAN applications, migration of VMs across WAN links poses [126,127] three additional challenges: 1) shared storage systems and/or storage area networks for VM disks may not always be available in WAN scenarios and, thus, in addition to random-access memory (RAM) transfer, disk state migration is required in this case (*storage migration issue*); 2) the bandwidth-delay product<sup>1</sup> of a WAN is typically high compared to buffering resources of the network [128], thus adversely impacting on both the total time of the migration and the VM downtime (*high bandwidth-delay issue*); 3) maintaining network level (i.e., IP addresses) reachability after migration is a difficult task in a WAN environment, since moving across different networks forces the VM to get a new IP address and, consequently, breaks existing network connections (*network reconfiguration issue*). To make WAN migration appealing, the requirements in terms of consistency, responsiveness, reliability, and scalability have to be studied thoroughly for cloud-based edge networks.

The paper is organized as follows. Section 4.2 describes some future network scenarios enabled by the technology advances in processing, storage, networking, and embedded communications. Section 4.3 provides a mathematical modeling of VM live migration across a WAN, by linking the performance of the RAM migration process to the main network parameters. Monte Carlo simulation results, obtained in a Matlab environment, are presented in Section 4.4. In Section 4.5, final remarks elaborate about the lesson learnt and the future steps.

## 4.2 Network scenarios

Today, traditional networks are suffering an “ossification”, which is creating several limitations for fast and flexible deployment, as well as adaptation of network functionality, services, and management policies. Launching new services is quite complex and expensive. In order to cope with the growing dynamism of *Information and Communication Technology* (ICT) markets, it is becoming increasingly urgent to find technologies and solutions solving the above mentioned limitations in future networks. Moreover, there is the need of reducing operational and capital expenditures (OpEx and CapEx). OpEx reduction can be achieved by

---

<sup>1</sup>Roughly speaking, the bandwidth-delay product of a data connection is the round-trip delay times the capacity of the underlying physical link.

easing human operators (and reducing human mistakes) in managing and automatically configuring equipment and network functionality. CapEx reduction can be achieved by postponing network resources investments (e.g., optimized use of available resources), for example, by exploiting layer and cross layer “constrained optimizations” (e.g., through several network applications in charge of load balancing, traffic engineering, optimized resource allocations, etc.). Eventually, in contrast to today, where competition exists only at the application level, future network should open new dimensions of business: incentives, cooperation, and competition will boost the long-term value of the network – like in ecosystems, where evolution selects the winning species, winning services will succeed, grow, and promote further investments, while losing ideas will fade away.

One of the most promising scenarios is that, in the short-medium term, SDN and NV principles will mature to bring a profound innovation at the edge of traditional networks, where, by the way, “intelligence” is already migrating. In this scenario, technology advances are bringing into the reality the concrete possibility of using tools and the solutions adopted in data centers for managing and orchestrating clouds of virtual resources. This will offering to network operators not only the ability to dynamically instantiate, activate, and re-allocate resources and network functions, but even programming them according to need and policies. Nevertheless this scenario has several challenges [126, 127]: one of these, covered by this paper, is deploying systems and methods capable of seamless migration of ensembles of VMs across WAN connections.

### 4.3 Live migration of virtual machines across WANs

The considered scenario is composed of a source physical machine (SPM) and a destination physical machine (DPM) that can be connected to each other by means of a WAN. We assume that the physical resources, i.e., central processing unit (CPU), memory, and input/output (I/O) devices of both source and destination are virtualized, so that multiple VMs, each of them self-contained with its own operating system (OS), can execute specific applications on the physical machine.

Hereinafter, we focus on live migration of a single VM from the source to the destination. Live migration of a VM across a WAN re-

quires [126, 127]: (i) network connection maintenance; (ii) disk state migration; (iii) RAM state migration. In this paper, we restrict our attention to RAM state migration, by assuming that: (a1) a protocol is used to separate the VM's identifier from its topological location, such as, the Locator/Identifier Separation Protocol (LISP) [129]; (a2) either a shared storage system for VM disks exists or a distributed replicated block device (DRBD) disk replication system [126] is employed to migrate storage to the destination.

Many migration techniques use a “pre-copy” mechanism [125] to *iteratively* copy the memory state of a VM from the source to the destination, while the OS continues to run. The OS of the VM has access to its own private, segmented name space; each segment known to the OS is sliced into equal-size units, called *pages*, to facilitate its mapping into the paged main memory. Let  $\mathcal{M} \triangleq \{m_1, m_2, \dots, m_M\}$  be the *set of memory pages* characterizing the OS of the VM, we consider a single source-destination link with capacity<sup>2</sup> of  $C$  pages per second, and a first-in first-out (FIFO) buffer of size  $B$  pages. Basically, pages are injected into the transport buffer by the upper layer protocol stack at a certain rate and, then, they are removed and transmitted by the physical link. In the sequel  $C^{-1}$  is referred to as the *service time*, which is the time needed to transmit a single page over the link. When the buffer is full, any page subsequently arriving is dropped (*buffer overflow*). After receiving a page, the destination is assumed to immediately send back an acknowledgement (ACK); such ACKs are cumulative in the sense that they also indicate the next page expected by the destination. Page drops due to buffer overflow are detected by either the receipt of duplicate ACKs or the expiration of a timer. In order not to complicate the analysis excessively, we assume that pages cannot be randomly lost after being transmitted over the physical link.

For the sake of simplicity, we assume that all the  $M$  pages experience the same (deterministic) propagation delay, which is denoted by  $\tau$ , and includes: (i) the time between the transmission of a page from the source and its arrival into the link buffer; (ii) the time between the transmission of the page on the link and its arrival at the destination; (iii) the time between the arrival of the page at the destination and the arrival of the corresponding acknowledgement at the source. Let  $T \triangleq \tau + 1/C$

---

<sup>2</sup>To simplify the presentation, we will assume that all the relevant network parameters are measured in units of pages, instead of bytes.

denote the propagation delay plus the service time, which will be referred to as *round-trip time*, and define the normalized buffer size  $B_{\text{norm}} \triangleq B/(CT) = B/(C\tau + 1)$ . Since we are concerned with transmission across a WAN, we restrict our attention to the case when  $B_{\text{norm}} \leq 1$  [128], i.e., when the buffer size  $B$  on the link is of the same order of magnitude as, or smaller than, the *bandwidth-delay product* [128] between the link capacity  $C$  and the round-trip time  $T$ . On the contrary, in LAN scenarios, it results that  $B_{\text{norm}} > 1$ .

### Congestion control algorithm

At the transport layer, the source-destination connection is assumed to use a congestion control algorithm, in order to regulate the amount of pages being injected into the WAN. To do this, the source uses a *congestion window* of size  $W$ , which sets a limit on the maximum number of pages that can be transmitted over the link before receiving an ACK. The value of  $W$  is varied dynamically in response to the network congestion: specifically, it is increased whenever a new page is acknowledged and is decreased whenever a page drop is detected. The maximum size of the congestion window in steady state is given [128] by  $W_{\text{max}} \triangleq B + CT$ , which is achieved when the buffer is fully occupied and there are  $CT$  pages travelling along the bit pipe. We assume that page drops occur at the window size  $W = W_{\text{max}}$  and, to simplify the analysis, we neglect the slow start phase [128]. The considered congestion control algorithm is an oversimplified version of the TCP-reno [130] (*Transmission Control Protocol-reno*) that can be summarized as follows:

- *Initialization*: set  $W = W_{\text{max}}/2$ .
- *Congestion avoidance phase*: when an ACK is received, if  $W < W_{\text{max}}$ , then  $W = W + 1/[W]$ , where  $[W]$  denotes the integer part of  $W$ .
- *Page dropping*: when  $W = W_{\text{max}}$ , a new *cycle* begins with  $W = W_{\text{max}}/2$ .

The time interval from the end of a congestion avoidance phase to the end of the next one is referred to [128] as a *cycle*: the evolution of the algorithm is periodic in the sense that successive cycles are identical. To evaluate the *average* page throughput  $\lambda$  of the connection, i.e., the number of pages transmitted per second, we report the main results of the

analysis carried out in [128] by using a continuous-time approximation of the congestion control evolution.

Let  $dW/dt$  denote the rate of window growth with time,  $dW/da$  the rate of window growth with arriving ACKs, and  $da/dt$  the rate at which the ACKs are arriving. In our case, it results that  $dW/da = 1/W$  and  $da/dt = \min\{W/T, C\}$ , which leads to

$$\frac{dW}{dt} = \frac{dW}{da} \frac{da}{dt} = \begin{cases} \frac{1}{T}, & W \leq CT; \\ \frac{C}{W}, & \text{otherwise.} \end{cases} \quad (4.1)$$

Let  $W(t)$  denote the value of the congestion window at time  $t$ , with  $W(0) = W_{\max}/2$ , eq. (4.1) shows that, when  $W \leq CT$ , one has that  $W(t) = W_{\max}/2 + t/T$  for  $t \in (0, t_1)$ , with

$$t_1 \triangleq T \left( CT - \frac{W_{\max}}{2} \right). \quad (4.2)$$

The number of pages transmitted during the interval  $t \in (0, t_1)$  is given by

$$n_1 = \int_0^{t_1} \frac{W(t)}{T} dt = \frac{W_{\max}}{2} \frac{t_1}{T} + \frac{t_1^2}{2T^2}. \quad (4.3)$$

When  $W > CT$ , it follows from (4.1) that  $W^2(t) = 2C(t - t_1) + (CT)^2$  for  $t \in (t_1, t_1 + t_2)$ , with

$$t_2 \triangleq \frac{W_{\max}^2 - (CT)^2}{2C} \quad (4.4)$$

where at the time  $t_1 + t_2$  the window size is equal to  $W_{\max}$  and a buffer overflow occurs. Since the link is fully utilized during the interval  $(t_1, t_1 + t_2)$ , the number of pages transmitted is

$$n_2 = C t_2 = \frac{W_{\max}^2 - (CT)^2}{2}. \quad (4.5)$$

The average page throughput assumes the expression

$$\lambda = \frac{n_1 + n_2}{t_1 + t_2} \quad (4.6)$$

which depends of the buffer size  $B$ , the link capacity  $C$ , and the round-trip time  $\tau$ : hence, the time needed to transmit a single page is  $1/\lambda$  on average.

### Migration algorithm

The main drawback of live migrating the VM's memory image stems from the fact that memory pages are continuously modified, or “dirtyed”, by the OS, and, hence, there is a high probability that those pages, which are frequently updated, may be transferred multiple times during the migration process. Since only the final version of a page is needed at the destination, repeated transfers lead to an unnecessary waste of resources. It has been observed in [125] that, in practice, a certain (possibly large) set of pages is seldom or never be modified by the OS, while the remaining ones are frequently dirtyed. In order to account for this fact, it is assumed in [131] that each page  $m_i$  is characterized by the probability that it is dirtyed at least one time during the transmission of a single page, for  $i \in \{1, 2, \dots, M\}$ . In Subection 4, we resort to a more general probabilistic model of the rewriting events, which is readily linked to the WAN parameters.

The migration process starts with the VM hypervisor marking all memory page as dirty. Then, the pre-copy algorithm [125] iteratively transfers dirty pages from the source to the destination until the number of pages remaining to be transferred is below a certain threshold  $M_{\max}$  or a maximum number of iterations  $K_m$  is reached. The hypervisor keeps track of those pages that are modified by using a *dirty page bitmap*, i.e., a memory structure where a bit is set for each dirty page. During live migration, the bitmap is scanned and, if a page is marked as dirty, it is transferred to the destination in the subsequent iteration. Let

$$\phi_0 : \{1, 2, \dots, M\} \rightarrow \{\phi_0^{(1)}, \phi_0^{(2)}, \dots, \phi_0^{(M)}\} \quad (4.7)$$

be an *initial page transfer ordering function*, which is assumed to be invertible and its inversion function is denoted by  $\phi_0^{-1}$ , whose choice depends on the dirty page rate, with  $\phi_0^{(i)} \in \{1, 2, \dots, M\}$  and  $\phi_0^{(i)} \neq \phi_0^{(j)}$  for  $i \neq j$ . On the basis of such an ordering, the pages are arranged in the new order  $m_{\phi_0^{(1)}}, m_{\phi_0^{(2)}}, \dots, m_{\phi_0^{(M)}}$ , wherein the position of page  $m_i$  turns out to be given by  $\phi_0^{-1}(i)$ , for  $i \in \{1, 2, \dots, M\}$ . We assume that only the pages belonging to  $\mathcal{M}_0 \triangleq \{m_{\phi_0^{(1)}}, m_{\phi_0^{(2)}}, \dots, m_{\phi_0^{(M_0)}}\}$  are live migrated, with  $M_0 \leq M$ , whereas the remaining  $M - M_0$  ones belonging to  $\overline{\mathcal{M}}_0 \triangleq \{m_{\phi_0^{(M_0+1)}}, m_{\phi_0^{(M_0+2)}}, \dots, m_{\phi_0^{(M)}}\}$  are transferred at the end of the migration process when the VM is stopped.

More precisely, the pre-copy migration process herein studied works as follows:

- At the first iteration ( $k = 0$ ), all the  $M_0$  pages belonging to  $\mathcal{M}_0$  are transmitted to the destination in an orderly way (*starting phase*), where  $m_{\phi_0^{(1)}}$  is the first page to be transferred, thus spanning a time interval of  $M_0/\lambda$  seconds.
- At the  $k$ th iteration, for  $k \in \{1, 2, \dots, k_{\text{end}}\}$ , after bitmap scanning, the pages in the subset  $\mathcal{D}_k \triangleq \{m_{d_k^{(1)}}, m_{d_k^{(2)}}, \dots, m_{d_k^{(M_k)}}\} \subseteq \mathcal{M}_0$  result to be marked as dirty, with  $M_k \leq M_0$ ,

$$d_k^{(i)} \in \{\phi_0^{(1)}, \phi_0^{(2)}, \dots, \phi_0^{(M_0)}\},$$

and  $d_k^{(i)} < d_k^{(j)}$  for  $i \neq j$ , and, hence, if  $M_k > M_{\text{max}}$ , they have to be retransmitted (*push phase*), thus spanning a time interval of  $M_k/\lambda$  seconds; specifically, let

$$\phi_k : \{1, 2, \dots, M_k\} \rightarrow \{\phi_k^{(1)}, \phi_k^{(2)}, \dots, \phi_k^{(M_k)}\} \quad (4.8)$$

be a  $k$ th page transfer ordering function, which is assumed to be invertible and its inversion function is denoted by  $\phi_k^{-1}$ , whose choice depends on the dirty page rate, with  $\phi_k^{(i)} \in \{d_k^{(1)}, d_k^{(2)}, \dots, d_k^{(M_k)}\}$  and  $\phi_k^{(i)} \neq \phi_k^{(j)}$  for  $i \neq j$ , all the  $M_k$  pages belonging to  $\mathcal{M}_k \triangleq \{m_{\phi_k^{(1)}}, m_{\phi_k^{(2)}}, \dots, m_{\phi_k^{(M_k)}}\}$  are live migrated in an orderly way, where  $m_{\phi_k^{(1)}}$  is the first page to be transferred.

- at the last iteration  $k = k_{\text{end}} + 1$ , where  $k_{\text{end}} = K_m$  if  $M_k > M_{\text{max}}$  for each  $k \in \{1, 2, \dots, K_m\}$  or  $k_{\text{end}} = k_f$  if  $M_{k_f} \leq M_{\text{max}}$  with  $k_f \in \{1, 2, \dots, K_m - 1\}$ , the VM is stopped and, let  $\mathcal{M}_{k_{\text{end}}+1} \subseteq \mathcal{M}_0$  denote the subset of cardinality  $M_{k_{\text{end}}+1} \leq M_0$  collecting the pages that are marked as dirty at the end of the push phase, the pages in  $\mathcal{M}_{k_{\text{end}}+1} \cup \overline{\mathcal{M}_0}$  are transmitted in an arbitrary order (*stop-and-copy phase*), which spans a time interval of  $M_{k_{\text{end}}+1}/\lambda + (M - M_0)/\lambda$  seconds.

When the complete memory image has been transferred, the VM is resumed at the destination and the live migration process is complete. The time  $T_{\text{down}}$  required to complete the stop-and-copy phase is referred to as *downtime*, whereas the time  $T_{\text{tot}}$  needed to collectively finish the

starting, push, and stop-and-copy phases is called *total migration time*. It is readily seen that

$$T_{\text{down}} = \frac{M_{k_{\text{end}}+1} + (M - M_0)}{\lambda} \quad (4.9)$$

$$T_{\text{tot}} = \frac{M_0}{\lambda} + \sum_{k=1}^{k_{\text{end}}} \frac{M_k}{\lambda} + T_{\text{down}} = \frac{M}{\lambda} + \sum_{k=1}^{k_{\text{end}}+1} \frac{M_k}{\lambda}. \quad (4.10)$$

To avoid service interruption, consistency issues, and unpredictable performance, the downtime has to be as small as possible. Moreover, in many scenarios, it is desirable to reduce the total migration time in order to free as fast as possible the VM resources for other use or to avoid waste of network resources, such as bandwidth and power.

#### 4.4 Numerical performance analysis

Herein, we aim at evaluating the average downtime  $\overline{T}_{\text{down}}$  and the average total migration time  $\overline{T}_{\text{tot}}$  by Monte Carlo computer simulations carried out in Matlab environment: both  $\overline{T}_{\text{down}}$  and  $\overline{T}_{\text{tot}}$  are obtained by averaging (4.9) and (4.10) over  $10^4$  Monte Carlo trials.

As first step, we have to specify the probabilistic model of the page rewriting events. For  $i \in \{1, 2, \dots, M\}$ , let  $N_i(t)$  denote the random number of rewriting events (the count) of page  $m_i$  at time  $t$ , assuming a zero count at  $t = 0$ . We assume that the sequence of rewritings in the counting process  $N_i(t)$  is a *Poisson point process* [132], i.e., rewriting events of page  $m_i$  occurs independently of one another, and at a fixed average rate of  $\gamma_i$  rewritings per second, and the event of two rewritings at precisely the same time is impossible, with  $N_i(t)$  statistically independent of  $N_j(t)$ , for  $i \neq j$ . We refer to  $\gamma_i$  as *average rewriting rate* of page  $m_i$ . Under these assumptions, the probability  $p_i(n)$  that the page  $m_i$  is dirtied at least one time during a time interval of duration  $n/\lambda$ , i.e., the average time needed to transmit  $n$  consecutive pages, is given by

$$p_i(n) = 1 - e^{-\frac{\gamma_i n}{\lambda}}. \quad (4.11)$$

It is worth noting that, if  $\gamma_i \gg \lambda/n$ , then  $p_i \approx 1$ , that is, the page  $m_i$  is almost surely dirtied during the transmission of  $n$  pages; this is just the case when live transfer of page  $m_i$  is wasteful of time, bandwidth, and

power. On the other hand, when  $\gamma_i \ll \lambda/n$ , it follows that  $p_i \approx 0$  and, hence, page  $m_i$  is not dirtied  $n/\lambda$  seconds almost surely.

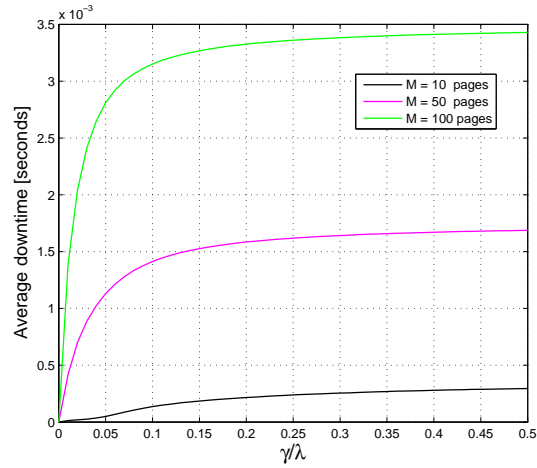
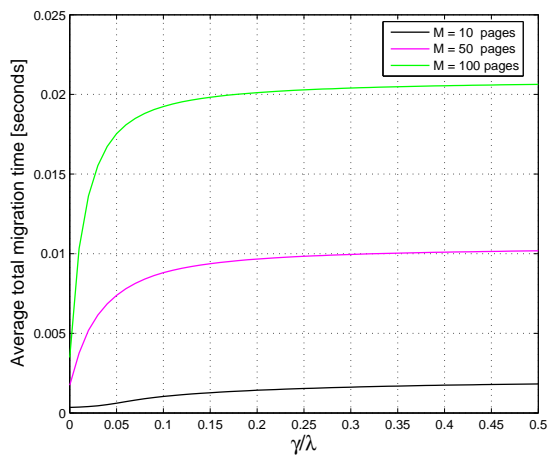
At the end of the  $k$ th iteration of the migration algorithm, for  $k \in \{0, 1, \dots, K_m\}$ , the probability  $p_i^{(k)}$  that page  $m_i$  is dirtied at least one time is given by

$$p_i^{(k)} = \begin{cases} p_i (M_k - \phi_k^{-1}(i) + 1), & k = L_i \\ p_i \left( M_{L_i} - \phi_{L_i}^{-1}(i) + 1 + \sum_{\ell=L_i+1}^k M_\ell \right), & k > L_i \end{cases} \quad (4.12)$$

where  $L_i \in \{0, 1, \dots, k\}$  is the index of the last iteration in which the page  $m_i$  has been retransmitted. For each iteration of the migration algorithm, the entries of the dirty page bitmap are randomly generated in each Monte Carlo trial as independent Bernoulli random variables with success (i.e., rewriting) probabilities given by (4.12).

For the sake of simplicity, we assume in the following example that all the  $M$  pages are characterized by the same average rewriting rate, i.e.,  $\gamma_i = \gamma$  for each  $i \in \{1, 2, \dots, M\}$ , and they are migrated in a random order (we used the `randperm` function of Matlab to ordering the pages at each iteration of the migration algorithm). Regarding the parameters of the migration algorithm, we set  $\mathcal{M}_0 = \mathcal{M}$  or, equivalently,  $M_0 = M$ , and we used as stop conditions  $M_{\max} = M/10$  and  $K_m = 5$ . Moreover, we fixed the WAN parameters as follows:  $C = 31250$  pages per second (i.e., the link capacity is 1 Gbps and the size of the pages is 4 kB),  $B = 5000$  pages, and  $\tau = 0.5$  seconds, which lead to  $\lambda = 28710$  pages per second and  $B_{\text{norm}} = 0.32$ .

Fig. 4.2 and Fig. 4.3 report, respectively, the average downtime  $\bar{T}_{\text{down}}$  and the average total migration time  $\bar{T}_{\text{tot}}$  as a function of the ratio  $\gamma/\lambda$  for different values of the number of pages  $M \in \{10, 50, 100\}$ . Results show that  $\bar{T}_{\text{down}}$  and  $\bar{T}_{\text{tot}}$  rapidly increase as the ratio  $\gamma/\lambda$  raises by (approximately) saturating to the values  $M/\lambda$  and  $(K_m + 1)(M/\lambda)$ , respectively, which correspond to the case in which all the  $M$  pages are dirtied at the end of each iteration of the migration algorithm. It can be argued that, with respect to the case when all the pages are transmitted while the VM is stopped (*non-live migration*), live migration leads to a significantly smaller downtime only when the average rewriting rate  $\gamma$  is a very small fraction of the average page throughput  $\lambda$ . For instance,

Figure 4.2: Average downtime versus  $\gamma/\lambda$ .Figure 4.3: Average total migration time versus  $\gamma/\lambda$ .

with reference to the case of  $M = 100$  pages, when  $\gamma$  is the 2.5% of  $\lambda$ , the difference between live and non-live migration is about 1.5 ms in terms of downtime. Finally, results not reported here for the sake of brevity show that, as expected,  $\bar{T}_{\text{down}}$  and  $\bar{T}_{\text{tot}}$  are monotonously decreasing functions of the WAN parameters  $B$  and  $C$ , whereas they monotonously increase

as a function of  $\tau$ ; however, migration performances are influenced more by the link capacity  $C$  than by the buffer size  $B$  and the propagation delay  $\tau$ .

## 4.5 Conclusions

This chapter has argued that, in the short-medium term, SDN and NV principles could bring a profound innovation at the edge of traditional networks. As a matter of fact, we are already witnessing a migration of processing power, storage capability, and embedded communications towards the edge of the network, i.e. towards the end users. This combination of drivers and trends will create the conditions where the end users [both residential and small-to-medium enterprises (SMEs) and large enterprises (LEs)] will “drive the network dynamics” more and more: the edge will become a distributed networking and computing environment, a sort of commodity fabric, capable of offering and providing ICT services through a galaxy of ecosystems. This vision will require overcoming current network ossifications by introducing features for fast and flexible deployment, as well as adaptation of network functionality, services and management policies: one example of these features is the capability of orchestrating ensembles of VMs across multiple edge networks interconnected by WAN links. In particular, the contribution presented in this chapter has addressed the development of a mathematical model for performance analysis of live migration of a single VM over a WAN link. The derived model unveils the dependence of the total migration time and downtime of the VM memory transfer on the main WAN parameters, such as capacity, buffering resources, and propagation delay. In particular, the performance of a “pre-copy” migration algorithm with page ordering has been considered. Simulation results have shown that live migration across WANs allows to reduce the downtime only when the average rewriting rate of the pages is a very small fraction of the average page throughput. Future work will be focused on completing the theoretical analysis of the considered scenario, and validating the obtained result against real data migration figures; moreover, an interesting development is extending the main methodologies proposed in the paper to tackle the more challenging scenario of migrating multiple VMs across WAN links, as well as using the developed framework to improve migration performance through constrained optimization approaches.

# Conclusions

In this thesis work some results related to technologies which are candidate to be part of the fifth generation (5G) standard have been presented. Specifically, the treated topics fall in the area of cooperative approaches as well as in the area of the software defined networking (SDN) and network function virtualization (NFV) paradigms.

With regard to the first of the two areas, the study of a cooperative network has been faced in the case of both Gaussian and non-Gaussian noise while, with respect to the second one, the study of the virtual machine migration over wide area network (WAN) links has been carried out from a mathematical point of view.

The discussion related to cooperative systems corrupted by Gaussian noise has been presented throughout three different studies. Specifically, by assuming absence of channel state information, tight approximations on the average symbol error probability have been obtained for MIMO cooperative dual-hop amplify-and-forward multiple-relay systems, in the case of both zero forcing and minimum mean square error equalization at the destination node. Moreover, with regard to the zero forcing case, the performance gain of the cooperative scheme over direct transmission has been assessed and, under hypothesis of relay cluster, the optimal placement of the relay nodes has been analytically determined. In both the considered cases, results of Monte Carlo computer simulations showed a good agreement between the proposed bounds and the related exact symbol error probabilities with a growing accuracy when the signal to noise ratio and the number of cooperating nodes increase. Finally, by considering the two limit cases of full-instantaneous channel state information (F-CSI) availability and statistical-only channel state information (S-CSI) availability, both the source and relay processing optimization has been faced to show the impact of the channel knowledge level on the performance of the considered system. Although simulation results have

shown an impressive gain when the source and relay processing are optimized on the basis of the full-channel state information, the S-CSI based design also provides a remarkable performance improvement which, even if not comparable to that of the F-CSI design, it is achieved at a price far lower.

With reference to the case of systems corrupted by non-Gaussian noise, the design of a new frequency-domain equalizer, which is able to mitigate the intercarrier interference introduced by non-linear techniques, has been carried out for single-input single-output orthogonal frequency division multiplexing (OFDM) systems employing virtual carriers and blanking preprocessing. Then, the mathematical model for a cooperative decode-and-forward OFDM system characterized by distributed space-time block coding has been presented to show the performance improvements, with respect to the direct communication, achieved for different values of cooperating relays and different impulsive noise scenarios.

The last contribution presented in this thesis work has addressed the development of a mathematical model for performance analysis, in terms of downtime and total migration time, of a single virtual machine live migration over a WAN link. The presented model has been derived assuming a “pre-copy” migration algorithm with page ordering and the aim of this study has been to unveil the dependence of the performance metrics on the main WAN parameters. Simulation results have shown that live migration across WANs allows to reduce the downtime only when the average rewriting rate of the memory pages is a very small fraction of the average page throughput.

# Appendices



# Appendix A

## Proof of Lemma 1

The proof of Lemma 1 relies on a generalization of the *Kolmogorov's inequality* [64], which was originally developed for scalar random variables, to the case of random matrices:

**Theorem 4.** *Let  $\mathbf{X}_1, \mathbf{X}_2, \dots, \mathbf{X}_n$  be mutually independent random matrices with expectations  $\mathbb{E}(\mathbf{X}_k)$  and variances*

$$\text{VAR}(\mathbf{X}_k) \triangleq \mathbb{E}[\|\mathbf{X}_k - \mathbb{E}(\mathbf{X}_k)\|^2], \quad (\text{A.1})$$

for  $k \in \{1, 2, \dots, n\}$ , and define

$$\bar{\mathbf{X}}_k \triangleq \mathbf{X}_1 + \mathbf{X}_2 + \dots + \mathbf{X}_k \quad (\text{A.2})$$

$$\mathbf{E}_k \triangleq \mathbb{E}(\bar{\mathbf{X}}_k) = \mathbb{E}(\mathbf{X}_1) + \mathbb{E}(\mathbf{X}_2) + \dots + \mathbb{E}(\mathbf{X}_k) \quad (\text{A.3})$$

$$\begin{aligned} \text{VAR}(\bar{\mathbf{X}}_k) &\triangleq \mathbb{E}[\|\bar{\mathbf{X}}_k - \mathbf{E}_k\|^2] \\ &= \text{VAR}(\mathbf{X}_1) + \text{VAR}(\mathbf{X}_2) + \dots + \text{VAR}(\mathbf{X}_k). \end{aligned} \quad (\text{A.4})$$

For every  $t > 0$  the probability of the simultaneous realization of the  $n$  inequalities

$$\|\bar{\mathbf{X}}_k - \mathbf{E}_k\| < t \sqrt{\text{VAR}(\bar{\mathbf{X}}_k)}, \quad \text{for } k \in \{1, 2, \dots, n\} \quad (\text{A.5})$$

is at least  $1 - t^{-2}$ .

**Proof.** The proof is omitted since it can be obtained by following the same procedure delineated in [64], with minor modifications accounting only for the matrix nature of the involved random quantities.

In other words, based on such a theorem, the probability that at least one of the inequalities (A.5) does not hold is smaller than or equal to  $t^{-2}$ .

Let us now turn one's attention to the proof of Lemma 1. An equivalent way [64] to demonstrate that the matrix sequence  $\{\alpha_i \mathbf{G}_i \mathbf{G}_i^H\}_{i=1}^{N_C}$  obeys the strong law of large numbers is to show that, for every  $\epsilon > 0$ , with probability one there occur only finitely many of the events

$$\frac{\|\mathbf{S}_{N_C} - \mathbf{M}_{N_C}\|}{N_C} \geq \epsilon. \quad (\text{A.6})$$

With this goal in mind, let  $\nu \in \mathbb{Z}$  and define the event

$$\mathcal{A}_\nu \triangleq \left\{ \begin{array}{l} \text{there exists at least one } N_C \in (2^{\nu-1}, 2^\nu] \\ \text{such that } \frac{\|\mathbf{S}_{N_C} - \mathbf{M}_{N_C}\|}{N_C} \geq \epsilon \end{array} \right\}. \quad (\text{A.7})$$

By virtue of the Borel-Cantelli lemma [64], if

$$\sum_{\nu=1}^{+\infty} P(\mathcal{A}_\nu) < +\infty \quad (\text{A.8})$$

then with probability one only finitely many events  $\mathcal{A}_\nu$  occur, i.e., for a given  $\epsilon > 0$ , there exists a sufficiently large  $\bar{\nu}$  such that  $P(\mathcal{A}_{\bar{\nu}}) < \epsilon$ . Therefore, to accomplish the proof of Lemma 1, it suffices to prove that (2.13) implies (A.8). To this aim, we preliminarily observe that

$$\begin{aligned} P(\mathcal{A}_\nu) &\leq P(\{\text{there exists at least one } N_C \in (2^{\nu-1}, 2^\nu] \\ &\quad \text{such that } \|\mathbf{S}_{N_C} - \mathbf{M}_{N_C}\| \geq \epsilon 2^{\nu-1}\}) \\ &= 1 - P \left[ \bigcap_{k=2^{\nu-1}+1}^{2^\nu} \{\|\mathbf{S}_k - \mathbf{M}_k\| < \epsilon 2^{\nu-1}\} \right] \\ &\leq \frac{\text{VAR}[\mathbf{S}_{2^\nu}]}{\epsilon^2 2^{2(\nu-1)}} = 4 \frac{\text{VAR}[\mathbf{S}_{2^\nu}]}{\epsilon^2 2^{2\nu}} \end{aligned} \quad (\text{A.9})$$

where the second inequality directly comes from application of Theorem 4.

At this point, using (A.9) and accounting also for (2.12), we can write

$$\begin{aligned}
 \sum_{\nu=1}^{+\infty} P(\mathcal{A}_\nu) &\leq \frac{4N_R N_D^2}{\epsilon^2} \sum_{\nu=1}^{+\infty} \left(\frac{1}{4}\right)^\nu \sum_{i=1}^{2^\nu} \alpha_i^2 \sigma_{g,i}^4 \\
 &= \frac{4N_R N_D^2}{\epsilon^2} \sum_{i=1}^{+\infty} \alpha_i^2 \sigma_{g,i}^4 \sum_{\substack{\nu=1 \\ 2^\nu \geq i}}^{+\infty} \left(\frac{1}{4}\right)^\nu \\
 &\leq \frac{16N_R N_D^2}{3\epsilon^2} \sum_{i=1}^{+\infty} \frac{\alpha_i^2 \sigma_{g,i}^4}{i^2}
 \end{aligned} \tag{A.10}$$

where we have used the fact that, if  $2^{\nu_0} \geq i > 2^{\nu_0-1}$ , then

$$\begin{aligned}
 \sum_{\substack{\nu=1 \\ 2^\nu \geq i}}^{+\infty} \left(\frac{1}{4}\right)^\nu &= \sum_{\nu=\nu_0}^{+\infty} \left(\frac{1}{4}\right)^\nu = \left(\frac{1}{4}\right)^{\nu_0} \sum_{\nu'=0}^{+\infty} \left(\frac{1}{4}\right)^{\nu'} \\
 &= \frac{1}{2^{2\nu_0}} \frac{1}{1-\frac{1}{4}} \leq \frac{4}{3i^2}.
 \end{aligned} \tag{A.11}$$

In conclusion, if (2.13) holds, then from (A.10) the series  $\sum_{\nu=1}^{+\infty} P(\mathcal{A}_\nu)$  converges.

## Appendix B

### Proof of Theorem 1

It is shown [72, 133] that, conditioned on  $\mathbf{H}$ , the approximate value of  $\text{SINR}_n$  in (2.20) is a Gamma random variable with shape parameter  $k = N_D - N_B + 1$  and scale parameter  $\theta = (\gamma/\beta) \Sigma_n$ , where

$$\Sigma_n = \frac{1}{\left\{ \left[ \mathbf{F}_0^H \tilde{\mathbf{H}}^H (\boldsymbol{\Omega} \otimes \mathbf{I}_{N_R}) \tilde{\mathbf{H}} \mathbf{F}_0 \right]^{-1} \right\}_{nn}} \quad (\text{B.1})$$

and the entries of  $\tilde{\mathbf{H}} \triangleq [\text{diag}(\sigma_{h,1}^{-1}, \sigma_{h,2}^{-1}, \dots, \sigma_{h,N_C}^{-1}) \otimes \mathbf{I}_{N_R}] \mathbf{H} \in \mathbb{C}^{(N_C N_R) \times N_S}$  are i.i.d. ZMCSCG random variables having unit variance, with  $\boldsymbol{\Omega} \triangleq \text{diag}(\alpha_1 \sigma_{h,1}^2 \sigma_{g,1}^2, \alpha_2 \sigma_{h,2}^2 \sigma_{g,2}^2, \dots, \alpha_{N_C} \sigma_{h,N_C}^2 \sigma_{g,N_C}^2) \in \mathbb{R}^{N_C \times N_C}$ . Thus, remembering that for a Gamma random variable  $\Phi(y) = (1 - \theta y)^{-k}$  for  $y < \theta^{-1}$ , one has

$$\begin{aligned} \Phi_{\text{SINR}_n} \left( -\frac{u}{\sin^2 x}; \mathbf{H} \right) &\approx \frac{1}{\left( 1 + \frac{u\gamma}{\beta} \frac{\Sigma_n}{\sin^2 x} \right)^k} \\ &\approx (\sin^2 x)^k \left[ \frac{u\gamma}{\beta} \Sigma_n \right]^{-k} \end{aligned} \quad (\text{B.2})$$

where the last approximation holds for  $\gamma \gg 1$ . Substituting (B.2) in (2.17) and recalling the expressions of  $b$  and  $u$ , one has that  $P_{\text{coop},n}(e | \mathbf{H})$ , conditioned on  $\mathbf{H}$ , can be approximated as follows

$$P_{\text{coop},n}(e | \mathbf{H}) \approx 2\Theta(k) \left( 1 - \frac{1}{\sqrt{Q}} \right) \left[ \frac{3}{2(Q-1)} \frac{\gamma}{\beta} \Sigma_n \right]^{-k} \quad (\text{B.3})$$

where  $\Theta(v) \triangleq (2/\pi) \int_0^{\pi/2} (\sin^2 x)^v dx$ , with  $v \in \mathbb{R}$ .

According to (2.8), eq. (B.3) has to be averaged with respect to  $\mathbf{H} \in \mathbb{C}^{N_C N_R \times N_S}$  or, equivalently,  $\tilde{\mathbf{H}}$ . To this end, by partitioning  $\tilde{\mathbf{H}}$  as

$$\tilde{\mathbf{H}} \triangleq [\tilde{\mathbf{H}}_1^T, \tilde{\mathbf{H}}_2^T, \dots, \tilde{\mathbf{H}}_{N_C}^T]^T, \quad (\text{B.4})$$

with  $\tilde{\mathbf{H}}_i \in \mathbb{C}^{N_R \times N_S}$  for  $i \in \{1, 2, \dots, N_C\}$ , one obtains from (B.1) that

$$\mathbf{F}_0^H \tilde{\mathbf{H}}^H (\boldsymbol{\Omega} \otimes \mathbf{I}_{N_R}) \tilde{\mathbf{H}} \mathbf{F}_0 = \sum_{i=1}^{N_C} \mathbf{A}_i^H \mathbf{A}_i \quad (\text{B.5})$$

where

$$\mathbf{A}_i \triangleq \sqrt{\omega_i} \tilde{\mathbf{H}}_i \mathbf{F}_0 \in \mathbb{C}^{N_R \times N_B}, \quad (\text{B.6})$$

with  $\omega_i \triangleq \alpha_i \sigma_{h,i}^2 \sigma_{g,i}^2$  being the  $i$ th diagonal entries of  $\boldsymbol{\Omega}$ . It is readily seen that, for  $i \in \{1, 2, \dots, N_C\}$ , the matrix  $\mathbf{A}_i^H \mathbf{A}_i$  has a complex central Wishart distribution [69] with  $N_R$  degrees of freedom and covariance matrix  $(\omega_i/N_B) \mathbf{I}_{N_B}$ , provided that  $N_R \geq N_B$ . At this point, we can rely on the following general result:

**Lemma 3.** *Let  $\mathbf{X}_i \in \mathbb{C}^{N_B \times N_B}$  be a complex central Wishart matrix with  $\lambda_i \geq N_B$  degrees of freedom and covariance matrix  $\mathbf{K}_i$ , for  $i \in \{1, 2, \dots, N_C\}$ . The matrix  $\bar{\mathbf{X}} \triangleq \sum_{i=1}^{N_C} \mathbf{X}_i$  approximately has a complex central Wishart distribution with*

$$\bar{\lambda} \triangleq \frac{\text{tr} \left[ \left( \sum_{i=1}^{N_C} \lambda_i \mathbf{K}_i \right)^2 \right] + \text{tr}^2 \left( \sum_{i=1}^{N_C} \lambda_i \mathbf{K}_i \right)}{\sum_{i=1}^{N_C} \lambda_i [\text{tr}(\mathbf{K}_i^2) + \text{tr}^2(\mathbf{K}_i)]} \quad (\text{B.7})$$

degrees of freedom and covariance matrix

$$\bar{\mathbf{K}} \triangleq \frac{1}{\bar{\lambda}} \sum_{i=1}^{N_C} \lambda_i \mathbf{K}_i. \quad (\text{B.8})$$

**Proof.** See [65, Sec. 3]. By using Lemma 3 with  $\mathbf{X}_i = \mathbf{A}_i^H \mathbf{A}_i$ ,  $\lambda_i = N_R$ , and  $\mathbf{K}_i = (\omega_i/N_B) \mathbf{I}_{N_B}$ , the matrix in (B.5) approximately has a complex central Wishart distribution with  $N_R (\sum_{i=1}^{N_C} \omega_i)^2 / (\sum_{i=1}^{N_C} \omega_i^2)$  degrees of freedom and covariance matrix  $N_B^{-1} (\sum_{i=1}^{N_C} \omega_i^2) / (\sum_{i=1}^{N_C} \omega_i) \mathbf{I}_{N_B}$ .

Therefore, provided that  $N_C N_R > N_D$ , one has [72, 133] that  $\Sigma_n \sim \text{Gamma}(k, \theta)$ , with  $k = N_C N_R - N_S + 1$  and  $\theta = N_B^{-1} (\sum_{i=1}^{N_C} \omega_i^2) / (\sum_{i=1}^{N_C} \omega_i)$ , and, consequently,  $1/\Sigma_n$  is distributed as an inverse Gamma random variable. Following [36], after some calculations, one obtains

$$\mathbb{E}_{\mathbf{H}} [(\Sigma_n)^{-D}] = \frac{(N_C N_R - N_D - 1)!}{(N_C N_R - N_B)!} \left[ \frac{N_S \sum_{i=1}^{N_C} \omega_i}{\sum_{i=1}^{N_C} \omega_i^2} \right]^D, \quad (\text{B.9})$$

where  $D = N_D - N_B + 1$ . Averaging (B.3) with respect to  $\mathbf{H}$ , using (B.9), and recalling the expression of  $\omega_i$ , one obtains (2.19).

## Appendix C

### Proof of Theorem 2

The first part of the proof consists of showing that the approximate value of  $\text{SINR}_n$  given by (2.20) can be expressed as a random quadratic form [134]. The matrix  $\mathbf{C}$  in (2.15) can be rewritten as  $\mathbf{C} = \tilde{\mathbf{G}} \mathbf{F} \mathbf{H} \mathbf{F}_0$ , where the entries of  $\tilde{\mathbf{H}} \triangleq [\text{diag}(\sigma_{h,1}^{-1}, \sigma_{h,2}^{-1}, \dots, \sigma_{h,N_C}^{-1}) \otimes \mathbf{I}_{N_R}] \mathbf{H} \in \mathbb{C}^{(N_C N_R) \times N_S}$  and  $\tilde{\mathbf{G}} \triangleq \mathbf{G} [\text{diag}(\sigma_{g,1}^{-1}, \sigma_{g,2}^{-1}, \dots, \sigma_{g,N_C}^{-1}) \otimes \mathbf{I}_{N_R}] \in \mathbb{C}^{N_D \times (N_C N_R)}$  are i.i.d. ZMCSCG random variables having unit variance, with  $\mathbf{G}$  and  $\mathbf{F}$  defined previously, whereas  $\mathbf{F} \triangleq \text{diag}(\sqrt{\omega_1} \mathbf{F}_1, \sqrt{\omega_2} \mathbf{F}_2, \dots, \sqrt{\omega_{N_C}} \mathbf{F}_{N_C}) \in \mathbb{C}^{(N_C N_R) \times (N_C N_R)}$ , with  $\omega_i \triangleq \alpha_i \sigma_{h,i}^2 \sigma_{g,i}^2$ , for  $i \in \{1, 2, \dots, N_C\}$ . Let  $\mathbf{c}_n \in \mathbb{C}^{N_D}$  and  $\mathbf{C}_n \in \mathbb{C}^{N_D \times (N_B - 1)}$  denote the  $n$ th column of  $\mathbf{C}$  and the matrix obtained by striking  $\mathbf{c}_n$  out of  $\mathbf{C}$ , respectively, for  $n \in \{1, 2, \dots, N_B\}$ , it results (see, e.g., [72, 133]) that

$$\text{SINR}_n = \frac{\gamma}{\beta} \left[ \mathbf{c}_n^H \mathbf{c}_n - \mathbf{c}_n^H \mathbf{C}_n (\mathbf{C}_n^H \mathbf{C}_n)^{-1} \mathbf{C}_n^H \mathbf{c}_n \right]. \quad (\text{C.1})$$

It can be verified that, conditioned on  $\tilde{\mathbf{G}}$ , the matrix  $\mathbf{C}_n$  has a circular symmetric complex Gaussian distribution with mean  $\mathbf{O}_{N_D \times (N_B - 1)}$  and covariance matrix  $(\tilde{\mathbf{G}} \mathbf{F} \mathbf{F}^H \tilde{\mathbf{G}}^H) \otimes \mathbf{R}_n^*$ , where  $\mathbf{R}_n \in \mathbb{C}^{(N_B - 1) \times (N_B - 1)}$  is the nonsingular matrix  $\mathbf{F}_0^H \mathbf{F}_0$  deprived of its  $n$ th column and  $n$ th row. Therefore, we can equivalently express  $\mathbf{C}_n$  as  $\mathbf{C}_n = \tilde{\mathbf{G}} \mathbf{F} \tilde{\mathbf{H}}_{\text{red}} \mathbf{R}_n^{1/2}$ , where the entries of  $\tilde{\mathbf{H}}_{\text{red}} \in \mathbb{C}^{(N_C N_R) \times (N_B - 1)}$  are i.i.d. ZMCSCG random variables having unit variance and  $\mathbf{R}_n^{1/2}$  is the (Hermitian) square root of  $\mathbf{R}_n$ . Substituting such an expression of  $\mathbf{C}_n$  in (C.1), one obtains

$$\text{SINR}_n = \frac{\gamma}{\beta} \left[ \mathbf{c}_n^H \mathbf{P}_{\mathcal{N}(\Xi^H)} \mathbf{c}_n \right] \quad (\text{C.2})$$

where, by defining  $\Xi \triangleq \tilde{\mathbf{G}} \mathbf{F} \tilde{\mathbf{H}}_{\text{red}}$ ,

$$\mathbf{P}_{\mathcal{N}(\Xi^{\text{H}})} \triangleq \mathbf{I}_{N_{\text{D}}} - \Xi (\Xi^{\text{H}} \Xi)^{-1} \Xi^{\text{H}} \in \mathbb{C}^{N_{\text{D}} \times N_{\text{D}}} \quad (\text{C.3})$$

is the orthogonal projector onto  $\mathcal{N}(\Xi^{\text{H}})$ ; in particular, it results that:

i) *an orthogonal projector is Hermitian*, i.e.,

$$\mathbf{P}_{\mathcal{N}(\Xi^{\text{H}})}^{\text{H}} = \mathbf{P}_{\mathcal{N}(\Xi^{\text{H}})}; \quad (\text{C.4})$$

ii) *an orthogonal projector is idempotent*, i.e.,

$$\mathbf{P}_{\mathcal{N}(\Xi^{\text{H}})}^2 = \mathbf{P}_{\mathcal{N}(\Xi^{\text{H}})}. \quad (\text{C.5})$$

Moreover, it can be shown [72, 133] that

$$\mathbf{c}_n | \tilde{\mathbf{G}}, \mathbf{C}_n \sim \mathcal{CN}(-\mathbf{C}_n (\mathbf{R}_n^*)^{-1} \mathbf{r}_n^*, \tilde{\mathbf{G}} \mathbf{F} \mathbf{F}^{\text{H}} \tilde{\mathbf{G}}^{\text{H}} / \{(\mathbf{F}_0^{\text{T}} \mathbf{F}_0^*)^{-1}\}_{nn}), \quad (\text{C.6})$$

where  $\mathbf{r}_n \in \mathbb{C}^{N_{\text{B}}-1}$  represents the  $n$ th column of  $\mathbf{R}_n$  with its  $n$ th entry removed. Hence, we can equivalently express  $\mathbf{c}_n$  as  $\mathbf{c}_n = -\mathbf{C}_n (\mathbf{R}_n^*)^{-1} \mathbf{r}_n^* + (\tilde{\mathbf{G}} \mathbf{F} \mathbf{x}) / \{(\mathbf{F}_0^{\text{H}} \mathbf{F}_0)^{-1}\}_{nn}$ , where the entries of  $\mathbf{x} \in \mathbb{C}^{N_{\text{C}} N_{\text{R}}}$  are i.i.d. ZM-CSCG random variables having unit variance and we have also observed that  $\{(\mathbf{F}_0^{\text{T}} \mathbf{F}_0^*)^{-1}\}_{nm} = \{(\mathbf{F}_0^{\text{H}} \mathbf{F}_0)^{-1}\}_{nn}$ . Substituting such an expression of  $\mathbf{c}_n$  in (C.2) and observing that

$$\mathbf{C}_n^{\text{H}} \mathbf{P}_{\mathcal{N}(\Xi^{\text{H}})} = \mathbf{R}_n^{1/2} (\tilde{\mathbf{H}}_{\text{red}}^{\text{H}} \mathbf{F}^{\text{H}} \tilde{\mathbf{G}}^{\text{H}}) \mathbf{P}_{\mathcal{N}(\Xi^{\text{H}})} = \mathbf{O}_{(N_{\text{B}}-1) \times N_{\text{D}}}, \quad (\text{C.7})$$

one has

$$\text{SINR}_n = \delta_n \mathbf{x}^{\text{H}} \mathbf{Q} \mathbf{x} \quad (\text{C.8})$$

where  $\delta_n \triangleq (\gamma u) / [\beta \{(\mathbf{F}_0^{\text{H}} \mathbf{F}_0)^{-1}\}_{nn}]$  and  $\mathbf{Q} \triangleq \mathbf{F}^{\text{H}} \tilde{\mathbf{G}}^{\text{H}} \mathbf{P}_{\mathcal{N}(\Xi^{\text{H}})} \tilde{\mathbf{G}} \mathbf{F} \in \mathbb{C}^{(N_{\text{C}} N_{\text{R}}) \times (N_{\text{C}} N_{\text{R}})}$ . Under the assumption that  $N_{\text{C}} N_{\text{R}} \geq N_{\text{D}}$ , the matrix  $\tilde{\mathbf{G}} \mathbf{F} \in \mathbb{C}^{N_{\text{D}} \times (N_{\text{C}} N_{\text{R}})}$  is full-row rank with probability one and, consequently, one has  $\text{rank}(\mathbf{Q}) = \text{rank}(\mathbf{P}_{\mathcal{N}(\Xi^{\text{H}})}) = N_{\text{D}} - N_{\text{B}} + 1$ . At this point, by resorting to the Chernoff bound [?], the probability in (2.17) can be upper bounded as  $\Pr(E_{\text{coop},n} | \mathbf{G}, \mathbf{H}) \leq b \exp(-u \text{SINR}_n)$ , thus following from (2.13) that

$$\begin{aligned} P_{\text{coop},n}(e) &\leq b \mathbb{E}_{\tilde{\mathbf{G}}, \tilde{\mathbf{H}}_{\text{red}}, \mathbf{x}} [\exp(-u \text{SINR}_n)] \\ &= b \mathbb{E}_{\tilde{\mathbf{G}}} \left\{ \mathbb{E}_{\tilde{\mathbf{H}}_{\text{red}} | \tilde{\mathbf{G}}} \left[ \mathbb{E}_{\mathbf{x} | \tilde{\mathbf{G}}, \tilde{\mathbf{H}}_{\text{red}}} [\exp(-u \text{SINR}_n)] \right] \right\} \end{aligned} \quad (\text{C.9})$$

where we have also used the conditional expectation rule [135].

The second part of the proof lies in evaluating the ensemble averages in (C.10) with respect to  $\mathbf{x}$  and  $\tilde{\mathbf{H}}_{\text{red}}$ , given  $\tilde{\mathbf{G}}$ . First, accounting for (C.8), it results [136] that

$$\mathbb{E}_{\mathbf{x}|\tilde{\mathbf{G}},\tilde{\mathbf{H}}_{\text{red}}}[\exp(-u \text{SINR}_n)] = \det^{-1}(\mathbf{I}_{N_{\text{C}}N_{\text{R}}} + \delta_n \mathbf{Q}) . \quad (\text{C.10})$$

Second, following [134], it can be proven that

$$\mathbb{E}_{\tilde{\mathbf{H}}_{\text{red}}|\tilde{\mathbf{G}}}[\det^{-1}(\mathbf{I}_{N_{\text{C}}N_{\text{R}}} + \delta_n \mathbf{Q})] \approx \Upsilon_{N_{\text{B}}-1} \delta_n^{-(N_{\text{D}}-N_{\text{B}}+1)} \times \det^{-1}(\tilde{\mathbf{G}} \mathbf{F} \mathbf{F}^{\text{H}} \tilde{\mathbf{G}}^{\text{H}}) \quad (\text{C.11})$$

where the approximation holds for  $\gamma \gg 1$ ,

$$\Upsilon_p \triangleq \frac{\sum_{1 \leq i_1 < \dots < i_p \leq N_{\text{D}}} \left[ \prod_{j=1}^p \lambda_{i_j}(\tilde{\mathbf{G}} \mathbf{F} \mathbf{F}^{\text{H}} \tilde{\mathbf{G}}^{\text{H}}) \right]}{\binom{N_{\text{D}}}{p}} \quad (\text{C.12})$$

for  $p \in \{1, 2, \dots, N_{\text{D}}\}$ , and  $\{\lambda_i(\tilde{\mathbf{G}} \mathbf{F} \mathbf{F}^{\text{H}} \tilde{\mathbf{G}}^{\text{H}})\}_{i=1}^{N_{\text{D}}}$ , denote the eigenvalues of  $\tilde{\mathbf{G}} \mathbf{F} \mathbf{F}^{\text{H}} \tilde{\mathbf{G}}^{\text{H}}$ , which is nonsingular with probability one. The term at the numerator of  $\Upsilon_p$  is the elementary symmetric polynomial [137] of degree  $p$  in the  $N_{\text{D}}$  variables  $\lambda_1(\tilde{\mathbf{G}} \mathbf{F} \mathbf{F}^{\text{H}} \tilde{\mathbf{G}}^{\text{H}})$ ,  $\lambda_2(\tilde{\mathbf{G}} \mathbf{F} \mathbf{F}^{\text{H}} \tilde{\mathbf{G}}^{\text{H}})$ ,  $\dots$ ,  $\lambda_{N_{\text{D}}}(\tilde{\mathbf{G}} \mathbf{F} \mathbf{F}^{\text{H}} \tilde{\mathbf{G}}^{\text{H}})$ , i.e., the sum of all products of  $p$  out of the numbers  $\lambda_1(\tilde{\mathbf{G}} \mathbf{F} \mathbf{F}^{\text{H}} \tilde{\mathbf{G}}^{\text{H}})$ ,  $\lambda_2(\tilde{\mathbf{G}} \mathbf{F} \mathbf{F}^{\text{H}} \tilde{\mathbf{G}}^{\text{H}})$ ,  $\dots$ ,  $\lambda_{N_{\text{D}}}(\tilde{\mathbf{G}} \mathbf{F} \mathbf{F}^{\text{H}} \tilde{\mathbf{G}}^{\text{H}})$  with the indices in increasing order, whereas the binomial coefficient  $\binom{N_{\text{D}}}{p}$  in the denominator of  $\Upsilon_p$  is the number of terms in the numerator. In this regard, we capitalize on the following result:

**Lemma 4** (Maclaurin's inequality). *The following chain of inequalities holds*

$$\Upsilon_1 \geq \sqrt[2]{\Upsilon_2} \geq \dots \geq \sqrt[N_{\text{D}}]{\Upsilon_{N_{\text{D}}}} \quad (\text{C.13})$$

with equality if and only if all the  $\lambda_i(\tilde{\mathbf{G}} \mathbf{F} \mathbf{F}^{\text{H}} \tilde{\mathbf{G}}^{\text{H}})$  are equal.

**Proof.** See [137]. By virtue of Lemma 4 and, additionally, observing that  $\Upsilon_1 = \text{tr}(\tilde{\mathbf{G}} \mathbf{F} \mathbf{F}^{\text{H}} \tilde{\mathbf{G}}^{\text{H}})$ , it is seen that

$$\Upsilon_{N_{\text{B}}-1} \leq \text{tr}^{N_{\text{B}}-1}(\tilde{\mathbf{G}} \mathbf{F} \mathbf{F}^{\text{H}} \tilde{\mathbf{G}}^{\text{H}}) . \quad (\text{C.14})$$

The bound (2.34) follows by substituting (C.14), (C.11), (C.10) in (C.10) and, moreover, accounting for the expressions of the constants  $b$ ,  $u$ , and  $\delta_n$ .

## Appendix D

### Proof of Lemma 2

First of all, we observe that (see, e.g., [74])

$$\text{tr}(\tilde{\mathbf{G}} \mathbf{F} \mathbf{F}^H \tilde{\mathbf{G}}^H) \leq \text{tr}(\mathbf{F} \mathbf{F}^H) \text{tr}(\tilde{\mathbf{G}} \tilde{\mathbf{G}}^H). \quad (\text{D.1})$$

Let us order the eigenvalues of  $\tilde{\mathbf{G}} \mathbf{F} \mathbf{F}^H \tilde{\mathbf{G}}^H$  as

$$\lambda_1(\tilde{\mathbf{G}} \mathbf{F} \mathbf{F}^H \tilde{\mathbf{G}}^H) \leq \lambda_2(\tilde{\mathbf{G}} \mathbf{F} \mathbf{F}^H \tilde{\mathbf{G}}^H) \leq \dots \leq \lambda_{N_D}(\tilde{\mathbf{G}} \mathbf{F} \mathbf{F}^H \tilde{\mathbf{G}}^H), \quad (\text{D.2})$$

we rely on the following generalization of the Ostrowski's theorem [74]:

**Theorem 5.** *Let  $\lambda_1(\tilde{\mathbf{G}} \tilde{\mathbf{G}}^H) \leq \lambda_2(\tilde{\mathbf{G}} \tilde{\mathbf{G}}^H) \leq \dots \leq \lambda_{N_D}(\tilde{\mathbf{G}} \tilde{\mathbf{G}}^H)$  and  $\lambda_1(\mathbf{F} \mathbf{F}^H) \leq \lambda_2(\mathbf{F} \mathbf{F}^H) \leq \dots \leq \lambda_{N_C N_R}(\mathbf{F} \mathbf{F}^H)$  be the ordered eigenvalues of  $\tilde{\mathbf{G}} \tilde{\mathbf{G}}^H$  and  $\mathbf{F} \mathbf{F}^H$ , respectively, with  $N_C N_R \geq N_D$ , then*

$$\lambda_p(\tilde{\mathbf{G}} \mathbf{F} \mathbf{F}^H \tilde{\mathbf{G}}^H) = \theta_p \vartheta_p, \quad \text{for } p \in \{1, 2, \dots, N_D\} \quad (\text{D.3})$$

where

$$\lambda_1(\tilde{\mathbf{G}} \tilde{\mathbf{G}}^H) \leq \theta_p \leq \lambda_{N_D}(\tilde{\mathbf{G}} \tilde{\mathbf{G}}^H) \quad (\text{D.4})$$

and

$$\lambda_p(\mathbf{F} \mathbf{F}^H) \leq \vartheta_p \leq \lambda_{p+N_C N_R - N_D}(\mathbf{F} \mathbf{F}^H). \quad (\text{D.5})$$

**Proof.** See [138].

As a consequence of Theorem 5, we get

$$\begin{aligned} \det(\tilde{\mathbf{G}} \mathbf{F} \mathbf{F}^H \tilde{\mathbf{G}}^H) &= \prod_{p=1}^{N_D} \lambda_p(\tilde{\mathbf{G}} \mathbf{F} \mathbf{F}^H \tilde{\mathbf{G}}^H) = \left( \prod_{p=1}^{N_D} \theta_p \right) \left( \prod_{p=1}^{N_D} \vartheta_p \right) \\ &\geq \lambda_1^{N_D}(\tilde{\mathbf{G}} \tilde{\mathbf{G}}^H) \left[ \prod_{p=1}^{N_D} \lambda_p(\mathbf{F} \mathbf{F}^H) \right]. \end{aligned} \quad (\text{D.6})$$

Eq. (2.35) readily follows from (D.1) and (D.6)

# Appendix E

## Proof of Theorem 3

Since the matrix  $\mathbf{W}_{\text{dft}}$  is nonsingular, it results that

$$\text{rank}(\mathbf{C}\mathbf{H}\Theta) = \text{rank}[(\mathbf{I}_M - \mathbf{B})\mathbf{W}_{\text{idft}}\mathbf{H}\Theta]. \quad (\text{E.1})$$

Moreover, by virtue of assumption **(a3)**, one has  $\text{rank}(\mathbf{H}\Theta) = M_{\text{uc}}$ , which implies that  $\text{rank}(\mathbf{W}_{\text{idft}}\mathbf{H}\Theta) = M_{\text{uc}}$ , since  $\mathbf{W}_{\text{idft}}$  is a nonsingular matrix. The matrix  $(\mathbf{I}_M - \mathbf{B})\mathbf{W}_{\text{idft}}\mathbf{H}\Theta \in \mathbb{C}^{M \times M_{\text{uc}}}$  is full-column rank iff [79]  $\mathcal{N}(\mathbf{I}_M - \mathbf{B}) \cap \mathcal{R}(\mathbf{W}_{\text{idft}}\mathbf{H}\Theta) = \{\mathbf{0}_M\}$ . By construction, the  $m$ th diagonal entry of  $\mathbf{I}_M - \mathbf{B}$  is zero for each  $m \in \mathcal{B}$  and, thus,  $\text{rank}(\mathbf{I}_M - \mathbf{B}) = M - |\mathcal{B}| = |\overline{\mathcal{B}}|$ . Recalling that  $m_i$  denotes the  $i$ th element of  $\mathcal{B}$ , for  $i \in \{1, 2, \dots, |\mathcal{B}|\}$ , an arbitrary vector  $\boldsymbol{\mu} \in \mathbb{C}^M$  belongs to  $\mathcal{N}(\mathbf{I}_M - \mathbf{B})$  iff there exists a vector  $\boldsymbol{\beta} \in \mathbb{C}^{|\mathcal{B}|}$  such that  $\boldsymbol{\mu} = \boldsymbol{\Psi}\boldsymbol{\beta}$ , with  $\boldsymbol{\Psi} \triangleq [\mathbf{1}_{m_1}, \mathbf{1}_{m_2}, \dots, \mathbf{1}_{m_{|\mathcal{B}|}}] \in \mathbb{R}^{M \times |\mathcal{B}|}$ , where  $\mathbf{1}_m \in \mathbb{R}^M$  is the  $(m+1)$ th column of  $\mathbf{I}_M$ . Hence, an arbitrary vector  $\boldsymbol{\mu} \in \mathcal{N}(\mathbf{I}_M - \mathbf{B})$  also belongs to the subspace  $\mathcal{R}(\mathbf{W}_{\text{idft}}\mathbf{H}\Theta)$  iff there exists a vector  $\boldsymbol{\alpha} \in \mathbb{C}^{M_{\text{uc}}}$  such that  $\boldsymbol{\Psi}\boldsymbol{\beta} = \mathbf{W}_{\text{idft}}\mathbf{H}\Theta\boldsymbol{\alpha}$ . As a consequence, condition  $\mathcal{N}(\mathbf{I}_M - \mathbf{B}) \cap \mathcal{R}(\mathbf{W}_{\text{idft}}\mathbf{H}\Theta) = \{\mathbf{0}_M\}$  holds iff the system of equations  $\mathbf{H}\Theta\boldsymbol{\alpha} - \mathbf{W}_{\text{dft}}\boldsymbol{\Psi}\boldsymbol{\beta} = \mathbf{0}_M$  admits the unique solution  $\boldsymbol{\alpha} = \mathbf{0}_{M_{\text{uc}}}$  and  $\boldsymbol{\beta} = \mathbf{0}_{|\mathcal{B}|}$ . It can be seen [74] that this happens iff the matrix  $[\mathbf{H}\Theta, \mathbf{W}_{\text{dft}}\boldsymbol{\Psi}] \in \mathbb{C}^{M \times (M_{\text{uc}} + |\mathcal{B}|)}$  turns out to be full-column rank.



# Bibliography

- [1] Ericsson, “Ericsson mobility report - on the pulse of the networked society,” pp. 3719–3735, Nov 2014. [Online]. Available: <http://www.ericsson.com/res/docs/2014/ericsson-mobility-report-november-2014.pdf>
- [2] A. Osseiran, F. Boccardi, V. Braun, K. Kusume, P. Marsch, M. Maternia, O. Queseth, M. Schellmann, H. Schotten, H. Taoka, H. Tullberg, M. Uusitalo, B. Timus, and M. Fallgren, “Scenarios for 5G mobile and wireless communications: the vision of the METIS project,” *Communications Magazine, IEEE*, vol. 52, no. 5, pp. 26–35, May 2014.
- [3] Ericsson, “Operator opportunities in the internet of things,” pp. 3719–3735, Feb 2011. [Online]. Available: [http://www.ericsson.com/res/thecompany/docs/publications/ericsson\\_review/2011/er\\_edcp.pdf](http://www.ericsson.com/res/thecompany/docs/publications/ericsson_review/2011/er_edcp.pdf)
- [4] A. Osseiran, V. Braun, T. Hidekazu, P. Marsch, H. Schotten, H. Tullberg, M. Uusitalo, and M. Schellman, “The Foundation of the Mobile and Wireless Communications System for 2020 and Beyond: Challenges, Enablers and Technology Solutions,” in *Vehicle Technology Conference (VTC Spring), 2013 IEEE 77th*, June 2013, pp. 1–5.
- [5] P. Agyapong, M. Iwamura, D. Staehle, W. Kiess, and A. Benjebbour, “Design considerations for a 5G network architecture,” *Communications Magazine, IEEE*, vol. 52, no. 11, pp. 65–75, Nov 2014.
- [6] O. N. Foundation, “Software-defined networking: The new norm for networks,” *white paper*, 2012. [On-

- line]. Available: <https://www.opennetworking.org/images/stories/downloads/sdn-resources/white-papers/wp-sdn-newnorm.pdf>
- [7] ETSI, “Network Function Virtualisation - An introduction, Benefits, Enablers, Challenges & Call for Action,” *white paper*, Oct 2012. [Online]. Available: [https://portal.etsi.org/NFV/NFV\\_White\\_Paper.pdf](https://portal.etsi.org/NFV/NFV_White_Paper.pdf)
- [8] C. E. Shannon, “Two-way Communication Channels,” in *Proceedings of the Fourth Berkeley Symposium on Mathematical Statistics and Probability, Volume 1: Contributions to the Theory of Statistics*. Berkeley, Calif.: University of California Press, 1961, pp. 611–644. [Online]. Available: <http://projecteuclid.org/euclid.bsm/1200512185>
- [9] E. C. Van Der Meulen, *Transmission of information in a T-terminal discrete memoryless channel*. Dept. of Statistics, University of California, Berkeley: Ph.D. thesis, Dept. of Statistics, University of California, Berkeley, 1968.
- [10] —, “Three-Terminal Communication Channels,” *Advances in Applied Probability*, vol. 3, no. 1, pp. pp. 120–154, 1971.
- [11] S. P. E. Dahlman and J. Sköld, *4G LTE/LTE-Advanced for Mobile Broadband*. Academic Press.
- [12] N. Bhushan, J. Li, D. Malladi, R. Gilmore, D. Brenner, A. Damnjanovic, R. Sukhavasi, C. Patel, and S. Geirhofer, “Network densification: the dominant theme for wireless evolution into 5G,” *Communications Magazine, IEEE*, vol. 52, no. 2, pp. 82–89, February 2014.
- [13] ONF, *SDN definition*. [Online]. Available: <https://www.opennetworking.org/sdn-resources/sdn-definition>
- [14] N. McKeown, T. Anderson, H. Balakrishnan, G. Parulkar, L. Peterson, J. Rexford, S. Shenker, and J. Turner, “OpenFlow: Enabling Innovation in Campus Networks,” *SIGCOMM Comput. Commun. Rev.*, vol. 38, no. 2, pp. 69–74, Mar. 2008. [Online]. Available: <http://doi.acm.org/10.1145/1355734.1355746>

- [15] RAS, “5G radio network architecture,” *white paper*, Feb 2014. [Online]. Available: <http://www.ict-ras.eu/>
- [16] P. Demestichas, A. Georgakopoulos, D. Karvounas, K. Tsagkaris, V. Stavroulaki, J. Lu, C. Xiong, and J. Yao, “5G on the Horizon: Key Challenges for the Radio-Access Network,” *Vehicular Technology Magazine, IEEE*, vol. 8, no. 3, pp. 47–53, Sept 2013.
- [17] H. Niu, C. Li, A. Papathanassiou, and G. Wu, “RAN architecture options and performance for 5G network evolution,” in *Wireless Communications and Networking Conference Workshops (WCNCW), 2014 IEEE*, April 2014, pp. 294–298.
- [18] S. Zhidkov, “Analysis and comparison of several simple impulsive noise mitigation schemes for OFDM receivers,” *Communications, IEEE Transactions on*, vol. 56, no. 1, pp. 5–9, January 2008.
- [19] A. Molisch, *Wireless Communications (2nd ed.)*. Hoboken, New Jersey: John Wiley & Sons, 2011.
- [20] A. Goldsmith, *Wireless communications*. Cambridge University Press, 2005.
- [21] J. G. Proakis, *Digital Communications, 5th Edition*. New York: McGraw-Hill, 2007.
- [22] G. J. Foschini, “Layered space-time architecture for wireless communication in a fading environment when using multi-element antennas,” *Bell Labs Technical Journal*, vol. 1, no. 2, pp. 41–59, 1996. [Online]. Available: <http://dx.doi.org/10.1002/bltj.2015>
- [23] G. Golden, C. Foschini, R. Valenzuela, and P. Wolniansky, “Detection algorithm and initial laboratory results using V-BLAST space-time communication architecture,” *Electronics Letters*, vol. 35, no. 1, pp. 14–16, Jan 1999.
- [24] A. Paulraj, D. Gore, R. Nabar, and H. Bolcskei, “An overview of MIMO communications - a key to gigabit wireless,” *Proceedings of the IEEE*, vol. 92, no. 2, pp. 198–218, Feb 2004.
- [25] J. Proakis, *Encyclopedia of telecommunications*. Hoboken, New Jersey: John Wiley & Sons, 2003.

- 
- [26] M. Doelz, E. Heald, and D. Martin, "Binary Data Transmission Techniques for Linear Systems," *Proceedings of the IRE*, vol. 45, no. 5, pp. 656–661, May 1957.
- [27] S. Weinstein and P. Ebert, "Data Transmission by Frequency-Division Multiplexing Using the Discrete Fourier Transform," *Communication Technology, IEEE Transactions on*, vol. 19, no. 5, pp. 628–634, October 1971.
- [28] B. Hirosaki, "An Orthogonally Multiplexed QAM System Using the Discrete Fourier Transform," *Communications, IEEE Transactions on*, vol. 29, no. 7, pp. 982–989, Jul 1981.
- [29] J. Bingham, "Multicarrier modulation for data transmission: an idea whose time has come," *Communications Magazine, IEEE*, vol. 28, no. 5, pp. 5–14, May 1990.
- [30] G. Gelli, *Modulazione multiportante, sistemi OFDM e DMT*, Naples, Italy, 2001. [Online]. Available: <http://www.docenti.unina.it/giacinto.gelli>
- [31] F. Fitzek and M. Katz, *Cooperation in Wireless Networks: Principles and Applications*. The Netherlands: Springer, 2006.
- [32] D. Tse and P. Viswanath, *Fundamentals of Wireless Communication*. Cambridge: Cambridge University Press, 2005.
- [33] A. Sendonaris, E. Erkip, and B. Aazhang, "User cooperation diversity. Part I. System description," vol. 51, no. 11, pp. 1927–1938, Nov. 2003.
- [34] —, "User cooperation diversity. Part II. Implementation aspects and performance analysis," vol. 51, no. 11, pp. 1939–1948, Nov. 2003.
- [35] K. Loa, C.-C. Wu, S.-T. Sheu, Y. Yuan, M. Chion, D. Huo, and L. Xu, "IMT-advanced relay standards [WiMAX/LTE Update]," vol. 48, no. 8, pp. 40–48, Aug. 2010.
- [36] F. Verde, D. Darsena, and A. Scaglione, "Cooperative Randomized MIMO-OFDM Downlink for Multicell Networks: Design and Analysis," *Signal Processing, IEEE Transactions on*, vol. 58, no. 1, pp. 384–402, Jan 2010.

- [37] A. Scaglione, D. Goeckel, and J. Laneman, "Cooperative communications in mobile ad hoc networks," vol. 23, no. 5, pp. 18–29, Sep. 2006.
- [38] F. Verde and A. Scaglione, "Decentralized space-time block coding for two-way relay networks," in *Signal Processing Advances in Wireless Communications (SPAWC), 2010 IEEE Eleventh International Workshop on*, June 2010, pp. 1–5.
- [39] R. Savoia and F. Verde, "Performance Analysis of Distributed Space-Time Block Coding Schemes in Middleton Class-A Noise," *Vehicular Technology, IEEE Transactions on*, vol. 62, no. 6, pp. 2579–2595, July 2013.
- [40] S. Jin, M. McKay, C. Zhong, and K.-K. Wong, "Ergodic Capacity Analysis of Amplify-and-Forward MIMO Dual-Hop Systems," *Information Theory, IEEE Transactions on*, vol. 56, no. 5, pp. 2204–2224, May 2010.
- [41] J. Laneman, D. Tse, and G. Wornell, "Cooperative diversity in wireless networks: Efficient protocols and outage behavior," vol. 50, no. 12, pp. 3062–3080, Dec. 2004.
- [42] F. Verde and A. Scaglione, "Randomized space-time block coding for distributed amplify-and-forward cooperative relays," in *Acoustics Speech and Signal Processing (ICASSP), 2010 IEEE International Conference on*, March 2010, pp. 3030–3033.
- [43] F. Verde, "Design of randomized space-time block codes for amplify-and-forward cooperative relaying," in *Communications Control and Signal Processing (ISCCSP), 2012 5th International Symposium on*, May 2012, pp. 1–5.
- [44] ———, "Performance analysis of randomised space-time block codes for amplify-and-forward cooperative relaying," *Communications, IET*, vol. 7, no. 17, pp. 1883–1898, Nov 2013.
- [45] W. Guan and H. Luo, "Joint MMSE Transceiver Design in Non-Regenerative MIMO Relay Systems," *Communications Letters, IEEE*, vol. 12, no. 7, pp. 517–519, July 2008.

- 
- [46] C. Song, K.-J. Lee, and I. Lee, "MMSE Based Transceiver Designs in Closed-Loop Non-Regenerative MIMO Relaying Systems," *Wireless Communications, IEEE Transactions on*, vol. 9, no. 7, pp. 2310–2319, July 2010.
- [47] C. Xing, S. Ma, and Y.-C. Wu, "Robust Joint Design of Linear Relay Precoder and Destination Equalizer for Dual-Hop Amplify-and-Forward MIMO Relay Systems," *Signal Processing, IEEE Transactions on*, vol. 58, no. 4, pp. 2273–2283, April 2010.
- [48] Y. Rong, X. Tang, and Y. Hua, "A Unified Framework for Optimizing Linear Nonregenerative Multicarrier MIMO Relay Communication Systems," *Signal Processing, IEEE Transactions on*, vol. 57, no. 12, pp. 4837–4851, Dec 2009.
- [49] H.-J. Choi, C. Song, H. Park, and I. Lee, "Transceiver Designs for Multipoint-to-Multipoint MIMO Amplify-and-Forward Relaying Systems," *Wireless Communications, IEEE Transactions on*, vol. 13, no. 1, pp. 198–209, January 2014.
- [50] B. Chalise and L. Vandendorpe, "Performance analysis of linear receivers in a MIMO relaying system," *Communications Letters, IEEE*, vol. 13, no. 5, pp. 330–332, May 2009.
- [51] R. H. Louie, Y. Li, H. Suraweera, and B. Vucetic, "Performance analysis of beamforming in two hop amplify and forward relay networks with antenna correlation," *Wireless Communications, IEEE Transactions on*, vol. 8, no. 6, pp. 3132–3141, June 2009.
- [52] C. Song, K.-J. Lee, and I. Lee, "Performance Analysis of MMSE-Based Amplify and Forward Spatial Multiplexing MIMO Relaying Systems," *Communications, IEEE Transactions on*, vol. 59, no. 12, pp. 3452–3462, December 2011.
- [53] —, "MMSE-Based MIMO Cooperative Relaying Systems: Closed-Form Designs and Outage Behavior," *Selected Areas in Communications, IEEE Journal on*, vol. 30, no. 8, pp. 1390–1401, September 2012.
- [54] D. Darsena, G. Gelli, F. Melito, and F. Verde, "Performance analysis of amplify-and-forward MIMO-OFDM links with linear ZF

- equalization,” in *Communications Workshops (ICC), 2013 IEEE International Conference on*, June 2013, pp. 296–300.
- [55] H. Shi, T. Abe, T. Asai, and H. Yoshino, “Relaying Schemes Using Matrix Triangularization for MIMO Wireless Networks,” *Communications, IEEE Transactions on*, vol. 55, no. 9, pp. 1683–1688, Sept 2007.
- [56] J. Ma, P. Orlik, J. Zhang, and G. Li, “Pilot Matrix Design for Estimating Cascaded Channels in Two-Hop MIMO Amplify-and-Forward Relay Systems,” *Wireless Communications, IEEE Transactions on*, vol. 10, no. 6, pp. 1956–1965, June 2011.
- [57] T. Kong and Y. Hua, “Optimal Design of Source and Relay Pilots for MIMO Relay Channel Estimation,” *Signal Processing, IEEE Transactions on*, vol. 59, no. 9, pp. 4438–4446, Sept 2011.
- [58] W. Xu, X. Dong, and W.-S. Lu, “MIMO Relaying Broadcast Channels With Linear Precoding and Quantized Channel State Information Feedback,” *Signal Processing, IEEE Transactions on*, vol. 58, no. 10, pp. 5233–5245, Oct 2010.
- [59] C. Zhao and B. Champagne, “Joint Design of Multiple Non-Regenerative MIMO Relaying Matrices With Power Constraints,” *Signal Processing, IEEE Transactions on*, vol. 61, no. 19, pp. 4861–4873, Oct 2013.
- [60] A. Behbahani, R. Merched, and A. Eltawil, “Optimizations of a MIMO Relay Network,” *Signal Processing, IEEE Transactions on*, vol. 56, no. 10, pp. 5062–5073, Oct 2008.
- [61] H. Bolcskei, R. Nabar, O. Oyman, and A. Paulraj, “Capacity scaling laws in MIMO relay networks,” *Wireless Communications, IEEE Transactions on*, vol. 5, no. 6, pp. 1433–1444, June 2006.
- [62] S. Song and K. Letaief, “System Design, DMT Analysis, and Penalty for Non-Coherent Relaying,” *Communications, IEEE Transactions on*, vol. 60, no. 9, pp. 2489–2498, September 2012.
- [63] M. Hasna and M.-S. Alouini, “A performance study of dual-hop transmissions with fixed gain relays,” *Wireless Communications, IEEE Transactions on*, vol. 3, no. 6, pp. 1963–1968, Nov 2004.

- 
- [64] W. Feller, *An Introduction to Probability Theory and its Applications*. New York: John Wiley & Sons, 1968.
- [65] D. Nel and C. V. der Merwe, "A solution to the multivariate Behrens-Fisher problem," *Commun. Stat. - Theory Methods*, vol. 15, no. 2, pp. 3719–3735, 1986.
- [66] S. Yang and J.-C. Belfiore, "Optimal Space-Time Codes for the MIMO Amplify-and-Forward Cooperative Channel," *Information Theory, IEEE Transactions on*, vol. 53, no. 2, pp. 647–663, Feb 2007.
- [67] D. Gunduz, M. Khojastepour, A. Goldsmith, and H. Poor, "Multi-hop MIMO relay networks: diversity-multiplexing trade-off analysis," *Wireless Communications, IEEE Transactions on*, vol. 9, no. 5, pp. 1738–1747, May 2010.
- [68] M. Simon and M. Alouini, *Digital Communications Over Fading Channels*. New York: Cambridge University Press, 1990.
- [69] A. James, "Distributions of matrix variates and latent roots derived from normal samples," *Ann. Math. Statist.*, vol. 35, no. 2, pp. 475–501, 1964.
- [70] D. Gore, R. Heath, and A. Paulraj, "Transmit selection in spatial multiplexing systems," *Communications Letters, IEEE*, vol. 6, no. 11, pp. 491–493, Nov 2002.
- [71] A. Edelman, "Eigenvalues and Condition Numbers of Random Matrices," PhD thesis, Department of Mathematics, Massachusetts Institute of Technology, Cambridge, MA, 1989.
- [72] P. Li, D. Paul, R. Narasimhan, and J. Cioffi, "On the distribution of SINR for the MMSE MIMO receiver and performance analysis," vol. 52, no. 1, pp. 271–286, Jan. 2006.
- [73] M. Abramowitz and I. Stegun, *Handbook of Mathematical Functions with Formulas, Graphs, and Mathematical Tables*. New York: Dover, 1972.
- [74] R. Horn and C. Johnson, *Matrix Analysis*. New York: Cambridge University Press, 1990.

- [75] D. Darsena, G. Gelli, F. Melito, and F. Verde, "Performance analysis of amplify-and-forward multiple-relay MIMO systems with ZF reception," *Vehicular Technology, IEEE Transactions on*, vol. PP, no. 99, pp. 1–1, 2014.
- [76] S. Boyd and L. Vandenberghe, *Convex Optimization*. New York, NY, USA: Cambridge University Press, 2004.
- [77] Z. Wang and G. Giannakis, "Wireless multicarrier communications," *Signal Processing Magazine, IEEE*, vol. 17, no. 3, pp. 29–48, May 2000.
- [78] H. Suraweera and J. Armstrong, "Performance of OFDM-Based Dual-Hop Amplify-and-Forward Relaying," vol. 11, no. 9, pp. 726–728, Sep. 2007.
- [79] A. Ben-Israel and T. N. E. Greville, *Generalized Inverses*. New York: Springer-Verlag, 2002.
- [80] C. G. Khatri, "On Certain Distribution Problems Based on Positive Definite Quadratic Functions in Normal Vectors," *Ann. Math. Statist.*, vol. 37, no. 2, pp. 468–479, 04 1966. [Online]. Available: <http://dx.doi.org/10.1214/aoms/1177699530>
- [81] D. Palomar, J. Cioffi, and M.-A. Lagunas, "Joint Tx-Rx beamforming design for multicarrier MIMO channels: a unified framework for convex optimization," *Signal Processing, IEEE Transactions on*, vol. 51, no. 9, pp. 2381–2401, Sept 2003.
- [82] A. Toding, M. Khandaker, and Y. Rong, "Optimal Joint Source and Relay Beamforming for Parallel MIMO Relay Networks," in *Wireless Communications Networking and Mobile Computing (WiCOM), 2010 6th International Conference on*, Sept 2010, pp. 1–4.
- [83] S. Geman, "A Limit Theorem for the Norm of Random Matrices," *Ann. Probab.*, vol. 8, no. 2, pp. 252–261, 04 1980. [Online]. Available: <http://dx.doi.org/10.1214/aop/1176994775>
- [84] J. W. Silverstein, "The Smallest Eigenvalue of a Large Dimensional Wishart Matrix," *Ann. Probab.*, vol. 13, no. 4, pp. 1364–1368, 11 1985. [Online]. Available: <http://dx.doi.org/10.1214/aop/1176992819>

- 
- [85] P. Viswanath and V. Anantharam, "Optimal sequences and sum capacity of synchronous CDMA systems," *Information Theory, IEEE Transactions on*, vol. 45, no. 6, pp. 1984–1991, Sep 1999.
- [86] C. Mullis and R. Roberts, "Synthesis of minimum roundoff noise fixed point digital filters," *Circuits and Systems, IEEE Transactions on*, vol. 23, no. 9, pp. 551–562, Sep 1976.
- [87] J. C. T. Starr, M. Sorbara and P. Silverman, *DSL Advances*. Prentice Hall Professional, 2003.
- [88] A. H. H. Hrasnica and R. Lehnert, *Broadband Powerline Communications*. Wiley, 2004.
- [89] ETSI, *Radio broadcasting systems; Digital audio broadcasting (DAB) to mobile, portable and fixed receivers*. ETSI Standard 300 401, 1995.
- [90] ———, *Digital video broadcasting (DVB); Framing structure, channel coding and modulation for digital terrestrial television*. ETSI Standard EN 300 744 v1.6.1, 2008.
- [91] B. O'Hara and A. Petrick, *The IEEE 802.11 Handbook: A Designer's Companion*. IEEE Standards Publications, 2005.
- [92] "IEEE Standard for Local and metropolitan area networks Part 16: Air Interface for Broadband Wireless Access Systems Amendment 3: Advanced Air Interface," *IEEE Std 802.16m-2011 (Amendment to IEEE Std 802.16-2009)*, pp. 1–1112, May 2011.
- [93] 3GPP, *LTE; Evolved universal terrestrial radio access (E-UTRA) and evolved universal terrestrial radio access network (E-UTRAN); Overall description*. 3GPP Standard TS 36.300, 2011.
- [94] D. Darsena, G. Gelli, L. Paura, and F. Verde, "Widely linear equalization and blind channel identification for interference-contaminated multicarrier systems," *Signal Processing, IEEE Transactions on*, vol. 53, no. 3, pp. 1163–1177, March 2005.
- [95] S. Muller-Weinfurtner, "Optimum Nyquist windowing in OFDM receivers," *Communications, IEEE Transactions on*, vol. 49, no. 3, pp. 417–420, Mar 2001.

- [96] D. Darsena, G. Gelli, L. Paura, and F. Verde, "NBI-resistant zero-forcing equalizers for OFDM systems," *Communications Letters, IEEE*, vol. 9, no. 8, pp. 744–746, Aug 2005.
- [97] A. J. Redfern, "Receiver window design for multicarrier communication systems," *Selected Areas in Communications, IEEE Journal on*, vol. 20, no. 5, pp. 1029–1036, Jun 2002.
- [98] D. Darsena, G. Gelli, L. Paura, and F. Verde, "A Constrained Maximum-SINR NBI-Resistant Receiver for OFDM Systems," *Signal Processing, IEEE Transactions on*, vol. 55, no. 6, pp. 3032–3047, June 2007.
- [99] K. Van Acker, G. Leus, M. Moonen, O. van de Wiel, and T. Pollet, "Per tone equalization for DMT-based systems," *Communications, IEEE Transactions on*, vol. 49, no. 1, pp. 109–119, Jan 2001.
- [100] K. V. Acker, T. Pollet, G. Leus, and M. Moonen, "Combination of per tone equalization and windowing in DMT-receivers," *Signal Processing*, vol. 81, no. 8, pp. 1571 – 1579, 2001, special section on Signal Processing Techniques for Emerging Communications Applications. [Online]. Available: <http://www.sciencedirect.com/science/article/pii/S0165168401000731>
- [101] D. Darsena, "Successive narrowband interference cancellation for OFDM systems," *Communications Letters, IEEE*, vol. 11, no. 1, pp. 73–75, Jan 2007.
- [102] K. Vanbleu, M. Moonen, and G. Leus, "Linear and decision-feedback per tone equalization for DMT-based transmission over IIR channels," *Signal Processing, IEEE Transactions on*, vol. 54, no. 1, pp. 258–273, Jan 2006.
- [103] D. Darsena, G. Gelli, and F. Verde, "Universal Linear Precoding for NBI-proof Widely Linear Equalization in MC Systems," *J. Wirel. Commun. Netw., EURASIP*, vol. 2008, pp. 8:1–8:13, Jan 2008. [Online]. Available: <http://dx.doi.org/10.1155/2008/321450>
- [104] S. Trautmann and N. Fliege, "A new equalizer for multitone systems without guard time," *Communications Letters, IEEE*, vol. 6, no. 1, pp. 34–36, Jan 2002.

- 
- [105] D. Darsena and F. Verde, "Successive NBI Cancellation Using Soft Decisions for OFDM Systems," *Signal Processing Letters, IEEE*, vol. 15, pp. 873–876, 2008.
- [106] D. Middleton, "Statistical-Physical Models of Electromagnetic Interference," *Electromagnetic Compatibility, IEEE Transactions on*, vol. EMC-19, no. 3, pp. 106–127, Aug 1977.
- [107] A. Spaulding and D. Middleton, "Optimum Reception in an Impulsive Interference Environment—Part I: Coherent Detection," *Communications, IEEE Transactions on*, vol. 25, no. 9, pp. 910–923, Sep 1977.
- [108] D. Middleton, "Procedures for Determining the Parameters of the First-Order Canonical Models of Class A and Class B Electromagnetic Interference," *Electromagnetic Compatibility, IEEE Transactions on*, vol. EMC-21, no. 3, pp. 190–208, Aug 1979.
- [109] P. Delaney, "Signal detection in multivariate class-A interference," *Communications, IEEE Transactions on*, vol. 43, no. 2/3/4, pp. 365–373, Feb 1995.
- [110] M. Nassar, A. Dabak, I. H. Kim, T. Pande, and B. Evans, "Cyclostationary noise modeling in narrowband powerline communication for Smart Grid applications," in *Acoustics, Speech and Signal Processing (ICASSP), 2012 IEEE International Conference on*, March 2012, pp. 3089–3092.
- [111] S. Zhidkov, "Performance analysis and optimization of OFDM receiver with blanking nonlinearity in impulsive noise environment," *Vehicular Technology, IEEE Transactions on*, vol. 55, no. 1, pp. 234–242, Jan 2006.
- [112] A. Mengi and A. Vinck, "Successive impulsive noise suppression in OFDM," in *Power Line Communications and Its Applications (ISPLC), 2010 IEEE International Symposium on*, March 2010, pp. 33–37.
- [113] C.-H. Yih, "Iterative Interference Cancellation for OFDM Signals With Blanking Nonlinearity in Impulsive Noise Channels," *Signal Processing Letters, IEEE*, vol. 19, no. 3, pp. 147–150, March 2012.

- [114] J. Lin, M. Nassar, and B. Evans, "Impulsive Noise Mitigation in Powerline Communications Using Sparse Bayesian Learning," *Selected Areas in Communications, IEEE Journal on*, vol. 31, no. 7, pp. 1172–1183, July 2013.
- [115] D. Darsena, G. Gelli, F. Melito, F. Verde, and A. Vitiello, "Impulse noise mitigation for MIMO-OFDM wireless networks with linear equalization," in *Measurements and Networking Proceedings (M N), 2013 IEEE International Workshop on*, Oct 2013, pp. 94–99.
- [116] M. Mirahmadi, A. Al-Dweik, and A. Shami, "BER Reduction of OFDM Based Broadband Communication Systems over Multipath Channels with Impulsive Noise," *Communications, IEEE Transactions on*, vol. 61, no. 11, pp. 4602–4615, November 2013.
- [117] T. Al-Naffouri, A. Quadeer, and G. Caire, "Impulse Noise Estimation and Removal for OFDM Systems," *Communications, IEEE Transactions on*, vol. 62, no. 3, pp. 976–989, March 2014.
- [118] F. Verde, "Subspace-based blind multiuser detection for quasi-synchronous MC-CDMA systems," *Signal Processing Letters, IEEE*, vol. 11, no. 7, pp. 621–624, July 2004.
- [119] A. Cacciapuoti, G. Gelli, and F. Verde, "FIR Zero-Forcing Multiuser Detection and Code Designs for Downlink MC-CDMA," *Signal Processing, IEEE Transactions on*, vol. 55, no. 10, pp. 4737–4751, Oct 2007.
- [120] V. Pan, *Structured Matrices and Polynomials: Unified Superfast Algorithms*. Boston, MA, USA: BirkhÅduser, 2001.
- [121] *Channel models for HIPERLAN/2 in different indoor scenarios*. ETSI Normalization Committee, available on <http://www.etsi.org>. [Online]. Available: <http://www.etsi.org>
- [122] K. Gulati, M. Nassar, and M. DeYoung, "Matlab Interference modeling and mitigation toolbox 1.6," Apr 2011 available on <http://users.ece.utexas.edu/~bevans/projects/rfi/software/>.
- [123] S. Alamouti, "A simple transmit diversity technique for wireless communications," *Selected Areas in Communications, IEEE Journal on*, vol. 16, no. 8, pp. 1451–1458, Oct 1998.

- [124] T. Anderson, L. Peterson, S. Shenker, and J. Turner, "Overcoming the Internet impasse through virtualization," *Computer*, vol. 38, no. 4, pp. 34–41, April 2005.
- [125] C. Clark, K. Fraser, S. Hand, J. G. Hansen, E. Jul, C. Limpach, I. Pratt, and A. Warfield, "Live Migration of Virtual Machines," in *Proceedings of the 2Nd Conference on Symposium on Networked Systems Design & Implementation - Volume 2*, ser. NSDI'05. Berkeley, CA, USA: USENIX Association, 2005, pp. 273–286. [Online]. Available: <http://dl.acm.org/citation.cfm?id=1251203.1251223>
- [126] K. K. Ramakrishnan, P. Shenoy, and J. Van der Merwe, "Live Data Center Migration Across WANs: A Robust Cooperative Context Aware Approach," in *Proceedings of the 2007 SIGCOMM Workshop on Internet Network Management*, ser. INM '07. New York, NY, USA: ACM, 2007, pp. 262–267. [Online]. Available: <http://doi.acm.org/10.1145/1321753.1321762>
- [127] M. Mishra, A. Das, P. Kulkarni, and A. Sahoo, "Dynamic resource management using virtual machine migrations," *Communications Magazine, IEEE*, vol. 50, no. 9, pp. 34–40, September 2012.
- [128] T. Lakshman and U. Madhow, "The performance of TCP/IP for networks with high bandwidth-delay products and random loss," *Networking, IEEE/ACM Transactions on*, vol. 5, no. 3, pp. 336–350, Jun 1997.
- [129] L. Jakab, A. Cabellos-Aparicio, F. Coras, D. Saucez, and O. Bonaventure, "LISP-TREE: A DNS Hierarchy to Support the LISP Mapping System," *Selected Areas in Communications, IEEE Journal on*, vol. 28, no. 8, pp. 1332–1343, October 2010.
- [130] S. Floyd and V. Jacobson, "Berkeley TCP evolution from 4.3-tahoe to 4.3-reno," in *Proceedings of the 18th Internet Engineering Task Force*, 1990.
- [131] F. Checconi, T. Cucinotta, and M. Stein, "Real-time Issues in Live Migration of Virtual Machines," in *Proceedings of the 2009 International Conference on Parallel Processing*, ser. Euro-Par'09. Berlin, Heidelberg: Springer-Verlag, 2010, pp. 454–466. [Online]. Available: <http://dl.acm.org/citation.cfm?id=1884795.1884847>

- 
- [132] W. A. Gardner, *Introduction to Random Processes*. New York: McGraw-Hill, 1990.
- [133] M. Kiessling and J. Speidel, "Analytical performance of MIMO zero-forcing receivers in correlated Rayleigh fading environments," in *IEEE Signal Processing Advances in Wireless Communications (SPAWC)*, Jun. 2003, pp. 1–5.
- [134] ———, "Unifying performance analysis of linear MIMO receivers in correlated Rayleigh fading environments," in *Spread Spectrum Techniques and Applications, 2004 IEEE Eighth International Symposium on*, Aug 2004, pp. 634–638.
- [135] A. Papoulis, *Random variables, and Stochastic Processes (3rd ed.)*. Singapore: MacGraw-Hill, 1991.
- [136] N. R. Goodman, "Statistical Analysis Based on a Certain Multivariate Complex Gaussian Distribution (An Introduction)," *Ann. Math. Statist.*, vol. 34, no. 1, pp. 152–177, 03 1963. [Online]. Available: <http://dx.doi.org/10.1214/aoms/1177704250>
- [137] G. B. et al., *Problems in mathematical analysis*. Moscow: MIR Publishers, 2009.
- [138] N. J. Higham and S. H. Cheng, "Modifying the inertia of matrices arising in optimization," *Linear Algebra and its Applications*, vol. 275 - 276, no. 0, pp. 261 - 279, 1998, proceedings of the Sixth Conference of the International Linear Algebra Society. [Online]. Available: <http://www.sciencedirect.com/science/article/pii/S0024379597100155>